

54. A COMPOSITIONALLY NEARLY STEADY-STATE MAGMA CHAMBER AT THE COSTA RICA RIFT: EVIDENCE FROM BASALT GLASS AND MINERAL DATA, DEEP SEA DRILLING PROJECT SITES 501, 504, AND 505¹

James H. Natland,² A. C. Adamson,³ Christine Laverne,⁴ W. G. Melson,⁵ and Timothy O'Hearn⁵

ABSTRACT

The compositions of natural glasses and phenocrysts in basalts from Deep Sea Drilling Project Sites 501, 504, and 505, near the Costa Rica Rift, constitute evidence for the existence of a periodically replenished axial magma chamber that repeatedly erupted lavas of remarkably uniform composition. Magma compositions were affected by three general components: (1) injected magmas carrying (in decreasing order of abundance) plagioclase, olivine, and chrome-spinel phenocrysts (spinel assemblage); (2) injected magmas carrying plagioclase, clinopyroxene, and olivine phenocrysts, but no spinel (clinopyroxene assemblage); and (3) moderately evolved hybrids in the magma chamber itself. The compositions of the injected phenocrysts and minerals in glomerocrysts are as follows: plagioclase—An₈₅₋₉₄; olivine—Fo₈₇₋₈₉; clinopyroxene—high Cr₂O₃ (0.7–1.1%), endiopsidite (Wo₄₂En₅₁Fs₇), and aluminous chromian spinel (Cr/Cr + Al ≈ 0.3). These minerals resemble those thought to occur in upper mantle sources (9 kbars and less) of ocean-ridge basalts and to crystallize in magmas near those sources. In the magma chamber, more sodic plagioclase (An₇₉₋₈₅), less magnesian olivine (Fo₈₅₋₈₆) and low-Cr₂O₃ (0.1–0.4%) clinopyroxene formed rims on these crystals, grew as other phenocrysts, and formed cumulus segregations on the walls and floors of the magma chamber. In the spinel-assemblage magmas, magnesiochromite (Cr/Cr + Al = 0.4–0.5) also formed. Some cumulus segregations were later entrained in lavas as xenoliths.

The glass compositions define 16 internally homogeneous eruptive units, 13 of which are in stratigraphic order in a single hole, Hole 504B, which was drilled 561.5 meters into the ocean crust. These units are defined as differing from each other by more than analytical uncertainty in one or more oxides. However, many of the glass groups in Hole 504B show virtually no differences in TiO₂ contents, Mg/Mg + Fe²⁺, or normative An/An + Ab, all of which are sensitive indicators of crystallization differentiation. The differences are so small that they are only apparent in the glass compositions; they are almost completely obscured in whole-rock samples by the presence of phenocrysts and the effects of alteration. Moreover, several of the glass units at different depths in Hole 504B are compositionally identical, with all oxides falling within the range of analytical uncertainty, with only small variations in the rest of the suite. The repetition of identical chemical types requires (1) very regular injection of magmas into the magma chamber, (2) extreme similarity of injected magmas, and (3) displacement of very nearly the same proportion of the magmas in the chamber at each injection. Numerical modeling and thermal considerations have led some workers to propose the existence of such conditions at certain types of spreading centers, but the lava and glass compositions at Hole 504B represent the first direct evidence revealed by drilling of the existence of a compositionally nearly steady-state magma chamber, and this chapter examines the processes acting in it in some detail.

The glass groups that are most similar are from clinopyroxene-assemblage lavas, which have a range of Mg/Mg + Fe²⁺ of 0.59 to 0.65. Spinel-assemblage basalts are less evolved, with Mg/Mg + Fe²⁺ of 0.65 to 0.69, but both types have nearly identical normative An/An + Ab (0.65–0.66). However, the two lava types contain megacrysts (olivine, plagioclase, clinopyroxene) that crystallized from melts with Mg/Mg + Fe²⁺ values of 0.70 to 0.72. Projection of glass compositions into ternary normative systems suggests that spinel-assemblage magmas originated deeper in the mantle than clinopyroxene-assemblage magmas, and mineral data indicate that the two types followed different fractionation paths before reaching the magma chamber. The two magma types therefore represent neither a low- nor a high-pressure fractionation sequence. Some of the spinel-assemblage magmas may have had picritic parents, but were coprecipitating all of the spinel-assemblage phenocrysts before reaching the magma chamber. Clinopyroxene-assemblage magmas did not have picritic parents, but the compositions of phenocrysts suggest that they originated at about 9 kbars, near the transition between plagioclase peridotite and spinel peridotite in the mantle.

Two glass groups have higher contents of alkalis, TiO₂, and P₂O₅ than the others, evidently as a result of the compositions of mantle sources. Eruption of these lavas implies that conduits and chambers containing magmas from dissimilar sources were not completely interconnected on the Costa Rica Rift.

The data are used to draw comparisons with the East Pacific Rise and to consider the mechanisms that may have prevented the eruption of ferrobasalts at these sites.

¹ Cann, J. R., Langseth, M. G., Honnorez, J., Von Herzen, R. P., White, S. M., et al., *Init. Repts. DSDP*, 69: Washington (U.S. Govt. Printing Office).

² Deep Sea Drilling Project, Scripps Institution of Oceanography, La Jolla, California.

³ Department of Geology, University of Newcastle-upon-Tyne, Newcastle-upon-Tyne, NE1 7RU, United Kingdom.

⁴ Laboratoire de Géologie, Faculté des Sciences et Techniques, 3038 SFAX, Tunisia.

⁵ Department of Mineral Sciences, Smithsonian Institution, Washington, D.C.

INTRODUCTION

While the basalts from Deep Sea Drilling Project Sites 501, 504, and 505 on the Costa Rica Rift were being recovered during Legs 68 and 69, shipboard X-ray fluorescence analyses (in Etoubleau et al., this volume) provided almost no indication of significant geochemical variation despite obvious differences in the occurrence of phenocrysts. Unlike previous drilling in the eastern Pacific (Legs 34, 54, and 65), the drilling failed to reveal the presence of ferrobasalts. Instead, the basalts resembled many Mid-Atlantic-Ridge lavas in ranging from being nearly aphyric to having abundant phenocrysts, megacrysts, and glomerocrysts of plagioclase, lesser olivine, and either chrome spinel or clinopyroxene. The fluctuations in these phenocrysts, however, did not define geochemical units, as they did, for example, at Sites 332 and 395 on the Mid-Atlantic Ridge (Natland, 1979a). We were dealing with rocks for the most part so subtly different in chemistry that the effects of the accumulation of phenocrysts and of alteration obscured the boundaries between different eruptive units. Whole-rock analyses were nearly useless for determining chemical stratigraphy.

It was clear that the only way to acquire a chemical stratigraphy was to determine the compositions of basalt glasses from the chilled rinds of pillows and thin flows. These glasses would be free of the effects of alteration and phenocrysts and might suggest reasons for the differences in the populations of phenocrysts. Chief among these differences were (1) the occurrence of a distinctive emerald green clinopyroxene in some porphyritic lavas but not others and (2) the occurrence of chromian spinel in lavas that lacked the clinopyroxene. Accordingly, samples of basalt glass were taken for electron microprobe analyses, first from the cores of Legs 68 and 69 and later from the portion of Hole 504B that was drilled during Leg 70. The analyses were performed by O'Hearn at the Smithsonian Institution for inclusion there in the archive of glass analyses from the ocean crust that has been compiled by Melson and his co-workers for a number of years. Meanwhile, the compositions of primary silicates were also determined by electron microprobe in many samples in the course of studies on alteration minerals by Adamson and Laverne, which form other chapters in this volume. These primary mineral data provide a general reconnaissance of mineral chemistry, particularly for Hole 504B, which was drilled to a total depth in basement of 561.5 meters by the end of Leg 70. Finally, the glass compositions and mineral reconnaissance data were used to select four samples for detailed study. Natland examined the minerals in these samples by using the electron microprobe at the Scripps Institution of Oceanography.

The combination of all these data sets allows us to be quite specific about the magmatic processes that acted at this spreading plate boundary at the times these basalts erupted. Although the glass compositions indeed reveal the subtle differences not evident in the whole-rock compositions, they are nevertheless so similar that it seems likely that most of the lavas erupted from a sin-

gle, periodically replenished axial magma chamber that achieved, probably to the maximum extent possible in nature, a nearly steady-state composition. However, there is enough variability in glass compositions, as well as important differences in phenocryst compositions and occurrences, to suggest that magmas experienced quite different histories prior to injection into the magma chamber, which acted mainly to buffer compositions to a consistent homogeneous average. We can also see indications among the phenocrysts that more evolved magmas developed in the magma chamber than apparently ever erupted (at least to be sampled by the drill), probably because they were invariably mixed with little-fractionated magmas entering the chamber prior to any eruptions. And, at the other end of the spectrum of phenocryst compositions, we can detect indications of the compositions of magmas near their sources of melting in the mantle, trace the coalescence of early melts into larger magma batches, and follow their crystallization from depth in the mantle to eruption on the seafloor.

SETTING

The sites were drilled on the south flank of the Costa Rica Rift (Fig. 1) in crust aged 5.9 m.y. (Sites 501 and 504) and 3.9 m.y. (Site 505). Site 501, drilled during Leg 68, was the pilot hole for an unsuccessful reentry attempt in Hole 504A and the very successful Hole 504B, which was drilled during Legs 69 and 70. Hole 504B was later extended to 1075 meters into basement during Leg 83, and it is still open for further drilling. Three holes were drilled at Site 505 during Leg 69; the drilling in all proceeded with much difficulty in highly fractured, little altered basalts, and none of the holes exceeded 50 meters in basement penetration.

The Costa Rica Rift is one segment of the east-west trending Galapagos Spreading Center (Fig. 1). It has an intermediate spreading rate of 3.6 cm/yr. (Lonsdale and Klitgord, 1978). At present the rift lacks either the deep rift valley of truly slow-spreading ridges or the axial horst or shield volcano that is characteristic of the fast-spreading East Pacific Rise (Lonsdale, 1977; Lonsdale and Spiess, 1980) and of the Galapagos Spreading Center near the Galapagos Islands (Anderson and Noltimier, 1973). Near Sites 501 and 504, the topography is quite flat and the sediment cover is uniform in thickness (230–250 m), suggesting that in the past there has been even less relief near the axis of spreading than there is now. Near Site 505, the topography is rougher (see Searle, this volume), and basement outcrops are common. The topography was a prominent factor in the lower heat flow near Site 505 than near Sites 501 and 504 (Langseth et al., this volume), a contrast that is reflected in the fresher rock and greater drilling difficulty at Site 505.

LITHOLOGY OF BASALTS AND SAMPLE DISTRIBUTION

Pillows, thin flows, and more massive flows up to 15 meters thick were the principal lithologies recovered in Holes 501, 504A, and 504B, although dike zones were noted in two places in Hole 504B (Fig. 2). The basalts

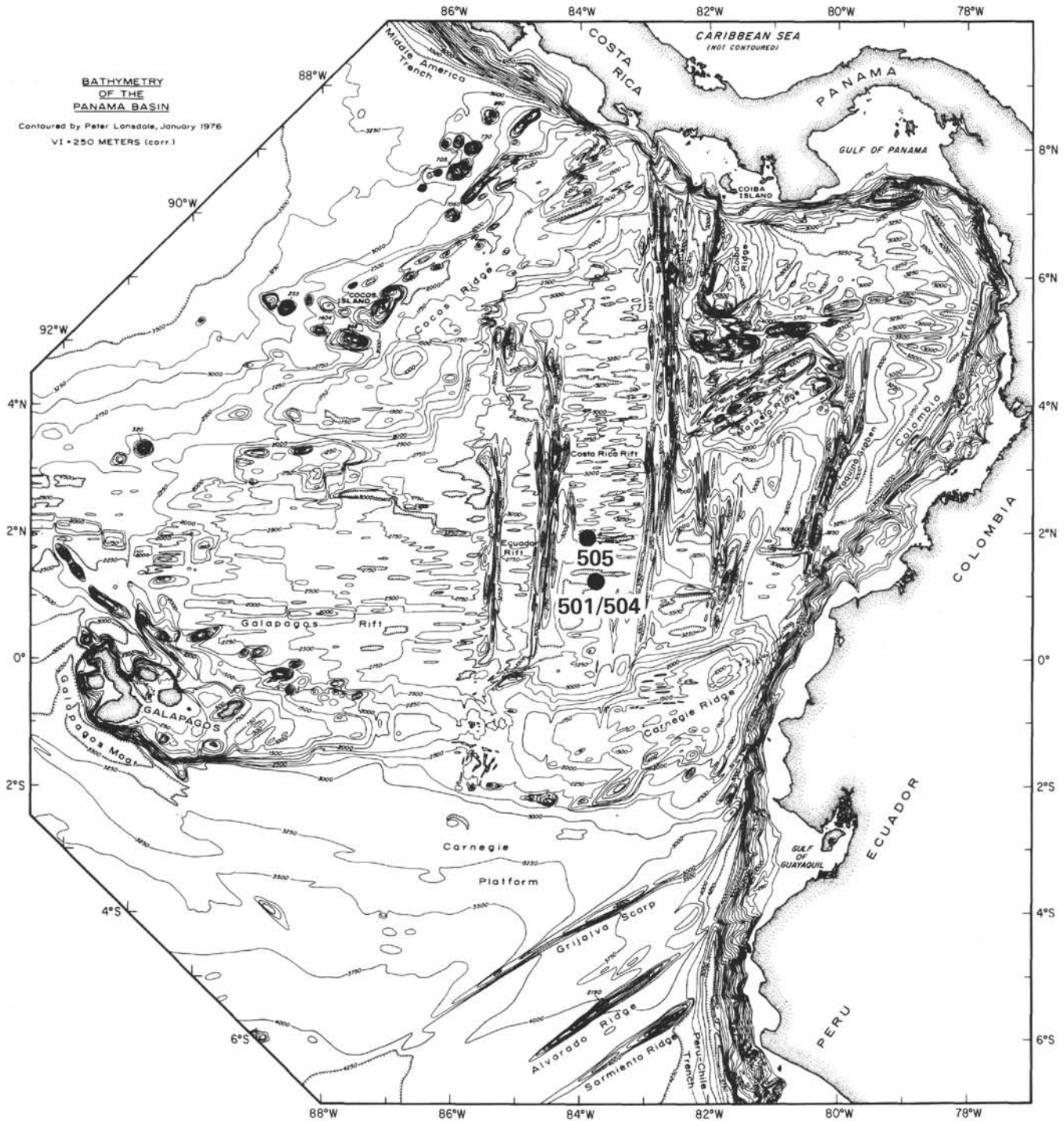
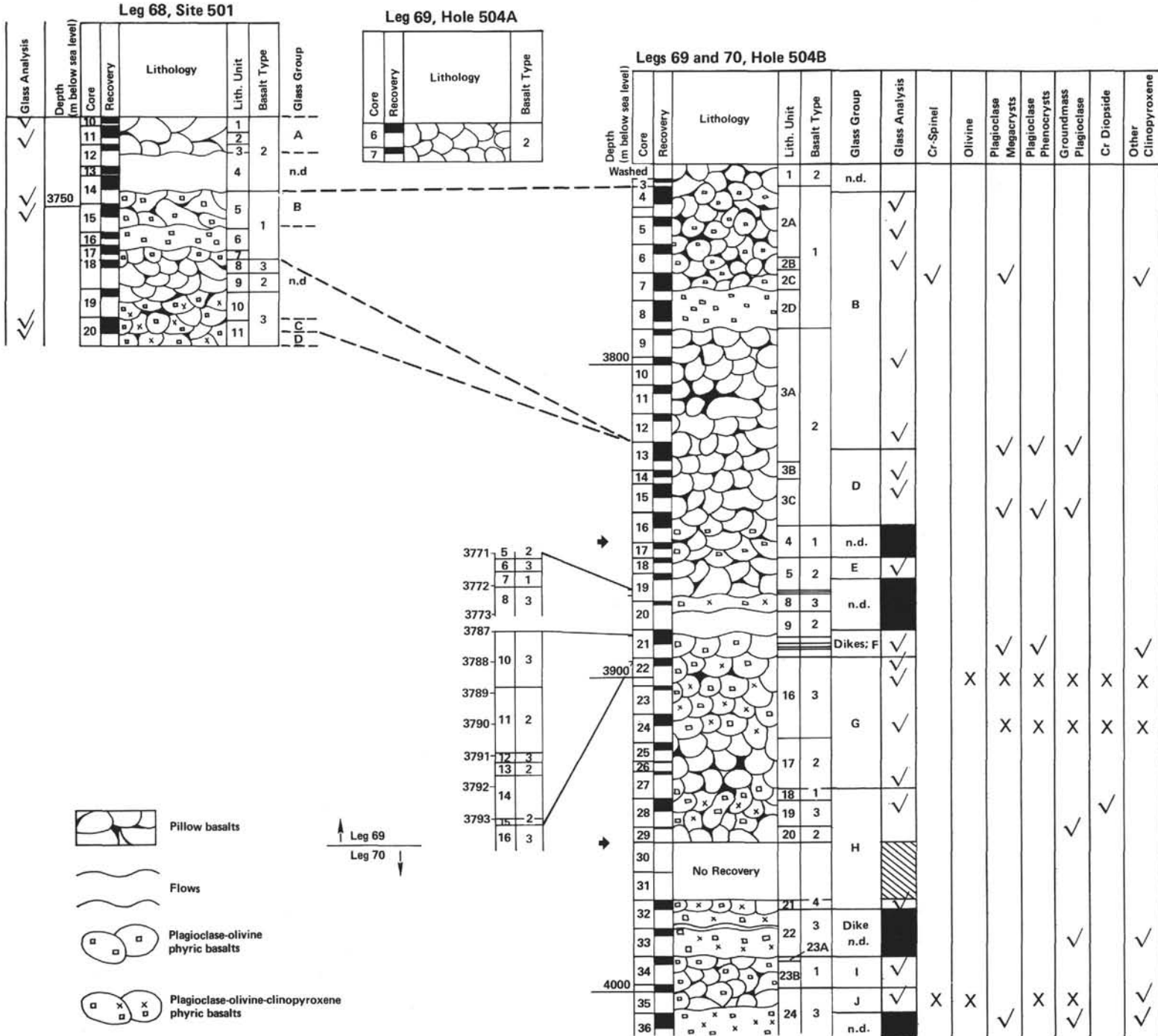


Figure 1. Locations of Sites 501, 504, and 505 south of the Costa Rica Rift, drilled during Legs 68 to 70. Bathymetry from Lonsdale and Klitgord (1978). Contour interval is 250 m.

were subdivided into five types by the shipboard parties on the basis of the abundance and occurrence of phenocrysts observed in hand specimens and thin sections. The five types are (1) plagioclase-olivine phyric basalt with essential chrome spinel; (2) aphyric and sparsely phyric basalts with variable proportions and occurrences of phenocrysts, mainly plagioclase; (3) plagioclase-olivine-clinopyroxene phyric basalt; (4) strongly porphyritic plagioclase-olivine-clinopyroxene phyric basalt; and

(5) moderately plagioclase-olivine phyric basalt lacking both chrome spinel and clinopyroxene.

Plagioclase is the dominant phenocryst in the porphyritic samples, constituting up to 25% of the rock, and it is 2 to 3 times as abundant as olivine and clinopyroxene phenocrysts. The feldspars range from large individual megacrysts up to 0.5 cm in length to microphe-
nocrysts less than 0.5 mm long; the latter appear mainly in glassy or spherulitic samples and can be observed



→ Re-entries

Basalt Petrographic Types

- 1 Plagioclase-olivine phyrlic basalt with essential chromite
- 2 Aphyric and sparsely phyrlic basalts with variable proportions and occurrences of phenocrysts
- 3 Plagioclase-olivine-clinopyroxene phyrlic basalt
- 4 Highly plagioclase-olivine-clinopyroxene phyrlic basalt
- 5 Moderately plagioclase-olivine phyrlic (no spinel or clinopyroxene)

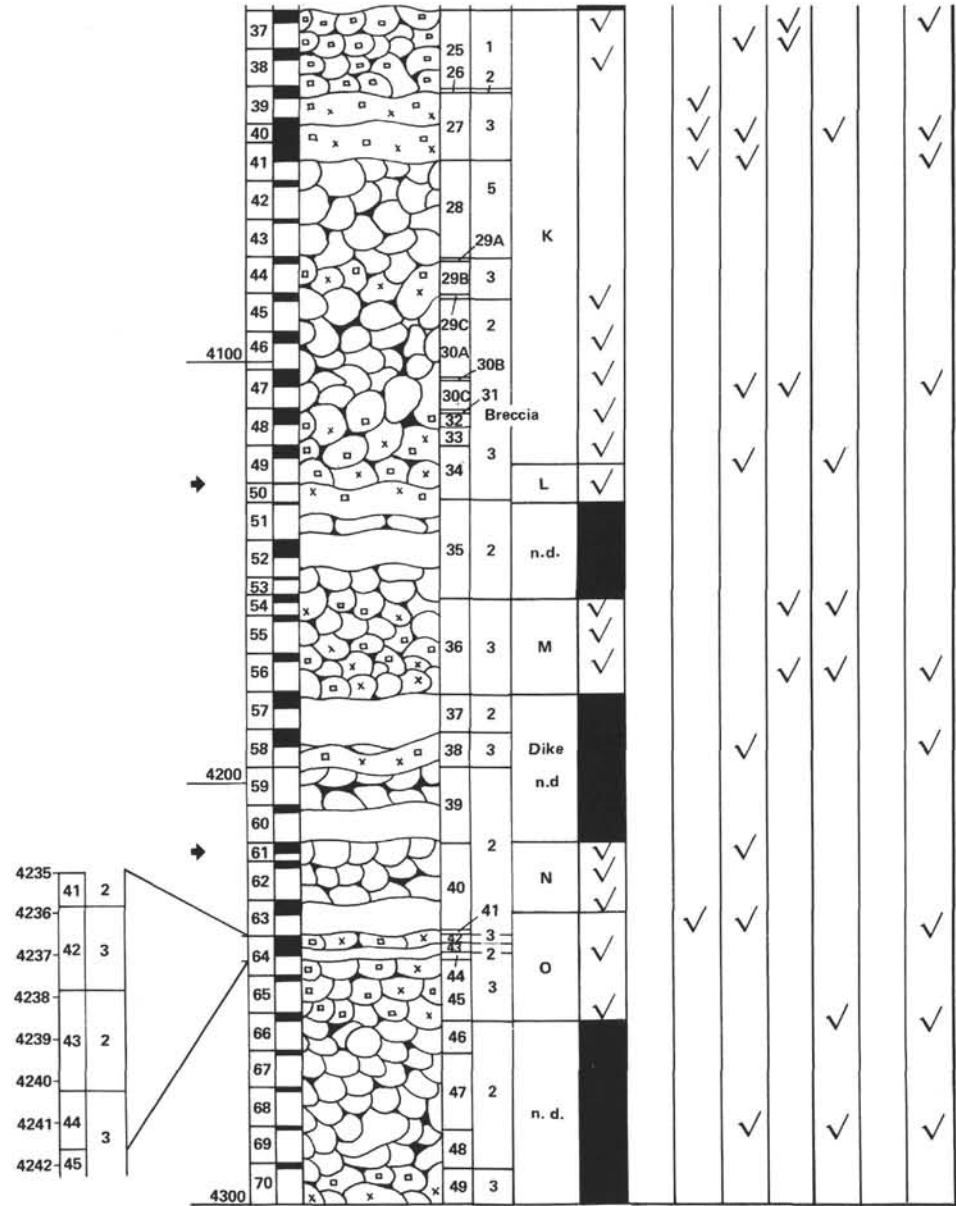


Figure 2. Lithologic summary of basement drilled at Holes 501, 504A, and 504B, giving lithologic units, petrographic types, and the distribution of glass groups, glass analyses, and mineral analyses. Checks indicate reconnaissance data, X's detailed mineral study.

under the microscope or with a hand lens. The plagioclases commonly occur grouped together in large glomerocrysts or in loose crystal clumps. Some of the larger glomerocrysts have larger than average crystals and contain olivine, but olivine phenocrysts usually occur singly or in intergrowths of two or three grains. In most samples from Sites 501 and 504, olivine is completely altered to clay minerals, but it is preserved to some extent in the glassy pillow margins, and it is fresh in samples from Site 505.

The distinctive emerald green clinopyroxene phenocrysts are commonly intergrown with plagioclase but not with olivine. Spinel occurs as euhedral or skeletal grains in the groundmass or enclosed within olivine and plagioclase phenocrysts. In most phyrlic samples, either clinopyroxene or Cr-spinel phenocrysts are present but not both. The basalt from Core 26 of Hole 505, in which clinopyroxene phenocrysts are fairly abundant, is an exception; Cr-spinel, although rare (1–2 grains per thin section), also occurs. Except in this instance, however, the basalts from Sites 501 and 504 contain one of the two phenocryst assemblages or are substantially aphyric. For convenience, we refer to the porphyritic basalts as spinel-assemblage or clinopyroxene-assemblage lavas, even though plagioclase is the most abundant phenocryst and olivine is more abundant than clinopyroxene in some samples. These definitions comprehend all of the porphyritic petrographic types defined by the shipboard parties except Type 5, which lacks diagnostic spinel and clinopyroxene but occurs in only one 20-meter interval in Hole 504B (Fig. 2). Of the various rock types, aphyric and sparsely phyrlic basalts are most abundant, making up perhaps half of the 561.5-meter section cored in Hole 504B (Fig. 2). Clinopyroxene-assemblage basalts are more abundant than spinel-assemblage lavas, occurring in Hole 505 and in Cores 19 to 24, 27 to 33, 36, 39, 40, 44, 48 to 50, 54 to 56, 58, 64 to 65, and 70 in Hole 504B. Spinel-assemblage lavas include all the basalts of Holes 505A and 505B and occur only in Cores 4 to 8, 16 to 17, 34, 35, and 38 of Hole 504B. Homogeneous glass groups comprise both phenocryst-poor and porphyritic lavas.

Two rock types not cored at these sites are olivine-rich basalts (picrites or, more properly, oceanites) and olivine-free basalts (which include ferrobasalts). These basalts represent the extremes of the compositions found in significant abundance in the ocean crust. Almost all of the Costa Rica Rift basalts are close to the compositional midpoint between these extremes. They are typical in many respects of the most abundant types of ocean crust basalt (cf. Wilkinson, 1982); therefore the petrogenetic processes that produced these basalts probably characterize many spreading ridge systems.

This chapter considers in turn each of the three data sets mentioned in the introduction—the glass composition data, the mineral reconnaissance data, and the data from the detailed study of selected samples. The chapter then discusses the general problem of magma generation at the Costa Rica Rift. Figure 2 shows the general distribution of data we obtained on glasses, the various phenocrysts, and groundmass minerals in Hole 504B. We

have additional data from Sites 501 and 505, but our main concern is Hole 504B, for which we have the most information.

GLASS SAMPLES

We obtained 68 new electron microprobe analyses of basaltic glasses from Sites 501, 504, and 505 (Table 1). Most of the analyses, 56 altogether, are from Hole 504B. Sample selection was dictated by the recovery of glass and the influence of alteration. At Site 505, both penetration into basalt and recovery in the three holes drilled were very small. No glass was recovered in Hole 505. Only one sample from Hole 505A and four samples from Hole 505B contained analyzable glass. Holes 501, 504A, and 504B are effectively the same site (Fig. 1). The principal gaps in the sampling of glasses in these holes coincide with thick units of massive basalt, which lack glass (Fig. 2), or occur where alteration is especially pervasive, as in the lowest cores of Hole 504B.

Sampling occurred in several stages (see footnote to Table 1); hence, analyses were obtained at different times. Samples were analyzed on an ARL nine-channel microprobe at the Department of Mineral Sciences, Smithsonian Institution, with techniques described in Melson et al. (1976) and Natland and Melson (1980). The homogeneity of glasses within chemical units judged to represent discrete eruptive events has been shown to be comparable to, or less than, the precision obtained by repeated analyses obtained by classical techniques on the Standard VG-2 (Melson, 1979). Some idea of sample homogeneity can be discerned from the average composition and standard deviation for each oxide of 24 glass chips from a single dredge haul from the East Pacific Rise (PL-1, 3°25.5'S, 102°35.7'W; Lonsdale, 1977) listed in Table 2. Values of twice the standard deviation (95% confidence limits) correspond closely to ranges for Standard VG-2 and DSDP Hole 395A Unit A₃ as given in Melson (1979). The reproducibility of analyses of homogeneous chemical types over time is quite good, as can be seen by examination of three analyses from a single section of Hole 504B, Core 35, all of which were sampled within a meter of each other (Table 1; VG nos. 5886, 5216, and 5453). The three analyses were obtained over a period of about 18 months, one in each of the three batches of analyses described in Table 1. Differences among the oxides all fall within the ranges for Standard VG-2 and the standard deviations for the chips from the dredge haul (PL-1 in Table 2), indicating that all three samples are of a single chemical type.

GLASS COMPOSITIONS

When the glass compositions are listed in order of depth, as in Table 1, many of the analyses are very similar to stratigraphically adjacent analyses. In order to determine how many chemical groups there were among the analyses, the following sorting procedure (which is also described in Natland and Melson [1980]) was used. The oxide differences between analyses were compared with the following tolerances (tolerances are given in wt.% of oxide): SiO₂ = 1.10, Al₂O₃ = 0.80, FeO* =

Table 1. Electron microprobe analyses of basaltic glasses, DSDP Sites 501, 504, and 505, Costa Rica Rift.

Original Sample No.	VG No.	SiO ₂	Al ₂ O ₃	FeO	MgO	CaO	Na ₂ O	K ₂ O	TiO ₂	P ₂ O ₅	Sum	Glass Group	
501-10-1, 9	5894	51.44	14.26	10.79	7.36	12.36	2.07	0.04	1.14	0.10	99.56	A	
11-1, 88	5895	51.12	14.28	10.74	7.59	12.26	2.05	0.05	1.11	0.10	93.30		
14-3, 133	5896	51.23	15.00	9.47	8.23	12.88	1.92	0.02	1.00	0.08	99.83		
15-1, 76	5897	50.98	15.16	9.27	8.30	12.87	1.87	0.03	0.98	0.09	99.55	B	
15-3, 147	5898	51.20	15.25	9.32	8.23	12.89	1.96	0.03	0.97	0.08	99.93		
20-2, 20	5899	51.25	14.44	10.55	7.64	12.66	1.92	0.03	1.04	0.09	99.62	C	
20-4, 130	5900	50.29	14.90	9.54	8.32	13.18	1.91	0.04	0.93	0.09	99.20		
504A-5-1, 98	5186	51.10	14.22	10.81	7.46	12.42	2.07	0.02	1.14	0.11	99.35	A	
504B-4-1, 138	5187	50.75	15.10	9.32	8.43	12.95	1.96	0.02	0.94	0.08	99.55	B	
4-2, 3	5188	50.99	15.23	9.28	8.44	12.83	1.91	0.02	0.98	0.11	99.79		
4-5, 70	5189	50.25	14.98	9.39	8.36	12.85	1.93	0.02	0.94	0.09	98.81		
5-1, 28	5190	50.87	15.02	9.49	8.52	12.90	1.94	0.03	0.96	0.10	99.83		
6-2, 2	5191	51.21	15.16	9.51	8.37	12.98	1.95	0.04	0.96	0.08	100.26		
10-2, 96	5192	51.29	15.04	9.30	8.39	12.94	2.15	0.03	0.99	0.08	100.21		
13-1, 75	5194	51.66	15.05	9.45	8.36	12.92	2.12	0.01	0.99	0.09	100.65		
14-2, 93	5195	51.56	14.49	9.94	8.14	12.78	1.91	0.02	0.95	0.07	99.86		
15-1, 72	5196	51.60	14.49	9.56	8.04	12.78	1.91	0.02	0.96	0.08	99.44		
15-3, 20	5197	51.41	14.52	9.74	8.03	12.84	1.91	0.02	0.93	0.07	99.47		D
15-4, 73	5198	51.59	14.66	9.81	8.13	12.88	1.86	0.02	0.98	0.08	100.01		
15-5, 12	5199	51.58	14.78	9.92	8.15	12.95	1.90	0.04	0.95	0.08	100.35		
16-4, 38	5880	50.77	15.21	8.68	8.35	11.72	2.76	0.25	1.01	0.09	98.84		E
21-3, 23	5882	51.02	14.90	9.37	8.28	13.36	1.81	0.02	0.85	0.10	99.71		
21-4, 99	5883	50.64	15.29	9.42	8.28	13.12	2.13	0.02	1.05	0.09	100.04		F
23-1, 7	5884	50.67	15.33	9.40	8.12	13.08	2.16	0.03	1.03	0.09	99.91		
24-2, 78	5201	50.70	14.50	9.50	7.98	12.94	2.02	0.02	0.98	0.09	98.73	G	
24-3, 70	5202	50.82	14.62	9.41	7.96	12.83	2.04	0.02	0.97	0.08	98.75		
27-1, 10	5204	50.85	14.41	9.61	7.92	12.88	2.13	0.01	1.01	0.09	98.91	H	
28-3, 3	5205	51.40	14.44	10.19	7.82	12.49	2.04	0.01	1.06	0.11	99.56		
32-1, 29	5450	51.65	14.23	10.58	7.55	12.38	1.85	0.04	1.08	0.09	99.45	I	
34-1, 126	5451	49.89	15.94	9.34	8.52	13.05	2.03	0.04	0.89	0.08	99.78		
34-2, 42	5452	49.98	15.88	9.43	8.56	12.93	2.10	0.03	0.90	0.07	99.88	J	
34-2, 129	5885	50.31	15.88	9.35	8.64	13.13	2.08	0.02	0.85	0.07	100.33		
34-2, 130	5215	49.67	15.85	9.30	8.49	13.15	2.09	0.02	0.91	0.07	99.55	K	
35-1, 15	5886	49.32	17.22	8.67	9.36	12.97	2.16	0.01	0.81	0.08	100.50		
35-1, 81	5216	48.87	16.98	8.43	9.21	12.97	2.12	0.02	0.83	0.07	99.50	L	
35-1, 108	5453	49.33	16.99	8.60	9.31	12.86	2.13	0.05	0.81	0.06	100.14		
37-1, 104	5454	50.79	14.94	10.03	8.12	12.95	2.04	0.04	0.96	0.08	99.95	M	
37-2, 1	5455	50.80	14.62	9.96	8.03	12.82	2.04	0.04	0.97	0.06	99.34		
38-1, 80	5456	51.02	14.90	9.91	8.19	12.97	2.06	0.04	0.97	0.06	100.12	N	
45-2, 4	5889	50.69	15.05	9.66	8.24	13.08	1.99	0.03	0.94	0.07	99.75		
46-1, 110	5217	51.08	14.56	9.91	7.88	12.98	2.13	0.04	1.00	0.09	99.67	O	
46-1, 113	5457	51.62	14.66	9.89	7.81	12.70	2.13	0.05	0.99	0.10	99.95		
46-3, 104	5458	51.29	14.79	9.86	7.81	12.84	2.07	0.05	1.06	0.08	99.85	P	
47-2, 38	5218	51.21	14.95	9.72	8.52	12.96	1.94	0.03	1.00	0.08	100.41		
48-2, 118	5459	51.59	14.61	9.80	8.08	12.66	1.86	0.05	0.91	0.08	99.64	Q	
49-1, 24	5460	50.96	14.70	9.91	7.98	12.84	2.00	0.04	0.98	0.07	99.48		
49-1, 86	5219	51.32	14.78	9.85	8.18	12.93	1.90	0.04	0.95	0.07	100.02	R	
49-1, 131	5220	51.78	14.64	9.84	8.08	12.72	1.87	0.02	0.96	0.10	100.01		
49-1, 135	5461	51.33	14.66	9.94	8.01	12.84	1.90	0.03	0.95	0.07	99.73	S	
49-2, 34	5462	51.76	14.59	9.92	7.98	12.78	1.89	0.03	0.94	0.07	99.96		
50-1, 19	5890	51.49	15.14	9.41	8.23	12.59	2.21	0.02	0.94	0.10	100.13	T	
54-2, 36	5891	51.15	15.04	9.84	7.72	12.33	2.53	0.10	1.32	0.16	100.19		
55-1, 111	5892	50.51	14.97	9.77	7.79	12.28	2.49	0.09	1.35	0.16	99.41	U	
56-1, 90	5893	50.51	14.86	9.69	7.75	12.32	2.46	0.09	1.37	0.16	99.21		
56-2, 75	5463	50.64	15.21	9.86	7.72	12.41	2.48	0.08	1.37	0.13	99.90	V	
61-1, 27	5464	50.82	15.06	10.19	8.24	12.69	1.91	0.03	1.06	0.11	100.11		
61-2, 79	5221	51.30	15.00	10.23	8.36	12.64	1.94	0.02	1.10	0.10	100.69	W	
62-2, 19	5465	50.72	14.78	10.06	8.17	12.59	1.90	0.02	1.09	0.08	99.41		
63-4, 19	5466	50.65	14.78	10.19	8.28	12.57	1.89	0.04	1.08	0.09	99.57	X	
64-1, 26	5467	50.97	14.70	9.64	7.95	12.85	1.94	0.04	1.04	0.09	99.22		
64-1, 27	5222	51.25	14.64	9.70	8.19	12.67	1.90	0.03	1.01	0.10	99.49	Y	
64-1, 91	5468	51.34	14.96	9.67	8.21	12.82	1.94	0.04	0.99	0.10	100.07		
66-1, 120	5469	51.48	14.73	9.80	8.00	12.83	2.01	0.04	1.03	0.08	100.00	Z	
505A-1-1, 56	5206	50.04	16.30	8.85	8.59	12.54	2.09	0.03	0.98	0.07	99.49		
505B-1-1, 24	5207	50.14	16.06	8.74	8.68	12.64	2.18	0.02	0.98	0.09	99.53	p	
2-1, 93	5208	50.28	15.95	8.80	8.72	12.64	2.13	0.02	0.95	0.09	99.58		
2-1, 119	5209	50.00	16.02	8.83	8.69	12.68	2.19	0.02	1.01	0.07	99.51		
5-1, 27	5210	49.76	16.10	8.80	8.70	12.51	2.12	0.05	0.99	0.08	99.11		

Note: VG Numbers 5186 to 5222 were sampled on board *Glomar Challenger* by J. Natland and J. Honnorez. VG Numbers 5450 to 5469 and 5880 to 5900 were sampled at the DSDP West Coast Repository by J. Natland at two separate times respectively between 12 and 18 months following Leg 70.

0.60, MgO = 1.00, CaO = 0.60, Na₂O = 0.30, K₂O = 0.08, TiO₂ = 0.30, and P₂O₅ = 0.08. Analyses were considered to belong to the same groups if (1) each analysis differed from every other by less than the stated tolerances for all nine oxides and (2) all analyses in the group were from the same site and appeared in consecutive (stratigraphic) order in Table 1. Groups defined in this way were taken to represent the compositions of individual eruptions on the seafloor (cf. Melson et al., 1976). Samples that met Criterion (1) and appeared in the same relative stratigraphic position in different holes

at the same site (treating Hole 501 as part of Site 504) were also construed as representing the same chemical group. The appearance of the same chemical group in different holes thus gave some information about the lateral extent of flows. Averages were compiled for each group, as well as standard deviations (where more than two analyses were involved), and these are listed along with CIPW norms in Table 2. There, for discussion and plotting purposes, the groups are given alphabetical designations. There are 16 groups in all; 15 of them appear at Sites 501 and 504, and 13 of these appear in a single

Table 2. Average analyses and standard deviations of glass groups.

Hole Glass Group Number of Samples	501, 504A A 3	501, 504B B 10	501 C 1	501, 504B D 6	504B E 1	504B F 1	504B G 5	504B H 2	
SiO ₂	51.22 ± 0.19	51.04 ± 0.38	51.25	51.34 ± 0.52	50.77	51.02	50.74 ± 0.09	51.53	
Al ₂ O ₃	14.25 ± 0.03	15.10 ± 0.10	14.44	14.64 ± 0.17	15.21	14.90	14.83 ± 0.44	14.34	
FeO*	10.78 ± 0.04	9.38 ± 0.09	10.55	9.75 ± 0.17	8.68	9.37	9.47 ± 0.09	10.39	
MgO	7.47 ± 0.12	8.36 ± 0.09	7.64	8.14 ± 0.10	8.35	8.28	8.05 ± 0.15	7.69	
CaO	12.35 ± 0.08	12.90 ± 0.05	12.66	12.90 ± 0.15	11.72	13.36	12.97 ± 0.13	12.44	
Na ₂ O	2.06 ± 0.01	1.97 ± 0.09	1.92	1.90 ± 0.02	2.76	1.81	2.10 ± 0.06	1.95	
K ₂ O	0.04 ± 0.02	0.03 ± 0.01	0.03	0.03 ± 0.01	0.25	0.08	0.02 ± 0.01	0.03	
TiO ₂	1.13 ± 0.02	0.97 ± 0.02	1.04	0.95 ± 0.02	1.01	0.85	1.01 ± 0.03	1.07	
P ₂ O ₅	0.10 ± 0.00	0.09 ± 0.01	0.09	0.08 ± 0.01	0.09	0.10	0.09 ± 0.005	0.10	
Mg no. ¹	0.552 (0.586)	0.614 (0.645)	0.563 (0.597)	0.598 (0.630)	0.632 (0.663)	0.612 (0.644)	0.602 (0.635)	0.619 (0.651)	
CIPW Norms ²									
Q	2.03	0.72	2.15	1.68	0.00	0.99	0.34	2.65	
Or	0.24	0.18	0.18	0.18	1.48	0.47	0.12	0.18	
Ab	17.42	16.66	16.23	16.06	23.33	15.30	17.75	16.49	
An	29.50	32.25	30.68	31.31	28.36	32.28	30.96	30.27	
Ne	0.00	0.00	0.00	0.00	0.00	0.00	0.00	0.00	
Di	Wo	12.96	12.98	13.14	13.40	12.16	13.89	13.66	12.83
	En	7.08	7.71	7.27	7.78	7.43	8.20	8.01	7.17
	Fs	5.40	4.59	5.35	4.97	4.03	4.99	4.97	5.13
Hy	En	11.45	13.02	11.68	12.40	7.70	12.34	11.95	11.90
	Fs	8.73	7.74	8.59	7.92	4.17	7.51	7.42	8.52
	Fo	0.00	0.00	0.00	0.00	3.91	0.00	0.00	0.00
Ol	Fa	0.00	0.00	0.00	0.00	2.34	0.00	0.00	
	Mt	2.21	1.92	2.17	2.01	1.78	1.92	1.95	2.14
Il	2.15	1.85	1.98	1.81	1.92	1.62	1.92	2.04	
Ap	0.23	0.21	0.21	0.18	0.21	0.23	0.21	0.23	
Σ	99.41	99.82	99.63	99.72	98.81	99.75	99.28	99.55	

¹ Mg/Mg + Fe²⁺. Numbers outside parentheses assume all iron as FeO*. Numbers inside parentheses assume Fe²⁺/Fe²⁺ + Fe³⁺ = 0.86.

² Computed on the basis of Fe²⁺/Fe²⁺ + Fe³⁺ = 0.86.

³ Natland and Melson (1980), their Glass Group U, from crest of East Pacific Rise near 3°S.

hole, Hole 504B. The distribution of glass groups with depth and the correlation between the holes at Sites 501 and 504 are shown in Figure 2. Some chemical characteristics of the groups and the petrographic types of the corresponding basalts (spinel assemblage, clinopyroxene assemblage, sparsely phyrlic) are listed in Table 3. From Figure 2, it is evident that glass groups span intervals that include both porphyritic and sparsely phyrlic basalts, demonstrating variable concentrations of phenocrysts within individual eruptive units. There are four spinel-assemblage groups (which include some aphyric and sparsely phyrlic intervals), seven clinopyroxene-assemblage groups (which also include some sparsely phyrlic and aphyric basalts), two groups that lack diagnostic phenocrysts, one group with mixed petrographic assemblages, and two others, described as less depleted, to be discussed shortly.

VARIATIONS AMONG GLASS GROUPS

Many of the glass groups are very similar in composition, and none is highly fractionated. All are hypersthene or quartz normative tholeiites (Table 2), and most have exceedingly low abundances of K₂O and P₂O₅, even for abyssal tholeiites. In these groups, both Na₂O and TiO₂ contents are also low. TiO₂ abundances, which are a sensitive indicator of the degree of fractionation, are less than 1.2% in all but one case and less than 1.0% in fully half of the glass groups (Table 3). Mg/Mg + Fe²⁺ ranges from 0.69 to 0.59, with most

groups falling in the range from 0.62 to 0.66. FeO* is no higher than 10.78%. Thus, none of the groups closely approaches the FETI compositions of Melson et al. (1976). For Groups F, I, and J, TiO₂ contents are particularly low (<0.90%). With 9.29% MgO, Mg/Mg + Fe²⁺ of 0.689, and CaO/Al₂O₃ of 0.76, Group J is the least fractionated glass group, and in fact it is the least evolved glass composition so far analyzed in the Galapagos Spreading Center (cf. Melson et al., 1976). It is appropriate to place it among the MGCA samples of Melson et al. (1976).

Two glass groups, Groups E and M, have higher Na₂O, K₂O, and P₂O₅ contents at comparable MgO abundances than the other glass groups. Group M has the highest TiO₂ content of all the glass groups. In Table 3, the two groups are clearly set off from the others by their lower normative An/An + Ab, a consequence of both lower CaO/Al₂O₃ and higher Na₂O. These samples are from two intervals in Hole 504B that whole-rock analyses show to be considerably enriched in large-ion-lithophile and other hygromagmatophile elements compared with other samples in the hole. The rocks have different ratios of Nb/Zr and La/Ta, indicating an origin from a less depleted mantle source than the remainder of the lavas (Etoubeau et al., this volume; Autio and Rhodes, this volume). They are designated as having less depleted compositions in Table 3. Despite these features of the trace element chemistry, the glass compositions still fall within the range observed among mid-

Table 2. (Continued).

504B I 4	504B J 3	504B K 14	504B L 1	504B M 4	504B N 4	504B O 4	505A, 505B P 5	PL ₂ -1 24 ³
49.96 ± 0.27	49.14 ± 0.24	51.23 ± 0.31	51.49	50.86 ± 0.44	50.87 ± 0.29	51.26 ± 0.22	50.04 ± 0.19	51.52 ± 0.34
15.89 ± 0.04	17.06 ± 0.14	14.70 ± 0.21	15.14	15.04 ± 0.14	14.91 ± 0.15	14.76 ± 0.14	16.09 ± 0.13	13.82 ± 0.17
9.36 ± 0.05	8.57 ± 0.12	9.87 ± 0.09	9.41	9.79 ± 0.08	10.17 ± 0.07	9.70 ± 0.07	8.80 ± 0.04	12.05 ± 0.13
8.55 ± 0.07	9.29 ± 0.08	8.07 ± 0.18	8.23	7.75 ± 0.03	8.26 ± 0.08	8.09 ± 0.13	8.68 ± 0.05	6.20 ± 0.12
13.07 ± 0.10	12.93 ± 0.06	12.86 ± 0.10	12.59	12.34 ± 0.05	12.62 ± 0.05	12.79 ± 0.08	12.60 ± 0.07	10.57 ± 0.08
2.08 ± 0.03	2.14 ± 0.02	1.99 ± 0.05	2.21	2.49 ± 0.03	1.91 ± 0.02	1.95 ± 0.05	2.14 ± 0.04	2.96 ± 0.05
0.02 ± 0.02	0.03 ± 0.02	0.04 ± 0.01	0.08	0.09 ± 0.01	0.03 ± 0.01	0.04 ± 0.01	0.03 ± 0.01	0.13 ± 0.01
0.89 ± 0.03	0.82 ± 0.01	0.9 ± 0.03	0.94	1.35 ± 0.02	1.08 ± 0.02	1.02 ± 0.02	0.98 ± 0.02	1.97 ± 0.05
0.07 ± 0.01	0.07 ± 0.01	0.08 ± 0.01	0.10	0.15 ± 0.01	0.10 ± 0.01	0.09 ± 0.01	0.08 ± 0.01	0.18 ± 0.02
0.619 (0.651)	0.659 (0.689)	0.593 (0.626)	0.609 (0.641)	0.585 (0.618)	0.591 (0.624)	0.598 (0.630)	0.637 (0.668)	
0.00	0.00	1.14	0.32	0.00	0.96	1.55	0.00	
0.12	0.18	0.24	0.47	0.53	0.18	0.24	0.18	
17.59	18.09	16.82	18.68	21.05	16.15	16.49	18.09	
33.95	36.84	31.04	31.14	29.58	32.01	31.39	34.19	
0.00	0.00	0.00	0.00	0.00	0.00	0.00	0.00	
12.68	11.18	13.43	12.78	12.77	12.48	13.11	11.58	
7.57	7.02	7.75	7.54	7.41	7.21	7.64	7.12	
4.44	3.46	5.05	4.59	4.75	4.68	4.84	3.78	
9.34	5.93	12.27	12.87	10.61	13.28	12.43	10.96	
5.47	2.92	8.00	7.83	6.79	8.63	7.88	5.82	
3.01	7.07	0.00	0.00	0.84	0.00	0.00	2.41	
1.95	3.85	0.00	0.00	0.59	0.00	0.00	1.42	
1.92	1.76	2.03	1.94	2.01	2.10	2.00	1.81	
1.69	1.56	1.85	1.79	2.57	2.05	1.94	1.86	
0.16	0.16	0.18	0.23	0.35	0.23	0.21	0.18	
99.87	100.02	99.80	100.18	99.86	99.95	99.69	99.41	

Table 3. Phenocryst assemblages and geochemical features of Costa Rica Rift basalts and associated glass groups.

Glass Group	Mg		CaO/Al ₂ O ₃	An/An + Ab	Cr (ppm) ¹	
	Mg + Fe ²⁺	TiO ₂			Range (no. samples)	Average
1) Spinel assemblage, sparsely phyrlic						
B	0.645	0.97	0.85	0.66	309–424 (9)	372
I	0.651	0.89	0.82	0.66	404 (1)	404
J	0.689	0.82	0.76	0.67	—	—
P	0.668	0.98	0.78	0.65	—	—
2) Clinopyroxene assemblage, sparsely phyrlic						
C	0.597	1.04	0.88	0.65	273–426 (5)	322
D	0.630	0.95	0.88	0.66	—	—
F	0.644	0.85	0.90	0.67	—	—
G	0.635	1.01	0.87	0.64	283–372 (3)	309
H	0.651	1.07	0.87	0.65	263–374 (8)	279
L	0.641	0.94	0.83	0.63	254 (1)	254
O	0.630	1.02	0.87	0.66	143–303 (2)	223
3) Sparsely phyrlic only						
A	0.586	1.13	0.87	0.63	—	—
N	0.624	1.08	0.85	0.66	313 (1)	313
Mixed						
K	0.626	0.97	0.87	0.63	133–398 (11)	332
4) Less depleted						
E	0.663	1.01	0.77	0.55	326 (1)	326
M	0.618	1.35	0.82	0.58	254 (1)	254
Averages						
1)	0.663 ± 0.020	0.92 ± 0.08	0.80 ± 0.04	0.66 ± 0.01		388
2)	0.633 ± 0.017	0.98 ± 0.08	0.87 ± 0.02	0.65 ± 0.01		277
3)	0.605	1.11	0.86	0.65		323
4)	0.640	1.18	0.80	0.57		290

¹ Data from Marsh et al. (this volume).

ocean-ridge basalts and are insufficiently rich in K_2O and P_2O_5 to be grouped with the KP-glasses (those enriched in K_2O and P_2O_5) of Melson et al. (1976), which have affinities with seamount and ocean-island alkalic olivine basalts. Their normative compositions (Table 2) are distinctly tholeiitic. Marsh et al. (this volume) describe these lavas as comparable to transitional or T-type mid-ocean-ridge basalts.

Some indication of the range of compositions found in the Costa Rica Rift sites is shown in a ternary plot of normative olivine, diopside, and silica (Fig. 3), which is based on the computational technique of Walker et al. (1979). If the two slightly more alkalic groups E and M (which plot farther from the silica apex than the other samples by virtue of their alkali contents) are disregarded, most of the glass groups form a closely-spaced cluster somewhat above the experimentally determined cotectic boundary between olivine and diopside. Similarly,

they plot near the cotectic boundary on a ternary plot of normative olivine, silica, and plagioclase (Fig. 4) that is also based on the procedure of Walker et al. (1979). This is consistent with the occurrence in many of the rock samples of phenocrysts of olivine, plagioclase, and clinopyroxene and the experimental determination of Aultio and Rhodes (this volume) that sparsely phyric Costa Rica Rift basalts from these sites are multiply saturated with all of these mineral phases at the 1-atm. liquidus.

Small but distinct differences in glass group compositions can be seen in Figure 3 between the four spinel-assemblage groups (B, I, J, and P) and the seven clinopyroxene-assemblage groups (C, D, F, G, H, and O). The differences are most pronounced for Groups I and J, which plot closer to the olivine–diopside side of the ternary diagram in Figure 3 than any of the other glass groups. These groups tend to weight the averages for spinel-assemblage glass groups in Table 3 to higher Mg/

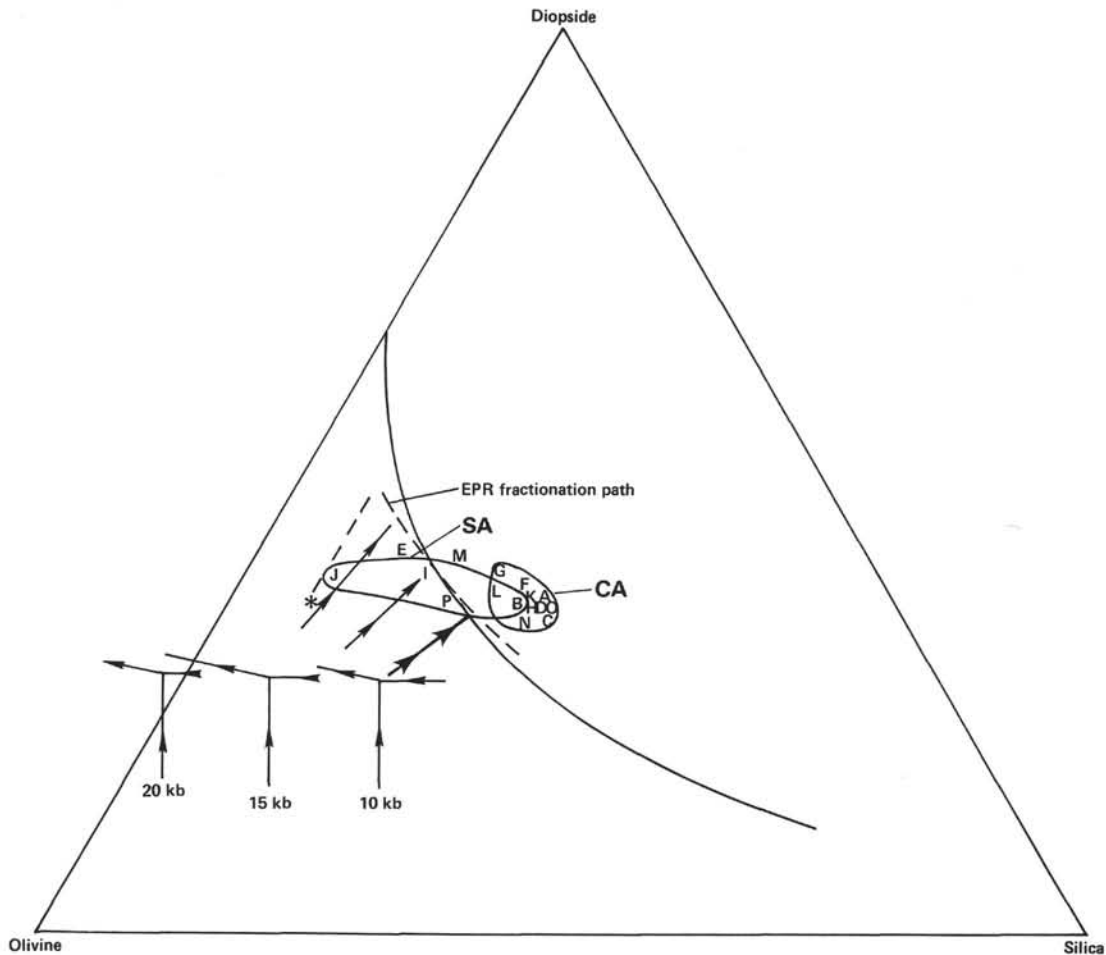


Figure 3. Glass group compositions from Table 2 plotted in a ternary diagram of normative olivine, diopside, and silica, calculated using the procedure of Walker et al. (1979). Field SA encloses spinel-assemblage glass groups; field CA encloses clinopyroxene-assemblage glass groups. The experimentally determined 1-atm. cotectic boundary of Walker et al. (1979) is shown, as are higher pressure (10, 15, and 20 kbar) phase boundaries of Stolper (1980). The dashed line represents the East Pacific Rise (9°N) fractionation trend calculated from glass data in Natland and Melson (1980). The asterisk is their proposed least fractionated parental glass composition for that fractionation trend. The double arrows are suggested low-pressure olivine-controlled fractionation trends for abyssal tholeiites originating at a range of pressures (10–15 kbars) and ascending to crustal levels. The bold double arrow is a possible such pathway leading to clinopyroxene assemblage lavas.

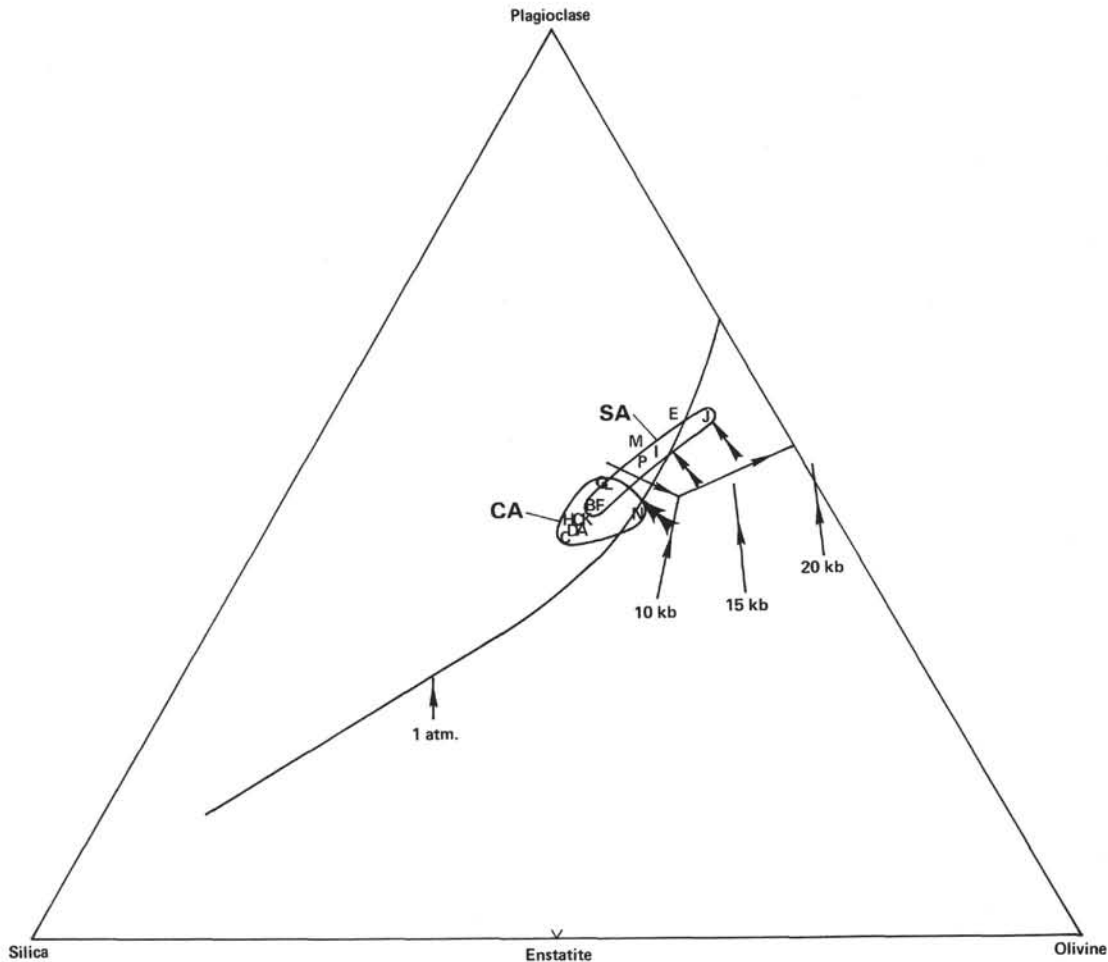


Figure 4. Normative olivine-plagioclase-silica ternary diagram for glass groups plotted using the procedure of Walker et al. (1979). 1-atm. and high-pressure phase boundaries, fields, notation, and double arrows are as in Figure 3.

Mg + Fe²⁺, lower TiO₂, and lower CaO/Al₂O₃. The two groups with only rare, nondiagnostic phenocrysts, A and N, and the mixed group, K, are geochemically similar to the clinopyroxene-assembly glass groups.

GROUP EQUIVALENCES

The close clustering of most of the glass groups on Figure 3 is one indication of the chemical uniformity of most of the basalts of the Costa Rica Rift sites. Melson et al. (1976) and Natland and Melson (1980) used a sorting procedure similar to that described above in which group averages were compared with each other; they were judged to be equivalent if they differed from each other for each oxide by less than half the tolerances described above. This criterion was taken to be a conservative gauge of the tendency of ridge crests to erupt lavas of the same composition from time to time or place to place. Most of the group equivalences in the earlier studies occurred in FETI glasses from faster spreading ridges. In the case of a single deep hole, such as Hole 504B, equivalences can be taken to represent the tendency to return to the same compositions within a short period of time (within, say, 10⁴ to 10⁶ yr.) at one point on a spreading center.

Despite the lack of FETI glasses, several equivalences exist in Hole 504B, and there are a number of comparisons for which equivalence fails by only small excesses above the stated tolerances in one or two oxides. The equivalences are B = G, C = H, and D = K = O. Very near equivalences are L ≈ G and B ≈ D. This is a remarkable number of equivalences or near equivalences in such a small set of glass groups. Most of the equivalences occur among the clinopyroxene-assembly groups (Table 3). One equivalence (B = G) and the near equivalence B ≈ D, however, occur between spinel-assembly and clinopyroxene-assembly lavas. Partly because of this, samples from Groups B and G were selected for detailed mineralogical study, described later in this chapter.

Crystallization differentiation is perhaps the most important cause of chemical variations among abyssal tholeiites. A number of oxides are particularly sensitive to fractionation of olivine, plagioclase and clinopyroxene, namely those that are more or less systematically excluded from the crystal lattices of those minerals. The oxides that vary particularly strongly as a result of crystal fractionation are K₂O, P₂O₅, Na₂O, and TiO₂ (e.g., Kay et al., 1970; Clague and Bunch, 1976). Of these,

relative to its typical abundance, TiO_2 is most precisely determinable with the microprobe. If we consider this oxide as diagnostic of the degree of fractionation of the glass groups, a remarkable feature of the Hole 504B glass groups emerges: there is virtually no variation due to crystal fractionation among them. The following groups have equivalent TiO_2 contents, all falling within the small tolerance of 0.15% (which is based on analytical precision and comparison to variation among other homogeneous glass groups): B, C, D, G, K, L, O, and P. These include both spinel- and clinopyroxene-assemblage lavas. Groups A, H, and N (two sparsely phyrlic, the other clinopyroxene phyrlic) fall barely outside this grouping on the high side, and Group I (spinel-assemblage) falls outside on the low side. Groups F (clinopyroxene assemblage) and J (spinel assemblage) have distinctively lower TiO_2 , with Group J the least evolved of all, plotting well away from the cotectic boundary on Figure 3 and toward the olivine apex. Groups E and M are excluded from this comparison because of their significantly higher contents of alkalis and P_2O_5 .

An important conclusion of this work, then, is that despite multiple saturation with olivine, plagioclase, and Cr-spinel or clinopyroxene (and thus having somewhat evolved or fractionated basaltic compositions), the glass groups show almost no variation that can be attributed to the extent of crystal fractionation. Moreover, although the spinel-assemblage glass groups tend to be slightly more magnesian than the clinopyroxene-assemblage groups, not all of them are, and in fact glass groups with identical compositions can have either phenocryst assemblage. Indeed, although there is a small range in $\text{Mg}/\text{Mg} + \text{Fe}^{2+}$, there are virtually no differences in normative $\text{An}/\text{An} + \text{Ab}$ among the glass groups (Table 3; Fig. 5), which might be expected if they represented a fractionation sequence.

How much of the variation in liquid compositions (i.e., glasses) might be related by crystallization fractionation? In many respects, possible parental compositions might be the low- TiO_2 spinel-assemblage groups, Groups I and J. However, these two groups have Na_2O as high or higher than almost all the remaining groups (again excluding E and M from comparison). K_2O and P_2O_5 cannot be determined with sufficient precision at the low abundances present in all of the glass groups to detect differences in the degree of fractionation. The only other available index of differentiation, Na_2O , suggests that Groups I and J are not precisely representative of magmas parental to the remaining glass groups. Differences between these two groups and the others occur in SiO_2 (Groups I and J are lower), Al_2O_3 (higher), CaO (slightly higher), and FeO^* (lower, especially J). These contrasts are quite typical between less- and more-fractionated abyssal tholeiites (cf. Clague and Bunch, 1976). However, differences among these oxides are too slight in the remaining glass groups (apart from Groups E and M) to show patterns of this type.

Group F has low TiO_2 and Na_2O but has clinopyroxene-assemblage phenocrysts, low Al_2O_3 , high SiO_2 , and not very high $\text{Mg}/\text{Mg} + \text{Fe}^{2+}$, suggesting that overall it is a fractionated (not parental) composition. The

alkali-enriched groups (Groups E and M) have lower CaO when compared at comparable values of MgO than the other groups (a characteristic that is manifested also as lower $\text{CaO}/\text{Al}_2\text{O}_3$ in Table 3). The lower CaO is also a feature of glasses from transitional and alkalic olivine basalts of seamounts near the crest of the East Pacific Rise at $8^\circ 30' \text{N}$ (Natland and Melson, 1980) and may reflect melting at somewhat greater depths in the mantle; the high-pressure phase boundaries and alternative fractionation paths on Figure 3 support this hypothesis.

MINERAL DATA

We obtained 194 separate mineral analyses from 45 samples from Sites 501, 504, and 505, although a number of the mineral analyses are from different parts of the same grains (core, rim, etc.). There are, all together, 17 spot analyses of spinels, 19 of olivines, 116 of plagioclases, and 43 of clinopyroxenes. We also obtained the compositions of 6 glass inclusions in plagioclase megacrysts from one sample.

Of the mineral analyses, 114 make up the mineral reconnaissance and 80 the detailed sample study. The reconnaissance includes 9 olivine analyses, 84 plagioclase analyses, and 21 clinopyroxene analyses. The detailed sample study includes all 17 spinel analyses, 10 olivine analyses, 32 plagioclase analyses, 22 clinopyroxene analyses, and the 6 glass inclusion analyses. For reference, we have compiled a mineral data index (Table 4) listing sample identification and location information and the table numbers where information on each sample may be found. Table 4 also suggests the general distribution of mineral analyses within the various holes (see also Fig. 2) and shows the glass groups for the different samples. Mineral data were obtained on samples from intervals corresponding to spinel-assemblage Groups B, J, and P, clinopyroxene-assemblage Groups D, G, H, and O, aphyric-sparsely phyrlic Groups A and N, mixed-assemblage Group K, and less-depleted Group M. No mineral data were obtained on samples from Groups C, E, F, I, or L.

The olivine data are sparse, mainly because olivine is almost completely altered in samples from Holes 501, 504A, and 504B. However, analyses of olivine were obtained from samples having both of the principal phenocryst assemblages, including the least evolved spinel-assemblage group, Group J. Spinel data are equally sparse, partly because spinel occurs in rocks corresponding to only four glass groups and partly because it is rare even in those samples (1–5 grains per sample). Furuta and Tokuyama (this volume) report numerous Cr-spinel data in phyrlic samples from Holes 505A and 505B (glass group P). Our spinel data are from a Group J sample (the least fractionated group) and from a Group B sample.

We have obtained the greatest number of analyses for plagioclase, which is the most abundant phenocryst phase and the most readily analyzed mineral in the groundmass. The preponderance of plagioclase analyses in the reconnaissance data in part prompted the detailed sample study, which concentrated more heavily on spinel, olivine, and clinopyroxene.

Table 4. Electron microprobe mineral analysis index.

Leg	Piece Number	Sample Number (interval in cm)	Glass Group	Phenocryst Assemblage	Table Containing Data				
					Spinel	Olivine	Plagioclase	Clinopyroxene	
68	238	501-15-3, 63-65 ^a	B	Spinel	9	10	11		
69	48	504A-6-3, 12-15	A	Aphyric-sparsely phytic			6		
	65	7-1, 50-53	A	Aphyric-sparsely phytic			6		
	466	504B-7-2, 98-102	B	Spinel			6		
	476	7-3, 27-30	B	Spinel			6		
	791	13-3, 66-69	B	Spinel			6		
	956	16-1, 4-7	D	Clinopyroxene			6		
	1254	21-4, 120-124	G	Clinopyroxene			6	7	
	1326	23-1, 115-116 ^a	G	Clinopyroxene		10	11	12	
	1361	24-2, 58-62 ^a	G	Clinopyroxene			11	12	
	1378	24-3, 30-33	G	Clinopyroxene			6		
	1558	28-5, 19-22	H	Clinopyroxene				7	
	1560	29-1, 11-14	H	Clinopyroxene			6		
	70	207	504B-33-2, 48-52	n.d. ^b	n.d.			6	7
		287	35-2, 24-26 ^a	J	Spinel	9	10	11	
		289	35-2, 53-56	J	Spinel				7
		314	36-2, 121-123	n.d.	n.d.			6	7
342		37-1, 15-17	K	Mixed			6		
383		37-2, 118-120	K	Mixed			6	7	
390		37-3, 10-13	K	Mixed				7	
397		37-3, 49-52	K	Mixed			6		
496		39-2, 144-147	K	Mixed		5			
507		40-1, 37-39	K	Mixed		5	6	7	
533		40-2, 89-91	K	Mixed			6		
548		40-3, 56-58	K	Mixed		5			
594		41-1, 118-120	K	Mixed		5		7	
605		41-2, 75-77	K	Mixed			6		
804		47-1, 7-11	K	Mixed			6	7	
922		49-1, 51-54	K	Mixed			6		
1061		54-1, 31-34	M	Less depleted			6		
1099		56-1, 2-4	M	Less depleted			6	7	
1189		58-1, 9-13	n.d.	n.d.			6	7	
1192		58-1, 35-38	n.d.	n.d.			6		
1315		61-3, 1-4	N	Aphyric-sparsely phytic			6		
1392		63-4, 7-10	O	Clinopyroxene			6		
1398		63-4, 65-69	O	Clinopyroxene			6		
1400	63-4, 90-91	O	Clinopyroxene		5				
1450	64-3, 87-92	O	Clinopyroxene			6	7		
1519	66-2, 106-109	n.d.	n.d.			6	7		
1548	69-1, 106-112	n.d.	n.d.			6			
69	93	505-26-1, 3-5	n.d.	n.d.			6		
69	107	505B-2-1, 25-28	P	Spinel			6	7	
	142	2-2, 100-103	P	Spinel			6		
	175	3-1, 109-112	P	Spinel			6		
	199	5-1, 50-60	P	Spinel			6		

^a Detailed study sample.^b No glass data.

The clinopyroxene data are principally from clinopyroxene-assemblage lavas, mainly Groups G and H. There is a great diversity of clinopyroxene compositions that depends on whether the clinopyroxene appears as phenocrysts, xenocrysts, or groundmass minerals. Only groundmass clinopyroxenes occur in spinel-assemblage lavas, where they are intergrown with plagioclase and titanomagnetite, the last mineral to crystallize. We obtained no data on titanomagnetites (but see chapters by Furuta, and Pertsev and Boronikhin in this volume).

MINERAL COMPOSITIONS

The reconnaissance mineral data are presented in Tables 5, 6, and 7 (olivines, plagioclases, and clinopyroxenes, respectively), along with structural formulae and general compositions (Fo, An, and WoEnFs). The glass group that corresponds to each analysis is also given.

Analytical procedures for the reconnaissance data are given in chapters in this volume by Adamson and by Laverne.

The distribution of the plagioclase compositions is summarized in Table 8. Tables 9 to 12 give the results of mineral analyses and structural formulae from the four samples selected for detailed study; data for spinels are

Table 5. Reconnaissance electron microprobe analyses of olivines, Holes 504B (Leg 70) and 505B (Leg 69).

	Hole 504B				Hole 505B				
	70/496	70/507	70/548	Leg/Piece 70/594 70/1400	69/142	69/175	69/175	69/175	
SiO ₂	40.50	40.04	40.49	40.01 40.71	41.30	40.59	40.48	39.80	
FeO ^a	12.20	12.22	13.18	12.81 12.27	12.39	11.88	12.31	10.62	
MnO	0.16	0.30	0.17	0.23 0.21	0.20	0.18	0.16	0.16	
MgO	46.89	47.40	46.49	47.38 47.12	46.90	47.25	47.29	48.09	
CaO	0.34	0.27	0.32	0.33 0.30	0.37	0.33	0.33	0.36	
NiO	0.12	0.13	0.15	0.19 0.08	—	—	—	—	
Cr ₂ O ₃	0.02	0.04	0.08	0.01 0.06	—	—	—	—	
	100.24	100.40	100.89	100.95 100.75	101.16	100.23	100.57	99.03	
Structural Formulae ^a									
Si	1.007	0.990	0.999	0.987 1.002	1.010	1.002	0.998	0.998	
Mn	0.003	0.006	0.004	0.005 0.004	0.004	0.004	0.003	0.003	
Ni	0.003	0.003	0.003	0.004 0.002	—	—	—	—	
Cr	0.001	0.001	0.002	0.003 0.001	—	—	—	—	
Fe	0.252	0.253	0.272	0.264 0.252	0.254	0.245	0.254	0.220	
Mg	1.727	1.748	1.710	1.742 1.728	1.712	1.738	1.738	1.778	
Ca	0.009	0.007	0.009	0.009 0.008	0.010	0.009	0.009	0.010	
[Y] ^b	1.995	2.015	2.000	2.027 1.995	1.980	1.996	2.004	2.011	
Composition Glass Group Analyst ^b	Fog7.0 K L	Fog7.0 K L	Fog6.0 K L	Fog6.5 K L	Fog7.0 O L	Fog7.1 P A	Fog7.6 P A	Fog7.3 P A	Fog9.0 P A

^a Structural formulae calculated on the basis of 4 oxygens.^b A, Adamson; L, Laverne.

given in Table 9, olivines in Table 10, plagioclases in Table 11, and clinopyroxenes in Table 12. Glass inclusion compositions are presented in Table 13. The analytical procedures used to acquire these data are summarized in the appendix.

Table 6. Reconnaissance electron microprobe analyses of plagioclases, Holes 504B, 504A, 505B, and 505.

Hole 504B																	
	Leg/Piece																
	69/466	69/466	69/476	69/476	69/791	69/791	69/791 ^d	69/791 ^d	69/956 ^d	69/956	69/956	69/956	69/956 ^d	69/956	69/956	69/956	69/1254 ^d
SiO ₂	47.52	47.05	47.60	45.96	48.37	49.18	53.07	53.12	45.43	46.92	47.13	46.86	52.45	46.92	48.74	45.46	50.26
Al ₂ O ₃	34.32	32.96	32.97	33.20	32.95	31.82	31.04	27.03	30.60	32.49	33.37	33.13	28.43	33.23	33.02	32.01	30.65
FeO*	0.32	0.45	0.44	0.37	0.39	0.69	1.10	1.72	0.35	0.45	0.40	0.43	1.60	0.49	0.47	0.74	1.05
MgO	0.00	0.00	0.00	0.00	0.00	0.00	0.29	1.21	0.00	0.22	0.00	0.00	0.23	0.00	0.00	0.21	0.55
CaO	18.27	17.50	17.96	18.24	17.45	16.54	15.15	13.17	16.73	17.52	17.81	17.82	13.19	18.06	17.77	17.70	15.61
Na ₂ O	0.86	1.34	1.15	0.86	1.21	1.94	2.90	3.43	1.55	1.09	1.14	1.15	3.98	1.41	1.43	1.26	2.57
K ₂ O	0.00	0.00	0.00	0.00	0.00	0.00	0.00	0.00	0.00	0.00	0.00	0.00	0.00	0.00	0.00	0.00	0.00
	101.29	99.30	100.12	98.63	100.37	100.18	103.54	99.76	94.66	98.69	98.85	99.38	99.89	100.12	101.41	97.37	100.70
Structural Formulae ^a																	
Si	8.621	8.712	8.742	8.585	8.834	9.002	9.361	9.716	8.826	8.738	8.767	8.667	9.599	8.642	8.828	8.626	9.156
Al	7.339	7.195	7.139	7.311	7.096	6.868	6.455	5.828	7.010	7.134	7.098	7.224	6.134	7.216	7.048	7.161	6.584
Fe	0.048	0.069	0.068	0.057	0.060	0.106	0.162	0.262	0.058	0.069	0.062	0.066	0.245	0.075	0.072	0.117	0.160
Mg	0.000	0.000	0.000	0.000	0.000	0.000	0.076	0.329	0.000	0.061	0.000	0.000	0.063	0.000	0.000	0.061	0.150
Ca	3.551	3.473	3.535	3.651	3.414	3.244	2.863	2.581	3.483	3.496	3.551	3.531	2.587	3.564	3.450	3.599	3.047
Na	0.301	0.481	0.408	0.310	0.427	0.687	0.992	1.215	0.585	0.392	0.412	0.413	1.413	0.505	0.501	0.462	0.909
K	0.000	0.000	0.000	0.000	0.000	0.000	0.000	0.021	0.000	0.000	0.000	0.000	0.000	0.000	0.000	0.000	0.000
Composition	Ang2.2	Ang7.8	Ang9.7	Ang2.2	Ang8.8	Ang2.5	Ang7.4	Ang8.0	Ang5.6	Ang9.9	Ang9.6	Ang9.5	Ang6.7	Ang7.6	Ang7.3	Ang8.6	Ang7.0
Crystal Type ^b	C	C	C	C	C	R	R	M	C	C	C	C	M	C	C	R	R
Glass Group	B	B	B	B	B	B	B	B	C	D	D	D	D	D	D	D	G
Analyst ^c	A	A	A	A	A	A	A	A	A	A	A	A	A	A	A	A	A

^a Structural formulae calculated on the basis of 32 oxygens.
^b C, phenocryst (core); R, phenocryst (rim); M, microlite.
^c A, Adamson; L, Laverne.
^d Analysis is somewhat suspect; see text.

Table 6. (Continued).

Hole 504B																
	Leg/Piece															
	70/605	70/804 ^d	70/804 ^d	70/804	70/922	70/922	70/922	70/922	70/922	70/1061	70/1061 ^d	70/1061	70/1099	70/1099	70/1099	70/1189
SiO ₂	45.76	44.82	52.29	45.64	45.96	49.72	46.47	46.91	46.68	51.13	50.15	52.92	56.10	51.67	52.52	52.76
Al ₂ O ₃	33.20	32.78	22.87	33.01	32.43	29.45	32.62	32.45	28.88	21.53	28.22	27.06	30.00	30.25	29.38	
FeO	0.26	0.33	4.42	0.39	0.32	0.82	0.38	0.38	0.34	0.99	4.06	0.93	0.99	0.53	0.74	0.79
MgO	0.23	0.00	1.04	0.00	0.00	0.00	0.00	0.00	0.27	4.51	0.33	0.10	0.23	0.31	0.19	
CaO	18.14	17.99	11.66	18.07	17.61	14.68	17.62	17.23	17.96	13.11	14.89	12.52	8.71	11.86	12.30	12.21
Na ₂ O	1.31	0.92	4.18	0.96	1.05	2.82	1.23	1.34	1.19	3.65	2.88	4.62	5.91	3.99	3.51	4.30
K ₂ O	0.00	0.00	0.00	0.00	0.00	0.00	0.00	0.00	0.00	0.00	0.00	0.00	0.10	0.00	0.03	0.00
	98.89	96.84	96.47	98.08	97.37	97.07	98.32	98.30	98.77	97.97	98.02	99.54	98.98	98.28	99.66	99.62
Structural Formulae ^a																
Si	8.538	8.535	10.003	8.578	8.580	9.341	8.696	8.764	8.700	9.508	9.570	9.682	10.190	9.515	9.537	9.610
Al	7.304	7.359	5.158	7.312	7.221	6.522	7.196	7.148	7.165	6.333	4.845	6.087	5.796	6.514	6.477	6.310
Fe	0.040	0.052	0.707	0.062	0.050	0.129	0.059	0.059	0.053	0.154	0.648	0.142	0.150	0.082	0.112	0.120
Mg	0.064	0.000	0.296	0.000	0.000	0.000	0.000	0.000	0.060	1.282	0.091	0.027	0.063	0.084	0.052	
Ca	3.626	3.671	2.389	3.639	3.564	2.955	3.532	3.449	3.586	2.612	3.045	2.454	1.696	2.341	2.394	2.383
Na	0.473	0.338	1.552	0.351	0.385	0.831	0.447	0.484	0.428	1.317	1.067	1.640	2.082	1.425	1.236	1.519
K	0.000	0.000	0.000	0.000	0.000	0.000	0.000	0.000	0.000	0.000	0.000	0.000	0.000	0.000	0.007	0.000
Composition	Ang8.5	Ang1.6	Ang6.6	Ang1.2	Ang0.3	Ang7.8	Ang8.8	Ang7.7	Ang9.3	Ang6.5	Ang7.1	Ang5.9	Ang4.9	Ang2.2	Ang6.0	Ang1.1
Crystal Type ^b	C	C	R	C	C	M	C	C	C	M	R	M	M	M	M	M
Glass Group	K	K	K	K	K	K	K	K	K	M	M	M	M	M	M	M
Analyst ^c	A	A	A	A	A	A	A	A	A	A	A	A	L	L	L	L

Table 6. (Continued).

Hole 505B										Hole 505					
	Leg/Piece														
	69/107	69/107	69/142	69/142	69/142 ^d	69/142 ^d	69/142	69/142	69/175 ^d	69/175 ^d	69/199	69/93	69/93	69/93	69/93
SiO ₂	50.33	50.34	45.62	45.17	51.20	55.81	45.88	46.58	46.75	45.66	46.84	47.51	48.44	48.58	50.32
Al ₂ O ₃	30.74	31.05	34.30	34.32	21.33	26.70	34.12	32.89	31.27	32.35	33.12	32.78	32.41	31.55	31.13
FeO*	0.54	0.44	0.22	0.28	6.44	1.60	0.26	0.37	0.42	0.32	0.41	0.40	0.34	0.32	0.50
MgO	0.00	0.00	0.00	0.00	3.24	0.00	0.00	0.00	0.00	0.00	0.00	0.00	0.00	0.00	0.00
CaO	15.47	15.81	18.70	19.01	14.93	11.38	18.81	17.56	16.54	17.43	17.70	17.58	17.36	16.44	15.32
Na ₂ O	2.28	2.45	0.76	0.83	2.43	4.85	0.95	1.34	1.60	1.15	1.19	1.27	1.60	1.87	2.45
K ₂ O	0.00	0.00	0.00	0.00	0.15	0.00	0.00	0.00	0.00	0.00	0.00	0.00	0.00	0.00	0.00
	99.35	100.09	99.60	99.61	99.68	100.48	100.01	98.71	96.59	96.92	99.26	99.54	100.15	98.76	99.85
Structural Formulae															
Si	9.242	9.191	8.446	8.382	9.664	10.055	8.468	8.682	8.883	8.667	8.679	8.768	8.876	9.004	9.197
Al	6.656	6.684	7.485	7.508	4.746	5.672	7.424	7.221	7.005	7.239	7.234	7.132	7.002	6.894	6.706
Fe	0.083	0.067	0.034	0.044	1.017	0.241	0.041	0.057	0.067	0.051	0.063	0.062	0.052	0.051	0.076
Mg	0.000	0.000	0.000	0.000	0.911	0.000	0.000	0.000	0.000	0.000	0.000	0.000	0.000	0.000	0.000
Ca	3.043	3.093	3.710	3.780	3.020	2.198	3.719	3.506	3.367	3.545	3.514	3.476	3.408	3.265	3.001
Na	0.810	0.867	0.274	0.299	0.890	1.693	0.337	0.484	0.589	0.424	0.428	0.456	0.570	0.672	0.869
K	0.000	0.000	0.000	0.000	0.020	0.000	0.000	0.000	0.000	0.000	0.000	0.000	0.000	0.000	0.000
Composition	Ang7.0	Ang7.8	Ang3.1	Ang2.7	Ang7.2	Ang5.5	Ang1.7	Ang7.9	Ang5.1	Ang9.3	Ang9.1	Ang8.4	Ang5.7	Ang2.9	Ang7.5
Crystal Type ^b	C	C	C	C	R	M	C	C	C	C	C	C	C	C	M
Glass Group	P	P	P	P	P	P	P	P	P	P	P	n.a.	n.a.	n.a.	n.a.
Analyst ^c	A	A	A	A	A	A	A	A	A	A	A	A	A	A	A

Table 6. (Continued).

Hole 504B																	
Leg/Piece																	
69/1254	69/1254	69/1378	69/1560 ^d	70/207 ^d	70/207 ^d	70/314 ^d	70/314 ^d	70/314	70/342	70/383	70/383	70/383 ^d	70/397	70/507	70/507	70/533	70/533
46.63	48.08	45.32	49.40	52.06	54.47	52.73	54.99	48.84	49.11	46.77	52.15	50.59	48.07	53.17	51.50	47.28	47.18
33.30	32.56	32.68	28.94	29.40	27.52	27.98	26.77	30.18	30.46	32.50	29.12	28.65	33.56	28.15	30.30	31.88	32.24
0.46	0.30	0.36	2.24	0.69	1.12	1.26	1.27	0.55	0.55	0.53	1.08	1.05	0.25	0.80	0.78	0.34	0.40
0.00	0.00	0.00	0.75	0.34	0.16	0.00	0.00	0.00	0.00	0.00	0.00	0.81	0.19	0.13	0.25	0.23	0.00
18.01	16.97	17.87	12.52	13.21	11.55	12.52	10.87	15.44	15.38	17.38	13.41	14.76	16.94	11.73	14.70	16.49	17.13
1.13	1.53	1.10	2.46	3.62	4.91	4.29	5.29	2.64	2.15	1.40	3.55	2.76	1.57	4.71	3.43	1.84	1.46
0.00	0.00	0.00	0.00	0.13	0.01	0.00	0.00	0.00	0.00	0.00	0.00	0.00	0.00	0.01	0.00	0.00	0.00
99.53	99.42	97.34	98.28	99.45	99.74	98.78	99.19	97.65	97.65	98.58	99.30	98.64	100.65	98.69	100.95	98.06	98.42
Structural Formulae ^a																	
8.629	8.852	8.584	9.226	9.527	9.908	9.722	10.035	9.161	9.184	8.723	9.563	9.389	8.757	9.771	9.327	8.839	8.805
7.264	7.065	7.298	6.372	6.344	5.902	6.081	5.759	6.673	6.715	7.146	6.296	6.268	7.208	6.100	6.470	7.025	7.093
0.071	0.047	0.056	0.350	0.106	0.170	0.194	0.194	0.086	0.086	0.082	0.165	0.163	0.038	0.123	0.118	0.053	0.063
0.000	0.000	0.000	0.209	0.093	0.043	0.000	0.000	0.000	0.000	0.000	0.000	0.224	0.052	0.036	0.067	0.064	0.000
3.572	3.348	3.627	2.903	2.591	2.251	2.473	2.125	3.103	3.082	3.473	2.635	2.934	3.307	2.310	2.853	3.304	3.425
0.406	0.544	0.404	0.890	1.285	1.732	1.534	1.872	0.960	0.781	0.507	1.261	1.001	0.555	1.679	1.205	0.668	0.473
0.000	0.000	0.000	0.000	0.000	0.000	0.000	0.000	0.000	0.000	0.000	0.000	0.000	0.000	0.002	0.000	0.000	0.000
An _{99.8}	An _{86.0}	An _{90.0}	An _{76.5}	An _{66.8}	An _{56.5}	An _{61.7}	An _{53.2}	An _{76.4}	An _{79.8}	An _{87.3}	An _{67.6}	An _{74.6}	An _{85.6}	An _{57.9}	An _{70.3}	An _{83.2}	An _{87.9}
C	C	C	M	M	M	M	M	C	R	C	R	R	C	M	M	C	C
G	G	G	H	I	I	J	J	J	K	K	K	K	K	K	K	K	K
A	A	A	A	L	L	A	A	A	A	A	A	A	L	L	L	A	A

Table 6. (Continued).

Hole 504B													Hole 504A		Hole 505B		
Leg/Piece																	
70/1192	70/1315	70/1315	70/1315	70/1315	70/1392	70/1398	70/1450	70/1450	70/1519	70/1519	70/1548	70/1548	70/1548	69/48	69/65	69/107	69/107
48.99	45.49	46.65	46.80	46.31	51.21	44.86	51.19	50.20	51.51	49.48	52.05	49.47	46.66	54.38	47.18	55.90	50.79
31.30	33.25	32.49	32.66	33.24	30.15	33.65	30.80	30.39	29.18	30.65	30.41	25.04	32.32	29.18	32.54	25.48	28.82
0.49	0.49	0.30	0.50	0.40	0.67	0.35	0.58	0.43	0.95	0.55	0.98	2.29	0.40	1.46	0.43	1.41	0.93
0.28	0.00	0.00	0.00	0.00	0.24	0.00	0.33	0.33	0.24	0.22	0.34	3.43	0.00	0.00	0.00	0.00	0.26
15.80	18.29	17.37	17.92	17.97	13.62	18.59	13.95	13.71	13.90	15.39	14.73	14.71	17.27	12.30	17.53	9.98	14.18
2.13	0.99	1.19	0.95	0.98	3.27	0.60	3.09	2.98	3.40	2.86	3.12	2.15	1.57	4.09	1.32	5.71	3.20
0.00	0.00	0.00	0.00	0.00	0.00	0.00	0.01	0.00	0.00	0.00	0.00	0.00	0.00	0.00	0.00	0.00	0.00
99.05	98.50	98.00	98.84	98.90	99.17	98.04	99.95	98.03	99.18	99.16	101.62	97.09	98.22	102.10	99.01	98.47	98.17
Structural Formulae ^a																	
9.051	8.517	8.741	8.712	8.619	9.395	8.444	9.319	9.308	9.475	9.141	9.357	9.388	8.740	9.696	8.763	10.254	9.449
6.817	7.340	7.178	7.167	7.294	6.522	7.466	6.611	6.644	6.327	6.676	6.446	5.604	7.138	6.134	7.122	5.509	6.321
0.084	0.076	0.048	0.078	0.061	0.103	0.054	0.088	0.067	0.146	0.086	0.148	0.364	0.063	0.217	0.066	0.216	0.145
0.078	0.000	0.000	0.000	0.000	0.066	0.000	0.090	0.091	0.066	0.061	0.090	0.970	0.000	0.000	0.000	0.000	0.071
3.128	3.669	3.487	3.574	3.583	2.678	3.749	2.721	2.724	2.740	3.047	2.836	2.991	3.466	2.483	3.488	1.961	2.827
0.763	0.359	0.432	0.344	0.353	1.163	0.220	1.091	1.072	1.214	1.023	1.087	0.792	0.570	1.414	0.474	2.030	1.153
0.000	0.000	0.000	0.000	0.000	0.000	0.000	0.002	0.000	0.000	0.000	0.000	0.000	0.000	0.000	0.000	0.000	0.000
An _{80.4}	An _{91.1}	An _{89.0}	An _{91.2}	An _{91.0}	An _{69.7}	An _{94.5}	An _{71.4}	An _{71.8}	An _{61.3}	An _{74.9}	An _{72.3}	An _{79.1}	An _{85.9}	An _{63.7}	An _{88.0}	An _{49.1}	An _{71.0}
C	C	C	C	C	M	C	M	M	M	M	M	C	C	M	C	M	R
M	N	N	N	N	N	N	N	N	O	O	n.a.	n.a.	n.a.	A?	A?	P	P
A	A	A	A	A	L	A	L	L	A	A	A	A	A	A	A	A	A

Olivines have only a limited range of composition (Table 5, Fo₈₆₋₈₉; Table 10, Fo_{85.2-89.8}). There is a slight tendency for olivines in spinel-assembly lavas to be more forsteritic than those in clinopyroxene-assembly lavas, but this distinction would probably disappear if a larger number of fresh olivines could be analyzed. Individual samples have very similar olivine compositions (± 1 mol% Fo) regardless of the grain size of euhedral phenocrysts and microphenocrysts. Groundmass olivines with swallowtail and hopper crystal morphologies were not analyzed because they were usually altered.

Plagioclase compositions include analyses from phenocryst and megacryst cores, from rims of these minerals, and from groundmass microlites. There are slight differences in the way the reconnaissance plagioclase compositions were obtained, as evidenced by the way the data are reported in Table 6. The principal differences are in the minor oxide data, with FeO* reported higher and MgO considerably lower (not detected in

most samples) by Adamson than by Laverne. Several of the analyses have low totals (95–98%), and a few analyses of microlites obviously overlapped other minerals or mesostasis or were uncorrected for iron excitation in nearby minerals, since they tended to have unusually high FeO* and MgO. These somewhat suspect analyses are identified in Table 6 but are included because ratios of principal cations (Ca, Na, K) to each other are probably not influenced by these effects.

The principal features of the plagioclase data are (1) the exceptionally calcic compositions of many of the phenocryst cores (An₈₆₋₉₄), (2) the generally more sodic compositions of phenocryst rims (An₆₁₋₈₇), and (3) the still more sodic range of compositions (An₄₅₋₇₈) for microlites (Table 6). There is no obvious difference in the An content of phenocryst core compositions that distinguishes spinel-assembly from clinopyroxene-assembly plagioclases. Rim compositions depend greatly on the crystallinity of the rock; they tend to be more so-

Table 7. Reconnaissance electron microprobe analyses of clinopyroxenes.

Hole 504B										
Leg/Piece										
	69/1254	69/1558	69/1558	69/1558	69/1558	70/207	70/289	70/314	70/383	70/390
SiO ₂	52.11	52.70	52.41	53.04	50.56	50.93	53.17	52.06	46.42	51.22
TiO ₂	0.52	0.16	0.24	0.23	0.21	0.78	0.23	0.32	0.77	0.61
Al ₂ O ₃	5.15	2.48	2.70	2.04	2.07	4.68	2.29	2.61	1.55	4.81
FeO*	8.01	4.08	4.74	4.69	4.93	5.63	5.26	6.41	24.31	7.13
MgO	19.00	18.48	17.29	18.08	17.37	17.02	18.70	17.18	9.07	18.24
CaO	14.81	20.44	20.47	20.28	18.97	19.02	18.88	18.61	13.34	15.83
Na ₂ O ^a	—	—	—	—	—	0.22	0.14	—	—	0.21
K ₂ O	—	—	—	—	—	0.00	0.01	—	—	0.07
MnO	0.21	0.14	—	—	—	0.22	0.05	0.12	0.38	0.18
NiO	—	—	—	—	—	0.10	0.03	—	—	0.00
Cr ₂ O ₃	0.33	1.06	0.75	0.71	0.74	0.18	0.53	0.30	—	0.38
	100.14	99.54	98.60	99.07	94.85	98.78	99.29	97.61	95.84	98.68
Structural Formulae ^b										
Si	1.888	1.925	1.935	1.947	1.941	1.875	1.944	1.945	1.918	1.882
Al	0.112	0.075	0.065	0.053	0.059	0.125	0.056	0.055	0.076	0.118
Al	0.108	0.032	0.053	0.035	0.035	0.078	0.043	0.060	—	0.091
Ti	0.014	0.004	0.007	0.006	0.006	0.022	0.006	0.009	0.024	0.017
Cr	0.010	0.030	0.022	0.021	0.022	0.005	0.015	0.009	—	0.011
Ni	—	—	—	—	—	0.003	0.001	—	—	0.000
Fe	0.243	0.125	0.146	0.144	0.158	0.174	0.161	0.200	0.840	0.219
Mn	0.006	0.004	—	—	—	0.007	0.002	0.004	0.013	0.006
Mg	1.026	1.006	0.951	0.989	0.994	0.934	1.019	0.957	0.558	0.997
Ca	0.575	0.800	0.810	0.798	0.780	0.750	0.740	0.745	0.591	0.624
Na	—	—	—	—	—	0.016	0.010	—	—	0.015
K	—	—	—	—	—	<0.001	<0.001	—	—	0.003
Wo	31.2	41.4	42.4	41.4	40.4	40.2	38.5	39.2	29.8	34.0
En	55.6	52.1	49.9	51.2	51.4	50.1	53.1	50.3	28.0	53.8
Fs	13.2	6.5	7.7	7.4	8.2	9.7	8.4	10.5	42.2	12.2
Glass Group	G	H	H	H	H	n.a.	J	n.a.	K	K
Analyst ^c	A	A	A	A	A	L	L	A	A	L

^a Na₂O, K₂O, NiO not determined by Adamson.^b Structural formulae calculated on the basis of 6 oxygens.^c A, Adamson; L, Laverne.

dic in holocrystalline samples and overlap much of the groundmass microlite compositional range. In general, the more sodic rims and microlites crystallized after eruption and during cooling of pillows and flows. The melts from which these crystals grew were interstitial and considerably more evolved than the original bulk magma compositions.

The distribution of reconnaissance plagioclase compositions is shown in Figure 5. There is no difference between the spectrum observed for Site 504 and that observed for Site 505, nor are there obvious compositional breaks, such as those that occur in some Mid-Atlantic Ridge lavas, which have been cited as evidence for magma mixing (Dungan and Rhodes, 1978). Compared with plagioclase phenocrysts from other ridge crests, these phenocrysts are unusually calcic, despite their largely quartz-normative hosts (Table 2); their compositions reflect the low contents of Na₂O in the glasses. The very low K₂O abundances in the lavas are reflected in the almost total lack of K₂O in the plagioclases, even in the microlites. What cannot be determined precisely from samples with microlites is the range of compositions of the last plagioclases that may have grown in an axial magma chamber or conduit system prior to extrusion of the lavas as pillows. For this purpose, the compositions of small, tabular plagioclases near pillow rims with glassy or spherulitic groundmass textures would be ideal. Most of the analyses in Table 6 were from samples more crystalline than this. However, the most sodic cores of small phenocrysts, even in nearly holocrystalline lavas, might be appropriate, or the least sodic rims of large phenocrysts in any of the rocks. Probably this range is given by the upper anorthite content of phenocryst rims and the lower anorthite content of phenocryst cores (An₇₈₋₈₅)

in Table 8. These should be close to compositions in equilibrium with corresponding glasses (cf. Autio and Rhodes, this volume). A more precise determination of this for clinopyroxene-assemblage lavas was obtained in the detailed sample study described later. In any case, it appears that the highly calcic plagioclase megacrysts crystallized in less evolved melts, possibly prior to injection into a shallow magma chamber system.

The clinopyroxenes in Table 7 include some notably high in Cr₂O₃ (0.7–1.1%) that are quite magnesian, having a narrow range of calcic endiopside (Poldervaart and Hess, 1951) compositions. Other phenocrysts, which have less Cr₂O₃, are more augitic, and some groundmass grains are quite iron rich, with ferroaugite compositions. In other abyssal tholeiites, Cr-rich endiopsides have been interpreted as high pressure megacrysts or as xenocrysts of the upper mantle, and they are usually associated with highly calcic plagioclases (cf. Donaldson and Brown, 1977; Bender et al., 1978; Wilkinson, 1982).

In summary, the reconnaissance mineral data corroborate the inference from the uniformity of glass group compositions (Table 2) that little of the variation in the lavas can be attributed to pre-extrusive crystallization differentiation. Plagioclase phenocrysts have the same range of highly calcic compositions, and the same range in compositions of rims regardless of stratigraphic position or phenocryst assemblage. In individual, more crystalline samples, *in situ* post-eruptive differentiation proceeded to variable, but sometimes considerable degrees, producing sodic groundmass plagioclases and iron-rich interstitial pyroxenes. But many of the phenocrysts—the calcic plagioclases, Cr₂O₃-rich clinopyroxenes, olivine, and perhaps spinel—crystallized at a very early stage in

Table 7. (Continued).

	Hole 504B										Hole 505B
	Leg/Piece										69/107
	70/507	70/594	70/804	70/804	70/1099	70/1189	70/1189	70/1450	70/1519	70/1540	
SiO ₂	52.73	51.88	53.66	50.21	51.54	53.99	53.39	53.34	49.97	52.27	47.51
TiO ₂	0.41	0.50	0.51	0.73	1.06	0.32	0.34	0.21	0.87	0.51	1.33
Al ₂ O ₃	2.66	2.99	4.03	2.58	3.90	1.33	1.28	1.81	1.57	3.88	3.44
FeO	5.69	7.86	7.79	12.27	7.27	8.50	9.54	8.39	21.64	6.87	17.63
MgO	18.34	17.79	18.25	15.57	16.85	19.42	20.28	21.47	9.19	18.77	12.54
CaO	18.34	17.40	17.93	15.50	16.63	15.39	13.91	14.00	16.53	16.50	14.53
Na ₂ O	0.20	0.16	—	—	0.27	0.10	0.14	0.12	—	0.14	—
K ₂ O	0.00	0.02	—	—	0.02	0.00	0.00	0.00	—	0.00	—
MnO	0.07	0.19	0.18	0.24	0.25	0.17	0.30	0.21	0.40	0.25	0.39
NiO	0.00	0.00	—	—	0.00	0.03	0.00	0.00	—	0.00	—
Cr ₂ O ₃	0.48	0.01	0.22	0.14	0.14	0.07	0.00	0.00	—	0.27	0.15
	98.93	98.81	102.57	97.24	97.93	99.32	99.19	99.55	100.17	99.46	97.52
Structural Formulae ^b											
Si	1.930	1.915	1.910	1.925	1.908	1.972	1.960	1.941	1.948	1.902	1.868
Al	0.070	0.085	0.090	0.075	0.092	0.028	0.040	0.059	0.052	0.098	0.132
Al	0.045	0.045	0.079	0.042	0.078	0.029	0.016	0.019	0.020	0.069	0.028
Ti	0.011	0.014	0.014	0.021	0.030	0.009	0.009	0.006	0.026	0.014	0.039
Cr	0.014	<0.001	0.006	0.004	0.004	0.002	0.000	0.000	—	0.008	0.005
Ni	0.000	0.000	—	—	0.000	0.001	0.001	0.000	—	0.000	—
Fe	0.174	0.243	0.232	0.393	0.225	0.260	0.293	0.255	0.706	0.290	0.580
Mn	0.002	0.006	0.005	0.008	0.008	0.005	0.009	0.007	0.013	0.008	0.013
Mg	1.002	0.979	0.968	0.889	0.930	1.057	1.109	1.165	0.534	1.018	0.735
Ca	0.719	0.688	0.684	0.637	0.660	0.603	0.547	0.546	0.691	0.643	0.612
Na	0.014	0.012	—	—	0.020	0.007	0.010	0.009	—	0.010	—
K	0.000	0.001	—	—	0.001	0.000	0.000	0.000	—	0.000	—
Wo	37.9	35.9	36.3	33.2	36.2	31.3	27.9	27.7	45.9	34.3	31.7
En	52.8	51.1	51.4	46.3	51.0	54.9	56.7	59.1	27.7	54.2	38.2
Fs	9.3	13.0	12.3	20.5	12.8	13.8	15.4	13.3	36.4	11.5	30.1
Glass Group	K	K	K	K	M	n.a.	n.a.	0	n.a.	n.a.	P
Analyst	L	L	A	A	L	L	L	L	A	L	A

Table 8. Summary of plagioclase anorthite contents for cores, rims, and microlites, DSDP Sites 501, 504, and 505.

Phenocryst Assemblage	Glass Group	Cores	Rims	Microlites
Spinel assemblage (Holes 501, 504B, 505A, 505B)	B	86–92	74–85	68
	I	—	—	66
	J	83–86	76–78	53–62
Clinopyroxene assemblage (Hole 504B)	P	78–93	71–77	49–78
	C	—	—	—
	D	87–90	87	65
	F	—	—	—
	G	86–90	77	—
Aphyric-sparsely phytic (Hole 504B)	H	—	—	76
	L	—	—	—
	O	—	—	69–75
Mixed (Hole 504B)	A	—	—	—
	N	89–94	—	70–72
Less depleted (Hole 504B)	K	87–91	61–80	78
Less depleted (Hole 504B)	E	—	—	—
	M	—	74	45–66

the history of the lavas from much less evolved liquids, perhaps at elevated pressures. Alternatively, some of the minerals may represent xenocrysts of mantle (or magma chamber) wall rocks.

PHENOCRYST MORPHOLOGIES

Phenocryst morphologies, sizes, compositions, and crystallization relationships are complex, but they are the key to unraveling the pre-eruptive history of the basalts. Brief descriptions of phenocrysts and megacrysts, presented in outline form in Table 14, are representative of all thin sections examined, but the four samples selected for detailed study exemplify many of the features described. Groundmass crystal morphologies are

typical of pillow basalts described elsewhere (e.g. Kirkpatrick, 1979, and Natland, 1979b), ranging from glassy through a variety of spherulitic and microlitic textures, to subophitic textures, depending on distances from pillow rims and thickness of cooling units. In samples from Site 505, these are quite spectacularly developed (Fig. 6).

Plagioclase Phenocrysts and Glomerocrysts

The porphyritic rocks contain several, and in some cases many, large plagioclase megacrysts and glomerocrysts in a single sample. Glomerocrysts can include several mineral phases, as for example that shown in Figure 7A, which depicts a large zoned plagioclase enclosing subhedral olivine and Cr-spinel. Or they can consist entirely of anhedral plagioclase exhibiting distinctive adcumulus texture (Fig. 7B). Some of the larger glomerocrysts, however, are simply loose collections of large, unzoned plagioclases (Fig. 7C) that have grain boundaries at odd angles to twin planes, suggesting that they are xenocrysts. Other extremely irregular grains (Fig. 7D) are more obviously xenocrysts and have rounded margins suggesting the effects of partial solution of the mineral grain in a melt.

Many plagioclase megacrysts contain brown, formerly glassy inclusions of trapped basalt melt. The dark color reflects formation of spherulitic crystallites similar to those near pillow rims. Usually, these inclusions are rather sparse, but they can be fairly large in individual mineral grains (Fig. 7C). Rarely, a large megacryst will have myriads of smaller, irregular-shaped inclusions arranged paralleling twin planes in the plagioclase (Fig. 7E). The inclusion-bearing zones mantle solid cores and have solid rims. In other plagioclases, inclusions are smaller and bubble shaped. Some inclusions are restricted to a narrow border zone and are overgrown with

Table 9. Detailed sample study electron microprobe analyses of Cr-spinels.

Leg 70, Sample 504B-35-2, 24–26 cm (Group J)								
Analysis								
	1	2	3	4	5	6	7	8
SiO ₂	0.06	0.46	0.07	0.05	0.05	0.05	0.09	0.02
TiO ₂	0.22	0.25	0.22	0.32	0.34	0.38	0.29	0.23
Al ₂ O ₃	42.35	42.58	43.26	38.43	38.58	38.87	29.25	42.37
Fe ₂ O ₃ ^a	3.89	2.79	3.38	4.42	4.35	4.36	3.69	4.50
FeO*	9.80	11.91	10.34	11.20	11.25	11.07	11.69	10.40
MnO	0.15	0.10	0.14	0.22	0.18	0.16	0.13	0.23
MgO	19.31	18.22	19.13	18.00	18.00	18.21	16.72	18.75
NiO	0.26	0.28	0.21	0.21	0.25	0.20	0.17	0.21
Cr ₂ O ₃	26.43	25.29	25.88	29.58	29.59	29.30	39.92	25.51
	102.47	101.88	102.63	102.43	102.59	102.60	101.95	102.22
Structural Formulae ^b								
Si	0.013	0.100	0.015	0.011	0.011	0.011	0.021	0.004
Al	10.767	10.916	10.959	9.998	10.008	10.060	7.951	10.826
Cr	4.506	4.348	4.397	5.155	5.148	5.085	7.277	4.371
Fe ³⁺	0.631	0.457	0.547	0.733	0.720	0.720	0.640	0.734
Ti	0.036	0.041	0.036	0.053	0.056	0.063	0.050	0.037
Mg	6.206	5.905	6.126	5.914	5.903	5.958	5.745	6.056
Fe ²⁺	1.767	2.166	1.858	2.065	2.070	2.032	2.252	1.885
Mn	0.027	0.018	0.025	0.041	0.034	0.030	0.025	0.042
Ni	0.045	0.049	0.036	0.037	0.044	0.035	0.032	0.037
Cr/Cr + Al	0.295	0.289	0.286	0.340	0.034	0.336	0.478	0.288
Mg/Mg + Fe ²⁺	0.778	0.732	0.767	0.741	0.740	0.746	0.718	0.763
Crystal Type and Number ^c	C1	R1	C1	C2	C2	R2	C3	R3

^a Computed from stoichiometry.

^b Structural formulae computed from stoichiometry on the basis of 32 oxygens.

^c C, core; R, rim; I, intermediate point between core and rim. Numbers identify individual mineral grains.

a more sodic dendritic rim (Fig. 7F). Megacrysts with these various types of glass inclusions are remarkably similar to megacrysts in many Mid-Atlantic-Ridge porphyritic basalts (cf. photomicrographs in Muir and Tilly, 1964; Blanchard et al., 1976; Natland, 1979b; Dungan et al., 1979).

Numerically more abundant, but volumetrically less important, are second generation plagioclase phenocrysts and glomerocrysts (e.g., Natland, 1979b). These consist almost entirely of small, tabular plagioclases, usually with a single, central Carlsbad twin plane, stacked together in parallel fashion (Figs. 7G and H). Just as commonly, however, such crystals occur in loose skeins or clumps, in small groups of two or three crystals (Fig. 7I), and as single crystals in the groundmass (Fig. 7J), often with dendritic projections from crystal corners in spherulitic samples. We term these second generation crystals (to distinguish them from the plagioclase megacrysts and large glomerocrysts), but they represent a continuum of crystallization conditions up to the point of extrusion and rapid cooling of the lavas. This produces normal zoning on these tabular crystals (Fig. 7H) and formation of dendrites at the corners of crystals, marking termination of crystal growth. The first generation megacrysts and glomerocrysts include all the highly calcic plagioclases, which we have suggested crystallized early in the history of the magmas, perhaps at elevated pressure, and were carried from depth into any shallow axial magma chamber that may have existed. The second generation crystals, we suggest, largely grew after injection of magmas into such a system, during upward movement of magmas to the seafloor, and even following eruption.

Clinopyroxene Phenocrysts and Megacrysts

Clinopyroxene phenocryst morphologies are as diverse as those of the plagioclases. The photomicrographs of Figure 8 are partly from the two Group G clinopyroxene-assemblage samples investigated in detail, and some of the specific minerals shown have been analyzed. Figure 8A depicts a portion of a large gabbroic xenolith consisting of plagioclases poikilitically surrounded by clinopyroxenes. The pyroxenes crystallized from a more iron-rich melt than the host glass (Group G); hence, the xenolith is evidently a fragment removed from the walls of a magma chamber or shallow conduit system that originally contained a more fractionated melt. Other xenoliths with rounded, irregular margins (Fig. 8B) contain smaller plagioclases. Then there are all manner of partially resorbed phenocrysts with rounded crystal facets (Fig. 8C), and commonly, nearly round or cigar-shaped ellipsoids that may in part be marginally plated with plagioclase microlites (Fig. 8D and Fig. 7H, upper right). Faceted phenocrysts without resorbed margins are also common, and they often enclose one or more small, tabular plagioclases (Fig. 8E–G). Some of these euhedra can be quite tiny, no larger than genuine groundmass clinopyroxenes. The latter, however, tend to be anhedral, have irregular extinction, and are intergrown with small second-generation microphenocrysts or microlites (Fig. 7J).

Olivine Phenocrysts

Olivine crystal forms can usually only be discerned in thin section by the outline of oftentimes plucked alteration minerals. Those associated with plagioclase glomero-

Table 9. (Continued).

Leg 70, Sample 504B-35-2, 24-26 cm (Group J)				Leg 69, Sample 501-15-3, 63-65 cm (Group B)				
Analysis								
9	10	11	12	13	14	15	16	17
0.07	0.08	0.06	0.05	0.05	1.53	0.15	0.12	0.09
0.28	0.24	0.25	0.37	0.44	0.42	0.54	0.34	0.54
42.50	38.37	31.57	29.11	28.77	29.73	26.97	31.70	30.07
3.73	3.84	3.62	4.81	6.41	3.87	6.56	5.82	6.60
11.22	10.71	11.51	14.18	13.69	15.65	14.30	13.60	13.58
0.13	0.17	0.19	0.22	0.22	0.22	0.22	0.22	0.26
18.52	18.30	16.89	15.05	15.33	15.16	14.71	15.81	15.39
0.19	0.25	0.18	0.18	0.12	0.17	0.13	0.12	0.19
26.40	30.63	37.18	37.95	36.95	34.79	37.73	34.69	34.58
103.04	102.59	101.45	101.92	101.98	101.54	101.31	102.42	101.30
Structural Formulae								
0.015	0.018	0.014	0.012	0.012	0.355	0.036	0.027	0.021
10.798	9.941	8.531	8.005	7.907	8.134	7.530	8.558	8.263
4.498	5.322	6.738	6.998	6.810	6.383	7.064	6.281	6.372
0.605	0.635	0.624	0.844	1.125	0.676	1.169	1.003	1.158
0.045	0.040	0.043	0.065	0.077	0.073	0.096	0.059	0.095
5.948	5.994	5.770	5.232	5.326	5.243	5.192	5.396	5.346
2.022	1.968	2.206	2.766	2.669	3.037	2.832	2.605	2.647
0.024	0.032	0.037	0.043	0.043	0.043	0.044	0.043	0.051
0.033	0.044	0.033	0.034	0.022	0.032	0.025	0.022	0.036
0.294	0.349	0.441	0.466	0.463	0.440	0.484	0.423	0.435
0.746	0.753	0.723	0.654	0.666	0.633	0.647	0.674	0.669
13	13	13	C4	R4	C5	R5	C6	R6

Table 10. Detailed sample study electron microprobe analyses of olivine.

	Leg 70, 504B-35-2, 24-26 (Group J)			Leg 69, 501-15-3, 63-65 (Group B)			Leg 69, 504B-23-1, 115-116 (Group G)			
	Analysis									
	1	2	3	4	5	6	7	8	9	10
SiO ₂	39.94	39.64	40.16	40.06	39.78	39.35	39.36	39.65	39.15	39.11
FeO*	11.32	10.23	9.97	10.35	13.24	12.72	13.28	12.54	13.91	14.16
MnO	0.22	0.15	0.20	0.16	0.24	0.20	0.21	0.24	0.27	0.28
MgO	48.37	48.99	49.29	48.87	47.15	45.96	46.89	47.23	45.39	45.60
CaO	0.31	0.33	0.31	0.32	0.33	0.40	0.32	0.30	0.35	0.33
NiO	0.25	0.24	0.35	0.34	0.24	0.18	0.13	0.20	0.20	0.21
Cr ₂ O ₃	0.09	0.03	0.05	0.14	0.06	0.10	0.08	0.09	0.05	0.04
	100.51	99.69	100.40	100.26	101.05	99.34	100.27	100.24	99.34	99.75
Structural Formulae ^a										
Si	0.985	0.981	0.986	0.986	0.984	0.992	0.981	0.985	0.989	0.985
Mn	0.005	0.003	0.004	0.003	0.005	0.004	0.004	0.005	0.006	0.006
Ni	0.005	0.005	0.007	0.007	0.005	0.004	0.003	0.004	0.004	0.004
Cr	0.002	0.001	0.001	0.003	0.001	0.002	0.002	0.002	0.001	0.001
Fe	0.233	0.212	0.205	0.213	0.274	0.268	0.277	0.261	0.294	0.298
Mg	1.777	1.808	1.803	1.793	1.738	1.727	1.743	1.749	1.708	1.712
Ca	0.008	0.009	0.008	0.008	0.009	0.011	0.009	0.008	0.009	0.009
[Y] ⁶	2.030	2.037	2.028	2.027	2.032	2.015	2.038	2.029	2.022	2.030
Composition, Crystal Type ^b	Fog8.4 MC1	Fog9.5 PC2	Fog9.8 PC3	Fog9.4 PC4	Fog8.4 MC5	Fog8.6 MC6	Fog8.3 MC7	Fog7.0 PC8	Fog8.3 MC9	Fog5.2 MC10

^a Structural formulae calculated on the basis of 4 oxygens.^b M, microphenocryst; P, phenocryst; C, core. Numbers identify individual mineral grains.

crystals tend to be granular or anhedral. Isolated phenocrysts are usually anhedral in spinel-assembly lavas (Fig. 9A), but they can have skeletal forms (Fig. 9B). Groundmass olivines have swallowtail or hopper morphologies in microlitic samples (Fig. 9C), but they can form almost perfectly prismatic, tiny euhedra in glass (Fig. 9D).

Cr-Spinels

In samples corresponding to the least fractionated glass group, J, Cr-spinels are small euhedra occurring

in the groundmass or attached to olivines. A subjective impression is that they are scattered in the groundmass close to olivine phenocrysts and are rare away from them in the same thin section. In the somewhat more evolved spinel-assembly Group B and P samples, they have similar modes of occurrence (Figs. 9E and F), but they can also have partially skeletal outlines and contain altered or devitrified bubble-shaped glass inclusions (Fig. 9G). In samples from Holes 505A and 505B, they occur enclosed in both plagioclase (Fig. 7A) and olivine, and in the groundmass they can have vermicular rims

Table 11. Detailed sample study electron microprobe analyses of plagioclases.

	Leg 70, 504B-35-2, 24-26 cm (Piece 287, Group J)				Leg 69, 501-15-3, 63-65 (Piece 238, Group B)							Leg 69, 504B-24-2, 58-62 (Piece 1361, Group G)				
	1	2	3	4	5	6	7	8	9	10	11	12	13	14	15	16
SiO ₂	48.74	46.93	47.63	47.29	46.52	45.67	47.16	46.07	46.10	46.68	46.22	50.69	47.87	47.01	49.32	50.24
Al ₂ O ₃	32.71	33.99	33.63	33.73	33.99	34.69	33.50	34.19	34.35	33.81	33.92	31.04	33.01	33.10	32.05	30.79
FeO	0.39	0.40	0.37	0.36	0.52	0.38	0.33	0.34	0.43	0.47	0.39	0.54	0.50	0.40	0.52	0.54
MgO	0.27	0.24	0.24	0.17	0.12	0.23	0.27	0.22	0.21	0.22	0.25	0.25	0.26	0.26	0.27	0.26
CaO	16.67	18.29	17.90	17.83	18.16	18.88	17.67	18.57	18.09	18.35	18.32	14.93	17.26	17.59	15.87	14.86
Na ₂ O	2.21	1.38	1.67	1.63	1.52	1.09	1.54	1.10	1.23	1.45	1.40	2.83	1.66	1.57	2.29	2.55
K ₂ O	0.01	0.00	0.00	0.01	0.01	0.01	0.01	0.00	0.00	0.00	0.02	0.00	0.00	0.02	0.00	0.00
	101.00	101.23	101.44	101.02	100.84	100.95	100.48	100.49	100.41	100.98	100.52	100.28	100.56	99.95	100.32	99.24
Structural Formulae																
Si	8.858	8.552	8.650	8.623	8.521	8.368	8.639	8.463	8.468	8.538	8.493	9.224	8.752	8.662	8.998	9.230
Al	7.010	7.303	7.201	7.252	7.341	7.494	7.236	7.406	7.440	7.292	7.350	6.660	7.166	7.191	6.895	6.670
Fe	0.059	0.061	0.056	0.055	0.080	0.058	0.051	0.052	0.066	0.072	0.060	0.082	0.076	0.062	0.079	0.083
Mg	0.073	0.065	0.065	0.046	0.033	0.063	0.074	0.060	0.058	0.060	0.069	0.068	0.071	0.071	0.073	0.071
Ca	3.247	3.572	3.484	3.484	3.565	3.707	3.469	3.656	3.561	3.597	3.608	2.912	3.382	3.473	3.103	2.926
Na	0.779	0.488	0.588	0.576	0.540	0.387	0.547	0.392	0.438	0.514	0.499	0.999	0.589	0.561	0.810	0.909
K	0.002	0.000	0.000	0.002	0.002	0.002	0.002	0.000	0.000	0.000	0.005	0.000	0.000	0.005	0.000	0.000
Composition	Ang _{0.7}	Ang _{8.9}	Ang _{5.6}	Ang _{5.8}	Ang _{6.9}	Ang _{0.5}	Ang _{6.4}	Ang _{0.3}	Ang _{8.9}	Ang _{7.5}	Ang _{7.9}	Ang _{74.5}	Ang _{5.2}	Ang _{6.1}	Ang _{79.3}	Ang _{76.3}

Note: Structural formulae calculated on the basis of 32 oxygens.

^a Description of analyses: 1—Microcline; 2—Large anhedral megacryst with out glass inclusions; 3—Phenocryst; 4—One grain of glomerocryst; 5, 6—Very large skeletal megacryst (Fig. 7E). Analysis 5 is from the rounded core, 6 from the rim, and 11 from the skeletal mantle. Contains devitrified glass inclusions. (Analyses 1–3 of Table 13); 7—Core and rim of a large megacryst with glass inclusions (Analyses 4 and 5 of Table 13). Encloses spinel grain (Analyses 12 and 13 of Table 9); 9—Core of large megacryst containing two large and several smaller spherulitic inclusions (Analysis 6 of Table 13); 10—Small tabular crystal in glass; 11, 12—In gabbro xenolith, enclosed by clinopyroxene (Analyses 1 and 2 of Table 12); 13—In large glomerocryst with altered olivine; 14—Small crystal in glomerocryst with clinopyroxene; 15—In glomerocryst enclosed by clinopyroxene (Analyses 4–6 of Table 12); 16—In gabbro xenolith (Fig. 7B) with clinopyroxene (Analysis 7 of Table 12); 17—Plagioclase plating clinopyroxene in same gabbro xenolith (Fig. 7B); 18—In small glomerocryst with clinopyroxene; 19—In small glomerocryst with clinopyroxene (Analysis 10 of Table 12); 20—Small crystal intergrown with clinopyroxene phenocryst; 21—Small groundmass microphenocryst in cluster of plagioclases; 22—Large euhedral phenocryst with no glass inclusions; 23—Tabular crystal attached to clinopyroxene (Analysis 12 of Table 12); 24—Tabular crystal attached to small rounded clinopyroxene (Analysis 13 of Table 12); 25—In glomerocryst with altered olivine; 26—Euhedral crystal in glass; 27—Tabular crystal enclosed in rounded clinopyroxene phenocryst (Analysis 14 of Table 12); 28—Center of megacryst; 29, 30, 31—Various portions of the core of a large megacryst next to devitrified glass inclusion; 32—Center of megacryst.

Table 12. Detailed sample study electron microprobe analyses of clinopyroxenes.

	Leg 69, 504B-24-2, 58-62 (Piece 1361, Group G)										
	1	2	3	4	5	6	7	8	9	10	11
SiO ₂	52.21	51.88	50.98	51.96	52.13	51.54	51.95	51.21	51.33	51.66	50.63
TiO ₂	0.29	0.37	0.17	0.26	0.28	0.30	0.33	0.29	0.29	0.29	0.37
Al ₂ O ₃	1.80	2.30	3.55	2.38	2.55	2.56	2.93	3.33	3.09	2.66	3.32
FeO*	6.68	6.88	4.69	5.13	5.59	5.17	6.78	4.49	4.42	4.81	5.06
MgO	19.35	18.47	18.28	18.47	18.92	18.43	20.22	17.92	18.01	18.54	18.00
CaO	17.84	18.59	19.72	19.73	18.89	19.82	15.91	20.27	20.37	19.75	19.58
Na ₂ O	0.17	0.26	0.40	0.24	0.27	0.22	0.26	0.27	0.23	0.24	0.30
K ₂ O	0.00	0.01	0.02	0.00	0.01	0.01	0.01	0.02	0.00	0.03	0.02
MnO	0.14	0.24	0.17	0.17	0.16	0.18	0.27	0.07	0.18	0.12	0.16
NiO	0.05	0.00	0.06	0.08	0.03	0.08	0.05	0.04	0.12	0.06	0.04
Cr ₂ O ₃	0.14	0.11	1.02	0.45	0.44	0.39	0.26	1.12	1.04	0.50	0.78
	98.67	99.12	99.20	98.88	99.30	98.72	98.99	99.06	99.10	98.67	98.25
Structural Formulae											
Si	1.933	1.919	1.881	1.919	1.916	1.909	1.909	1.899	1.894	1.910	1.885
Al	0.067	0.081	0.119	0.081	0.084	0.091	0.091	0.111	0.106	0.090	0.115
Al	0.011	0.019	0.035	0.023	0.027	0.021	0.036	0.034	0.028	0.026	0.031
Ti	0.008	0.010	0.005	0.007	0.008	0.008	0.009	0.008	0.008	0.008	0.010
Cr	0.004	0.003	0.030	0.013	0.013	0.011	0.008	0.033	0.030	0.015	0.023
Ni	0.001	0.000	0.002	0.002	0.001	0.002	0.001	0.001	0.004	0.002	0.001
Fe	0.207	0.213	0.145	0.158	0.172	0.160	0.208	0.139	0.136	0.149	0.158
Mn	0.004	0.008	0.005	0.005	0.005	0.006	0.008	0.002	0.006	0.004	0.005
Mg	1.068	1.018	1.005	1.017	1.036	1.017	1.108	0.985	0.990	1.022	0.999
Ca	0.708	0.737	0.780	0.781	0.744	0.787	0.627	0.801	0.805	0.783	0.781
Na	0.012	0.019	0.029	0.017	0.019	0.016	0.019	0.019	0.016	0.017	0.022
K	0.000	<0.001	0.001	0.000	<0.001	<0.001	<0.001	<0.001	0.000	0.001	0.001
Composition	Wo	35.7	37.4	40.4	39.9	38.1	40.1	32.3	41.6	40.0	40.4
	En	53.9	51.7	52.0	52.0	53.1	51.8	57.0	51.2	52.3	51.5
	Fs	10.5	10.8	7.6	8.1	8.8	8.2	10.7	7.2	7.6	8.1

Note: Structural formulae calculated on the basis of 6 oxygens.

^a Description of analyses: 1, 2—Clinopyroxenes in gabbroic xenolith (Fig. 7A) enclosing plagioclase (Analysis 12, Table 11); 3—Rounded phenocryst similar to Figure 7E. 4, 5, 6—Clinopyroxenes in large, rounded glomerocryst, enclosing plagioclase (Analysis 15, Table 11); 7—Clinopyroxene in gabbroic xenolith (Fig. 7B), enclosing plagioclase (Analysis 16, Table 11); 8, 9—Core, rim of partly rounded euhedral phenocryst; has plagioclase (Analysis 17, Table 11) attached to rim; 10—Small, rounded phenocryst in groundmass. Next to plagioclase (Analysis 19, Table 11); 11—Large, rounded phenocryst; 12—Large euhedral phenocryst, not rounded, has small tabular plagioclase (Analysis 23, Table 11) intergrown on one edge; 13—Small, slightly rounded phenocryst, with tabular plagioclase (Analysis 24, Table 11) attached at one end; 14—Large, slightly rounded phenocryst (Fig. 7C) enclosing plagioclase (Analysis 27, Table 11); 15—Rounded, cigar-shaped phenocryst; 16—Small, angular xenocryst; 17—Small, angular xenocryst; 17—Small, angular xenocryst; 18, 19—Core (18), rim (19) of small angular phenocryst; 20—Small phenocryst; 21, 22—Core (21), rim (22) of small, slightly rounded phenocryst.

and even quite spectacular skeletal morphologies (Figs. 9H and I). Fisk and Bence (1980) and Furuta and Tokuyama (this volume) interpret such features as manifestations of resorption. However, such interior latticelike structure is not fundamentally different from that in the plagioclase megacryst of Figure 7E, and it probably had

similar origin. Both structures are a type of skeletal growth, the result of rapid heat loss from the melt. In both cases, exterior faceted crystal outlines are maintained, and there is no evidence for the distinctive rounding that marks the obviously partly resorbed plagioclase and clinopyroxene phenocrysts shown in Figures 7 and 8.

Table 11. (Continued).

	Leg 69, 504B-24-2, 58-62 (Piece 1361, Group G)					Leg 69, 504B-23-1, 115-116 (Piece 1326, Group G)										
	Analysis ^a															
	17	18	19	20	21	22	23	24	25	26	27	28	29	30	31	32
SiO ₂	47.99	45.85	46.76	46.69	47.12	46.55	46.71	46.62	47.00	46.41	47.14	46.56	46.97	46.19	46.73	46.20
Al ₂ O ₃	32.68	34.17	33.83	33.42	33.59	33.58	33.68	33.65	33.16	33.37	32.81	33.75	33.39	33.90	33.30	33.94
FeO*	0.51	0.35	0.55	0.41	0.42	0.41	0.52	0.46	0.44	0.46	0.49	0.41	0.47	0.42	0.39	0.42
MgO	0.24	0.20	0.23	0.26	0.27	0.23	0.21	0.24	0.23	0.23	0.24	0.26	0.25	0.22	0.20	0.20
CaO	16.53	17.87	17.52	17.47	17.58	7.68	17.33	17.39	16.98	17.15	17.13	17.68	17.51	17.72	17.04	17.49
Na ₂ O	1.78	1.38	1.42	1.36	1.48	1.36	1.48	1.41	1.54	1.66	1.77	1.55	1.46	1.09	1.60	1.26
K ₂ O	0.01	0.00	0.00	0.01	0.00	0.01	0.01	0.00	0.01	0.00	0.01	0.00	0.00	0.00	0.00	0.00
	99.74	99.82	100.31	99.62	100.46	99.82	99.93	99.77	99.36	99.28	99.59	100.21	100.05	99.32	99.36	99.51
Structural Formulae																
Si	8.825	8.470	8.584	8.623	8.632	8.588	8.603	8.598	8.691	8.607	8.712	8.563	8.641	8.541	8.654	8.543
Al	7.086	7.443	7.323	7.278	7.256	7.305	7.314	7.318	7.230	7.297	7.149	7.243	7.391	7.271	7.401	7.401
Fe	0.078	0.054	0.084	0.063	0.064	0.063	0.080	0.071	0.068	0.071	0.076	0.063	0.072	0.065	0.060	0.065
Mg	0.066	0.055	0.063	0.072	0.074	0.063	0.058	0.066	0.063	0.064	0.066	0.071	0.069	0.061	0.055	0.055
Ca	3.258	3.538	3.447	3.458	3.451	3.496	3.420	3.437	3.365	3.408	3.393	3.485	3.452	3.511	3.382	3.466
Na	0.635	0.494	0.506	0.487	0.526	0.487	0.529	0.504	0.552	0.597	0.634	0.553	0.521	0.391	0.575	0.452
K	0.002	0.000	0.000	0.002	0.000	0.002	0.002	0.000	0.002	0.000	0.002	0.000	0.000	0.000	0.000	0.000
Composition	Ang3.7	Ang7.7	Ang7.2	Ang7.7	Ang6.8	Ang7.8	Ang6.6	Ang7.2	Ang5.9	Ang5.1	Ang4.3	Ang6.3	Ang6.9	Ang0.0	Ang5.5	Ang8.5

Table 12. (Continued).

	Leg 69, 504B-23-1, 115-116 (Piece 1326, Group G)										
	Analysis ^a										
	12	13	14	15	16	17	18	19	20	21	22
SiO ₂	50.97	50.94	51.52	50.93	50.41	50.91	50.86	50.67	50.24	50.92	48.36
TiO ₂	0.28	0.22	0.25	0.32	0.37	0.25	0.28	0.38	0.45	0.30	0.59
Al ₂ O ₃	3.31	3.09	2.25	3.60	1.95	2.85	3.26	3.26	3.88	3.32	11.15
FeO*	4.59	4.31	4.58	4.88	13.06	4.40	4.92	5.10	5.22	4.60	5.46
MgO	18.17	17.91	18.51	18.18	15.61	17.88	18.08	17.59	17.52	17.82	16.60
CaO	18.62	19.98	19.70	19.31	16.18	20.05	19.47	19.64	19.44	19.81	17.75
Na ₂ O	0.32	0.35	0.30	0.16	0.20	0.20	0.12	0.44	0.32	0.27	0.34
K ₂ O	0.00	0.01	0.00	0.00	0.00	0.00	0.02	0.00	0.00	0.01	0.01
MnO	0.15	0.10	0.15	0.15	0.34	0.11	0.12	0.14	0.13	0.13	0.17
NiO	0.10	0.04	0.03	0.07	0.00	0.05	0.05	0.03	0.05	0.05	0.05
Cr ₂ O ₃	1.11	1.09	0.74	1.12	0.07	0.83	0.79	0.88	0.90	1.05	0.18
	97.63	98.04	98.04	98.76	98.20	97.51	98.01	98.14	98.15	98.27	100.67
Structural Formulae											
Si	1.900	1.897	1.917	1.883	1.927	1.905	1.895	1.890	1.847	1.892	1.744
Al	0.100	0.103	0.083	0.117	0.073	0.095	0.105	0.110	0.153	0.108	0.256
Al	0.046	0.033	0.016	0.040	0.015	0.31	0.038	0.033	0.018	0.037	0.218
Ti	0.008	0.006	0.007	0.009	0.011	0.007	0.008	0.011	0.013	0.008	0.016
Cr	0.033	0.032	0.022	0.033	0.002	0.025	0.023	0.026	0.027	0.031	0.005
Ni	0.003	0.001	0.001	0.002	0.000	0.002	0.001	0.001	0.002	0.001	0.001
Fe	0.143	0.134	0.143	0.151	0.418	0.138	0.153	0.159	0.163	0.143	0.165
Mn	0.005	0.003	0.005	0.005	0.011	0.003	0.004	0.004	0.004	0.004	0.005
Mg	1.010	0.994	1.027	1.002	0.890	0.997	1.004	0.978	0.974	0.987	0.892
Ca	0.744	0.797	0.786	0.765	0.663	0.804	0.777	0.785	0.777	0.789	0.686
Na	0.023	0.025	0.022	0.011	0.015	0.015	0.009	0.032	0.023	0.019	0.024
K	0.000	<0.001	0.000	0.000	0.000	0.000	0.001	0.000	0.000	<0.001	<0.001
Composition Wo	39.2	41.4	40.2	39.9	33.6	41.4	40.2	40.9	40.6	41.1	39.4
En	53.3	51.6	52.5	52.3	45.2	51.4	51.9	50.9	50.9	51.4	51.2
Fs	7.5	7.0	7.3	7.9	21.2	7.1	7.9	8.3	8.5	7.4	9.4

Phenocryst Incompatibilities and Associations

There are certain mineral interrelationships that do not occur in these samples. Glomerocrysts with all three silicate phases do not occur, nor does clinopyroxene occur in glomerocrysts with the large plagioclase adcumulus clumps of the type depicted in Figure 7B. This may be because large plagioclase-olivine glomerocrysts are rare (in samples where euhedral clinopyroxene pheno-

crysts are abundant, and rounded phenocrysts rare or absent), whereas the opposite relationship occurs when plagioclase-olivine glomerocrysts are abundant. This suggests that clinopyroxene phenocrysts entered solution more readily in magmas carrying abundant olivine and plagioclase megacrysts. In two senses, then, olivine and clinopyroxene phenocrysts appear to have been incompatible: they never precipitated together in a common magma, and even where they occur together in the

Table 13A. Detailed sample study electron microprobe analyses of glass inclusions in plagioclase megacrysts.

Sample 501-15-3, 63-65 cm, this study						
Analysis ^a						
	1	2	3	4	5	6
SiO ₂	49.85	50.07	50.69	50.11	51.23	51.84
TiO ₂	0.88	0.98	1.05	0.84	0.74	0.72
Al ₂ O ₃	17.04	15.24	17.03	15.59	15.38	15.28
FeO*	8.32	9.03	7.84	9.93	8.71	7.55
MgO	9.55	9.61	6.91	9.81	9.18	8.83
CaO	12.27	12.39	12.90	11.81	12.09	12.42
Na ₂ O	1.62	1.74	2.06	1.71	1.96	1.96
K ₂ O	0.08	0.29	0.30	0.38	0.18	0.07
P ₂ O ₅	0.11	0.14	0.11	0.12	0.08	0.04
MnO	0.20	0.16	0.21	0.19	0.18	0.19
Total	99.92	99.65	98.90	100.49	99.73	98.90
Mg ² /Mg + Fe	0.721	0.706	0.665	0.690	0.704	0.725
CaO/Al ₂ O ₃	0.720	0.813	0.797	0.756	0.786	0.813

Note: Mg/Mg + Fe is computed assuming that Fe²⁺/Fe²⁺ + Fe³⁺ = 0.86.

^a Description of analyses: 1, 2, 3—Inclusion in the large plagioclase megacryst of Figure 7E (Analyses 5, 6, and 11 of Table 11); 4, 5—Inclusions in a smaller megacryst (Analyses 7 and 8 of Table 11) enclosing a spinel (Analyses 12 and 13 of Table 9); 6—Inclusion in the center of another plagioclase phenocryst (Analysis 9 of Table 11).

Table 13B. Composition of Sample 501-15-3, 63-65 cm glass and average glass Group B composition.

	Sample 501-15-3, 63-65 cm ^a	Average Group B Composition ^b
SiO ₂	51.39	51.04
TiO ₂	1.04	0.97
Al ₂ O ₃	15.10	15.10
FeO*	9.41	9.38
MgO	8.30	8.36
CaO	13.15	12.90
Na ₂ O	2.03	1.97
K ₂ O	0.02	0.03
P ₂ O ₅	0.08	0.09
MnO	0.21	—
Total	100.73	99.84
Mg ² /Mg + Fe	0.657	0.633
CaO/Al ₂ O ₃	0.871	0.854

Note: Mg/Mg + Fe is computed assuming that Fe²⁺/Fe²⁺ + Fe³⁺ = 0.86.

^a Fresh glass rim; determined using Scripps Inst. microprobe.

^b From Table 2; based on Smithsonian Inst. microprobe data.

same rock, growth (or at least persistence) of olivine occurred at the expense of clinopyroxene. Obviously, such incompatibility would be even more marked between clinopyroxene and chromian spinel, which, in the spinel-assemblage lavas, first crystallized before olivine. The textural evidence is thus fairly convincing that these lavas contain phenocryst and glomerocryst assemblages out of equilibrium with each other, as well as their current hosts. This seems to be contradicted by the occurrence of small olivine and clinopyroxene crystals in the quenched glassy margins of these same samples, but

Table 14. Summary of phenocryst, megacryst, xenolith, and glomerocryst types.

Mainly or entirely plagioclase

- Large glomerocrysts with anhedral crystals ± intergrown olivine (S, C^a)
- Small glomerocrysts of loosely or compactly arranged tabular crystals (S, C)
- Large megacrysts
 - Solid core, skeletal mantle, solid rim (S, C)
 - Non-skeletal (S, C)
- Xenocrysts (C)
- Microphenocrysts of elongate crystals with dendritic terminations (S, C)

Olivine

- Individual euhedra (C) ± Cr-spinel (S)
- Linked multiple euhedra (C) ± Cr-spinel (S)
- Anhedra associated with plagioclase (see large plagioclase glomerocrysts in category above)

Clinopyroxene

- Gabbro xenoliths with plagioclase and cumulus textures (C)
- Partially resorbed phenocrysts ± plagioclase (C)
- Euhedral large phenocrysts (C)
- Microphenocrysts ± plagioclase (C)

Cr-spinel

- Euhedra in groundmass (S)
- Anhedra in other mineral grains (S)
- Skeletal crystals in groundmass (mixed)

^a S, occurs in spinel-assemblage lavas. C, occurs in clinopyroxene-assemblage lavas.

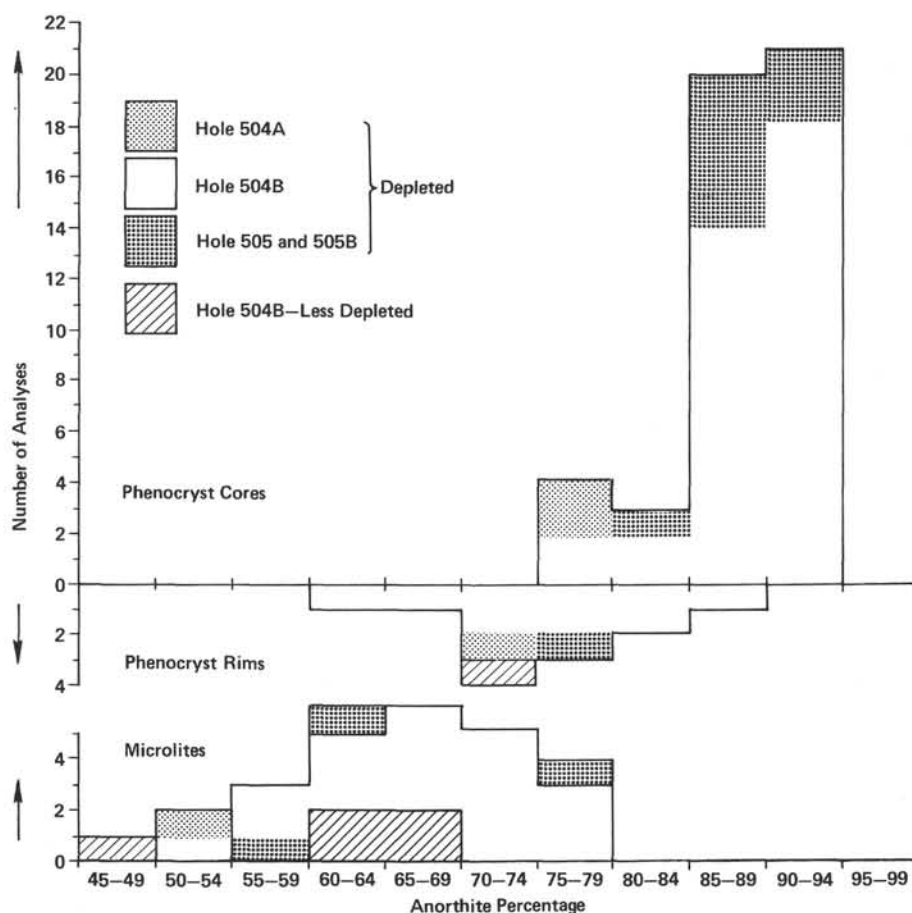


Figure 5. Histogram of reconnaissance plagioclase compositions (Table 5).

here kinetic effects may have been important, allowing olivine to crystallize metastably (e.g., Kirkpatrick et al., 1981). More important than this, however, the large phenocrysts and glomerocrysts crystallized from less fractionated melts than their current hosts, and resorption of clinopyroxene phenocrysts also occurred in magmas of different composition. Thus, mineral assemblages crystallized in equilibrium with the current host need have no bearing on the morphologies of megacrysts, or even necessarily what those minerals are.

There is no evidence that any clinopyroxene phenocrysts represent xenoliths or xenocrysts of the upper mantle. All of them, whether partially resorbed or not, crystallized from magmas after crystallization of small, tabular plagioclases, which they enclose. This is, in essence, a cumulus texture, even if in small crystal aggregates. Furthermore, resorption effects were insufficient to eliminate altogether original crystal outlines which manifestly were those of euhedral phenocrysts, some having high Cr_2O_3 and Al_2O_3 . These may have crystallized at high pressure, but they were not scavenged from the remnants of mantle source rocks.

The absence of Cr-spinel in the clinopyroxene-assemblage lavas of Hole 504B is evidently related to the occurrence of high- Cr_2O_3 clinopyroxenes (Irvine, 1977), although the absence of spinel, even enclosed in minerals of olivine-plagioclase glomerocrysts in Hole 504B

clinopyroxene-assemblage lavas, is a mystery. This evidence suggests that Cr-spinel and clinopyroxene phenocrysts are generally incompatible and that their occurrence in the same sample is unlikely, occurring only when there has been magma mixing. Among our samples only Hole 505 basalts have both, but other basalts having both Cr-spinel and clinopyroxene are known from the Mid-Atlantic Ridge (e.g., Type P₃ basalts of DSDP Hole 395A; Graham et al., 1979). Since there is good mineralogical evidence for mixing in Hole 395A lavas (Dungan et al., 1978), a hybrid origin for the Hole 505 lavas is plausible, although we have not investigated this in detail.

OBJECTIVES OF THE DETAILED SAMPLE STUDY

The detailed sample study was undertaken to investigate mineral interrelationships. The study was to be based upon the small but real differences among the glass groups, guidelines provided by the mineral reconnaissance data, and the petrographic information outlined in the previous section. Objectives were (1) to fill in some obvious gaps in the reconnaissance data, notably the compositions of Cr-spinels; (2) to delineate the compositions of clinopyroxenes occurring as phenocrysts, resorbed phenocrysts, and xenoliths; (3) to determine the compositions of plagioclases intergrown in one

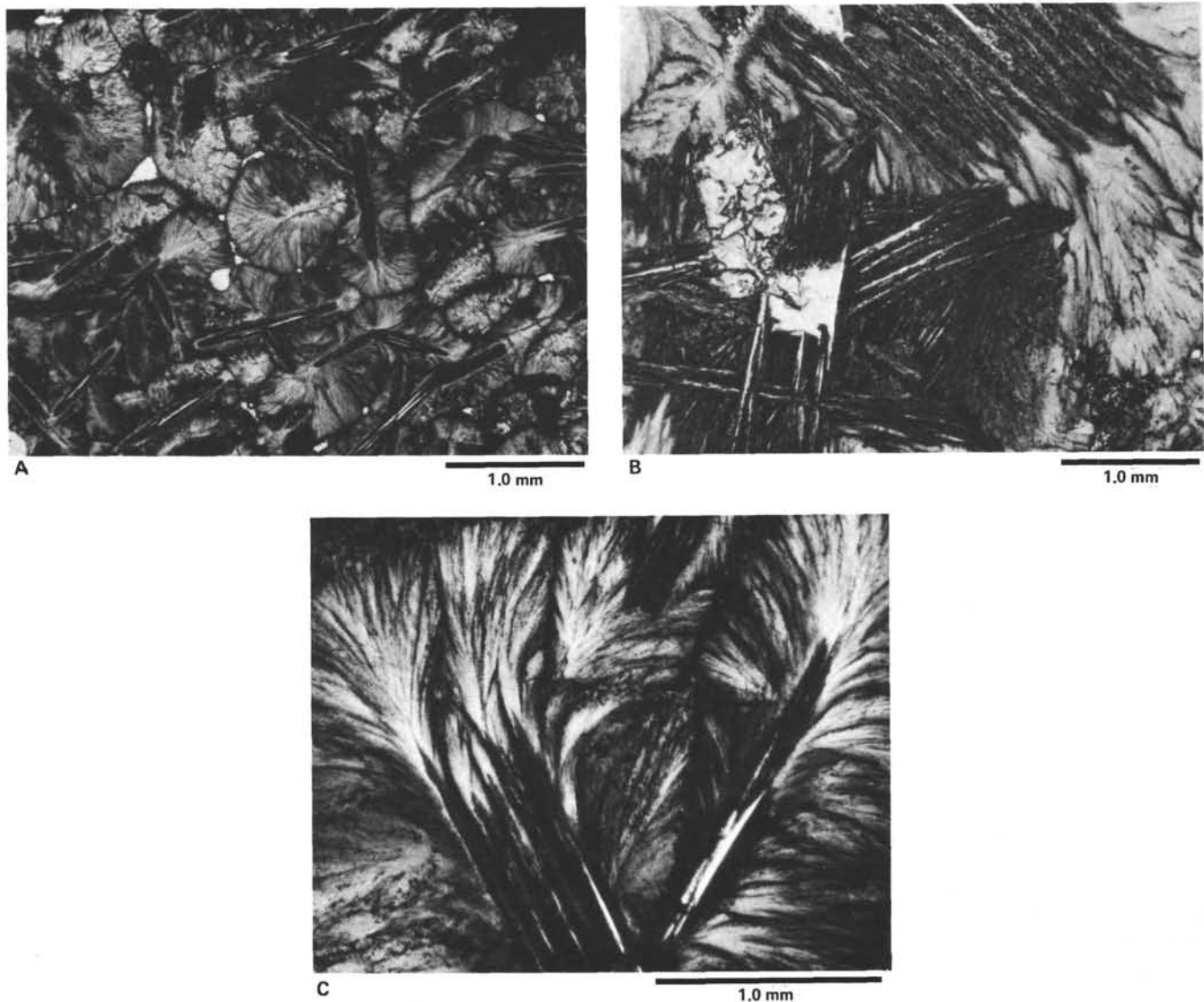


Figure 6. Spherulitic crystal morphologies and groundmass textures in Site 505 basalts. A–C. Sample 505B-3-2, 135–138 cm, plane polarized light. A. Zone of coalesced spherulites and plagioclase microlites. B. Sheaf spherulites and dendrites on a plagioclase crystal. C. Detail of sheaf spherulites radiating from plagioclase dendrites. D. Sample 505B-5-1, 14–17 cm, plane polarized light. Clinopyroxene dendrites and sparse titanomagnetite separated by (altered) glass. F. Sample 505B-5-1, 14–17 cm, crossed nichols. Curving clinopyroxene dendrites (coxcomb morphology) adjacent to larger plagioclase. G. Sample 505B-5-1, 14–17 cm, crossed nichols. Skeletal olivine hopper crystal in microlitic groundmass. The round object is a vesicle filled with clays and calcite.

form or another with olivine and clinopyroxene, and (4) to compare these with the compositions of plagioclases not associated with these minerals.

All four samples studied were thin sections prepared and polished on board *Glomar Challenger*. Two samples from the interval of Group G were studied because together they provided the fullest range of clinopyroxene phenocrysts, resorbed phenocrysts, and xenoliths. In one (Piece 1361), there are several gabbro xenoliths and a number of quite rounded phenocrysts. In the other (Piece 1326), these are rare, but euhedral phenocrysts are common, and fresh olivine occurs in the glass.

The Group B sample studied (Piece 238) is from Hole 501. It was selected partly because glass Groups B and G have essentially identical compositions, as discussed ear-

lier, and partly because this particular sample has glass containing unaltered olivine. A sample from Group J (Piece 287) was studied because of the high Mg/Mg + Fe²⁺ of the associated glass and its position away from the cotectic boundary and toward the olivine apex on Figure 3. The sample itself does not have glass, however.

MINERALS IN GROUP G (clinopyroxene-assembly) SAMPLES

Olivines

Only very tiny quench olivines were preserved unaltered in the two Group G samples studied. Their compositions (Fo_{85.2} and Fo_{85.3}; Table 10) are the most iron rich of all the olivines analyzed, and they are calculated

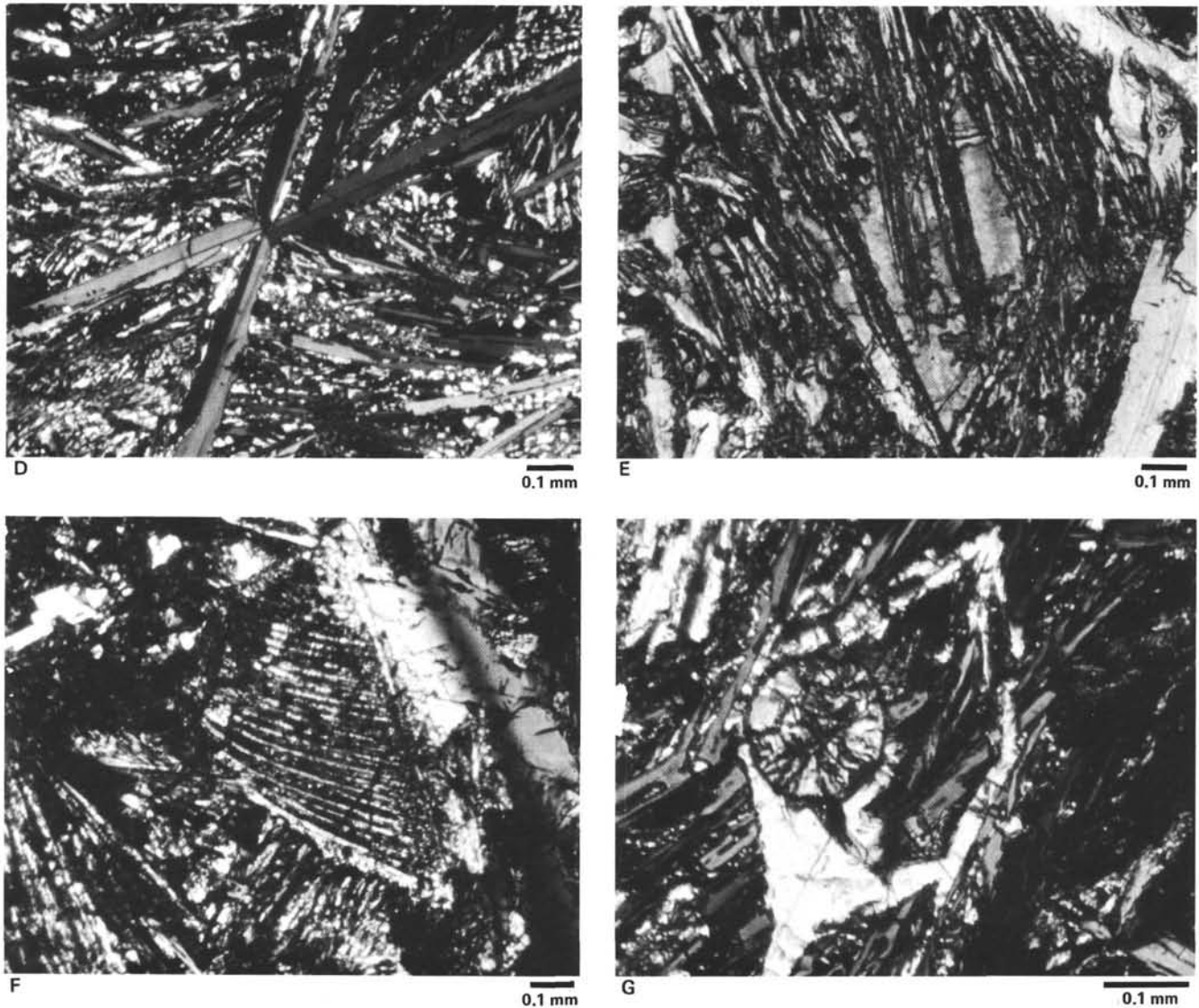


Figure 6. (Continued).

precisely in equilibrium with Group G glass having $Mg / (Mg + Fe^{2+}) = 0.635$ (Table 2) if the equation of Roeder and Emslie (1970) is used and if K_D^{Fe-Mg} is assumed to be 0.30.

Clinopyroxenes

In the samples studied, clinopyroxene spot analyses were obtained from 18 mineral grains. The minerals included clinopyroxenes from two gabbroic xenoliths (those of Figs. 8A and B), one glomerocryst consisting of several large, rounded clinopyroxenes enclosing small, tabular plagioclases, six rounded or partly rounded phenocrysts, two prismatic euhedral phenocrysts, four small angular phenocrysts, and one xenocryst of distinctly more iron-rich composition. They can be divided into two somewhat arbitrary compositional categories: those with high Cr_2O_3 (0.74–1.06%), and those with low Cr_2O_3 (0.11–0.50%). There is no correlation between composition and degree of rounding, since minerals of both categories form both rounded grains and prismatic

or angular euhedral crystals. In fact, the minerals with least Cr_2O_3 are those of the glomerocryst (0.39–0.45%) and the gabbro xenoliths (0.11–0.26%), and these themselves are distinctly rounded. Rounding, therefore, is not restricted to high- Cr_2O_3 clinopyroxenes, and there is no evidence for a mantle origin for them.

The high- Cr_2O_3 group has a very restricted range of compositions. The group is low in FeO^* and high in MgO and CaO , and its members plot close together as calcic endiopsides (Poldervaart and Hess, 1951) in the pyroxene quadrilateral (Fig. 10). The low- Cr_2O_3 clinopyroxenes are more iron rich and augitic, although some fall within the field of the high- Cr_2O_3 group shown on Figure 10.

The presumption that more diopsidic pyroxenes formed from less fractionated melts suggests that a systematic relationship should exist between Cr_2O_3 contents of clinopyroxenes and the compositions of the melts from which they precipitated. Duke (1976) has related the distribution of iron and magnesium between

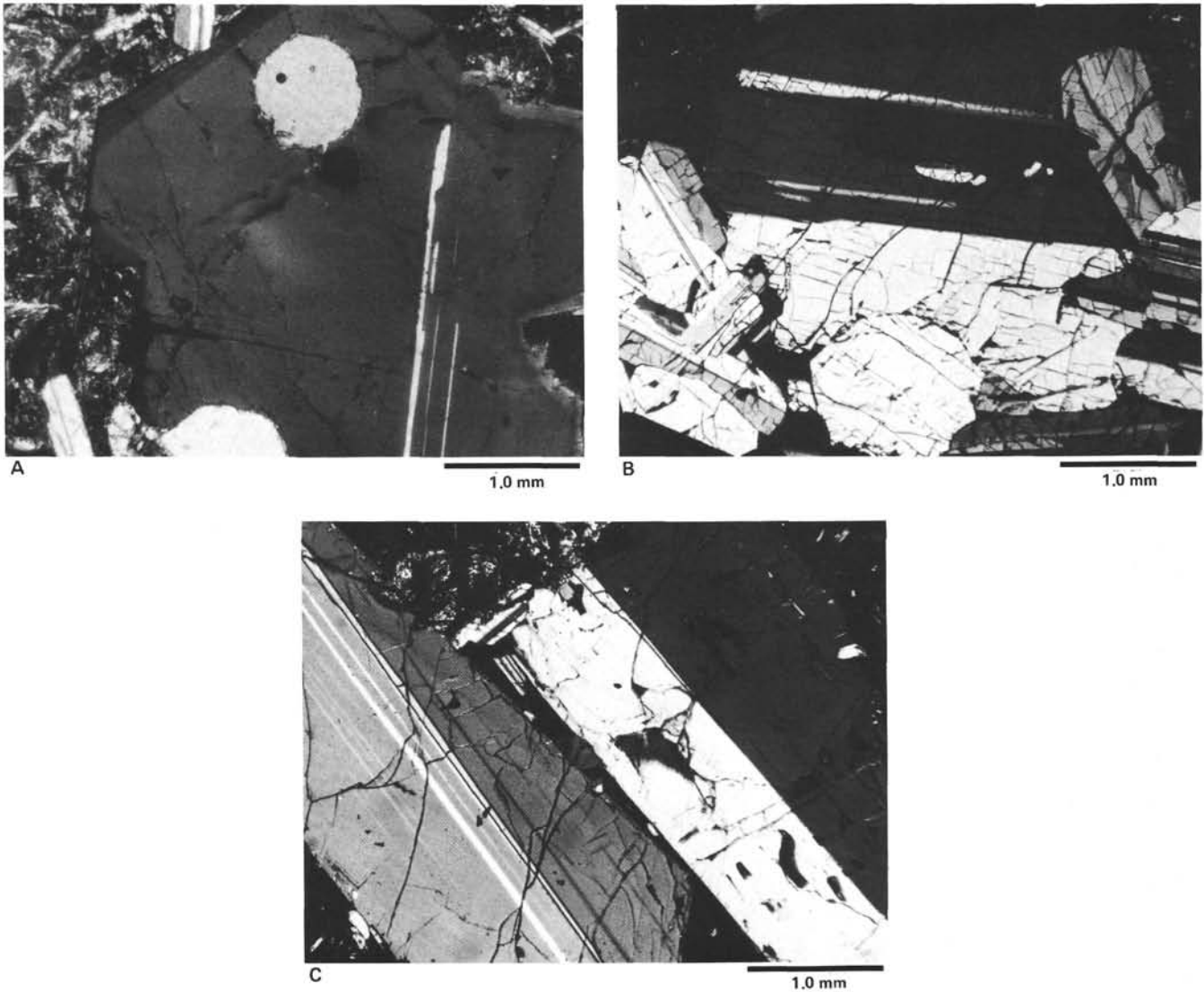


Figure 7. Plagioclase phenocrysts, megacrysts, and glomerocrysts in Costa Rica clinopyroxene-assemblage (CA), spinel-assemblage (SA), and mixed (M) basalts. A. Sample 505-25-1, 28–30 cm (M), crossed nichols. A partly faceted plagioclase phenocryst enclosing both olivine and Cr-spinel, sharply normally zoned at the rim. B. Sample 504B-23-1, 115–118 cm (CA), crossed nichols. A portion of a large plagioclase glomerocryst having accumulus texture. C. Sample 504B-28-4, 12–16 cm (CA), crossed nichols. Two large plagioclase crystals, one a megacryst containing devitrified glass inclusions, the other a xenocryst having external, probable fracture, surfaces at sharp angles to twin planes. D. Sample 505B-3-2, 135–138 cm (SA), crossed nichols. Highly irregular resorbed plagioclase phenocryst. E. Sample 501-15-3, 63–65 cm (SA), plane polarized light. Portion of large plagioclase megacryst showing part of rounded core at lower left, a wide mantle charged with devitrified glass inclusions, and a narrow rim at upper right without such inclusions. F. Sample 505B-3-2, 135–138 cm (SA), crossed nichols. A large plagioclase megacryst with a narrow skeletal zone containing glass inclusions and a narrow irregular rim with dendrites extending parallel to twin planes. G. Sample 504B-24-1, 12–15 cm (CA), crossed nichols. A collection of small tabular plagioclases clumped in parallel, but in which clump each crystal continued to grow after clumping (note curved and irregular boundaries between crystals). H. Sample 504B-24-2, 12–15 cm (CA), crossed nichols. A smaller three-crystal aggregate of plagioclases between two clinopyroxene crystals, one of which is markedly rounded by resorption. I. Sample 505B-3-2, 135–138 cm (SA), plane polarized light. A pair of small, equant plagioclases sharing a crystal face, one with a glass inclusion, and with an olivine crystal attached, sharing the center of a dark spherulite with a smaller plagioclase, itself attached to an olivine enclosing a tiny Cr-spinel. J. Sample 504B-4-2, 80–82 cm (SA), plane polarized light. Small, nearly tabular plagioclases with well developed dendrites paralleling their crystallographic axes.

calcic clinopyroxene and liquid, and we have used his equation (his p. 510) to calculate both the ratio $Mg/Mg + Fe^{2+}$ of liquids in equilibrium with each of the clinopyroxene analyses in Table 11 and a number of the reconnaissance analyses in Table 7. These are plotted against Cr_2O_3 of the pyroxenes in Figure 11. This figure shows clearly that there is a continuum of Cr_2O_3 contents in the calcic pyroxenes, but their Cr_2O_3 content at

first drops off very sharply with the decreasing $Mg/Mg + Fe^{2+}$ calculated for the melt. An approximate average trend is indicated by the solid curved line. It appears that the first, high- Cr_2O_3 clinopyroxenes separated from melts with $Mg/Mg + Fe^{2+} = 0.705$, about the value of the least fractionated glass compositions thus far found among ocean crust basalts, or the values calculated to be in equilibrium with olivines in those samples (cf. Frey

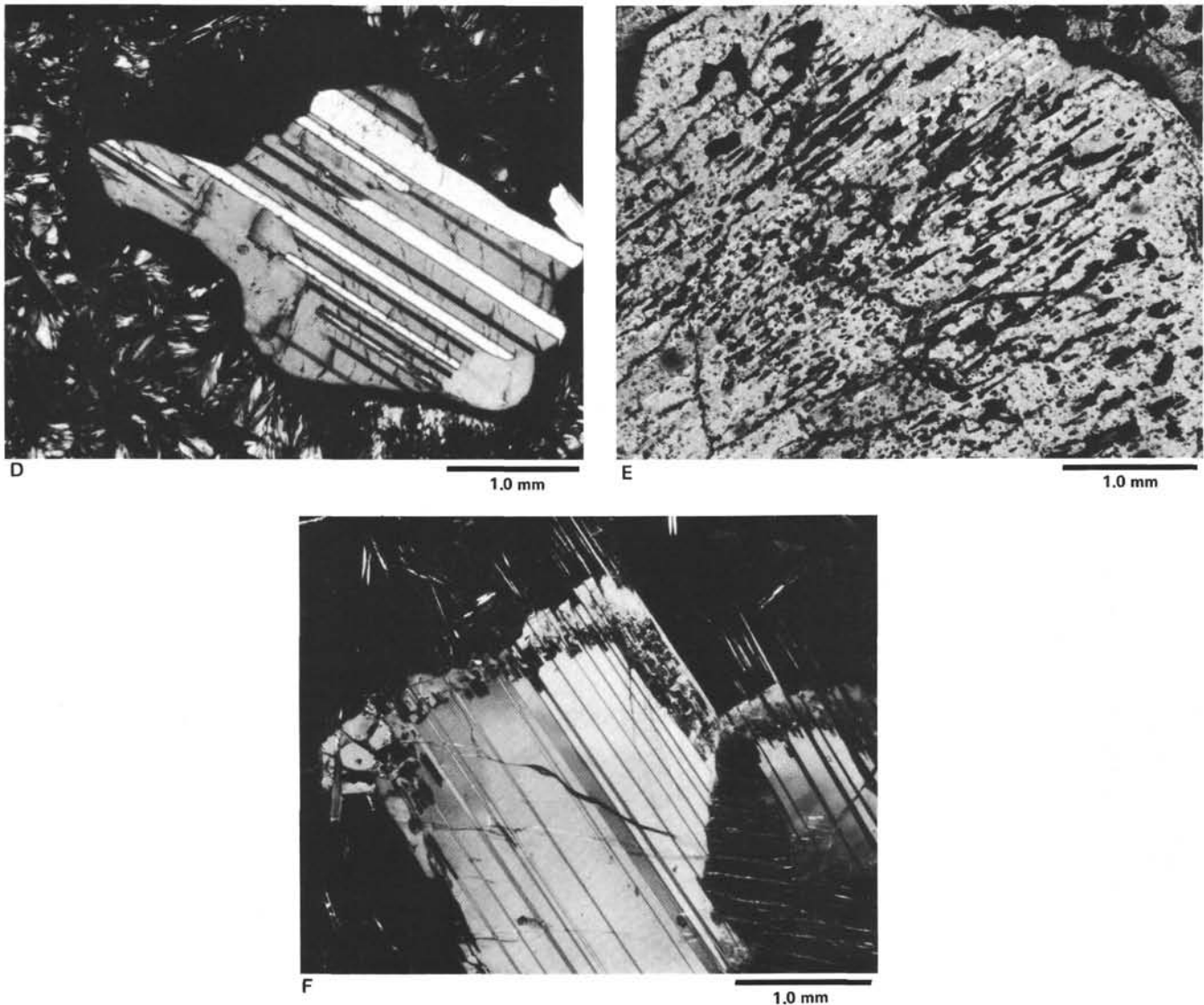


Figure 7. (Continued).

et al., 1974; Rhodes et al., 1979; Presnall et al., 1979; Wilkinson, 1982). If the Roeder and Emslie (1970) relationship is used, the olivine calculated to be in equilibrium with this melt has the composition $Fo_{88.9}$ (compared with the calculated and measured $Fo_{85.3}$ in equilibrium with Group G average glass of Table 2). We have no analyzed olivines from Group G (or other clinopyroxene-assemblage) lavas that are this forsteritic. However, this composition is close to that of several olivines that occur in spinel-assemblage lavas with higher $Mg/Mg + Fe^{2+}$.

There is a general correlation between Al_2O_3 and Cr_2O_3 in the data in Table 12 that is not really evident in previous data on low- and high- Cr_2O_3 clinopyroxenes in abyssal tholeiites, plotted together on Figure 12. Previously reported high- Cr_2O_3 clinopyroxenes almost always have greater than 3% Al_2O_3 , but some low- Cr_2O_3 clinopyroxenes have this much as well. Some authors have interpreted high Al_2O_3 in high- Cr_2O_3 calcic pyroxenes to reflect higher pressures at origin for these minerals than for the low- Cr_2O_3 clinopyroxenes (e.g.,

Donaldson and Brown, 1977; Wilkinson, 1982), although this interpretation may not have been entirely justified by the scatter of previous data. In our reconnaissance data a scatter also exists, but given the wider range of reconnaissance samples analyzed, the scatter may reflect analytical uncertainty or genuine variations caused by natural processes (e.g. kinetic effects). Wilkinson (1982) notes that TiO_2 and Na_2O contents increase in calcic pyroxenes as Cr_2O_3 content decreases, a trend that in general reflects the degree of fractionation. Such effects are evident in the groundmass clinopyroxenes of the reconnaissance data, but no similar inverse correlations exist in the detailed study data, because the range of fractionation represented is so small.

Plagioclases

We have also determined the compositions of plagioclases intergrown in glomerocrysts with low- and high- Cr_2O_3 clinopyroxenes. It was difficult to judge whether the two minerals separated from the same melt (or near-

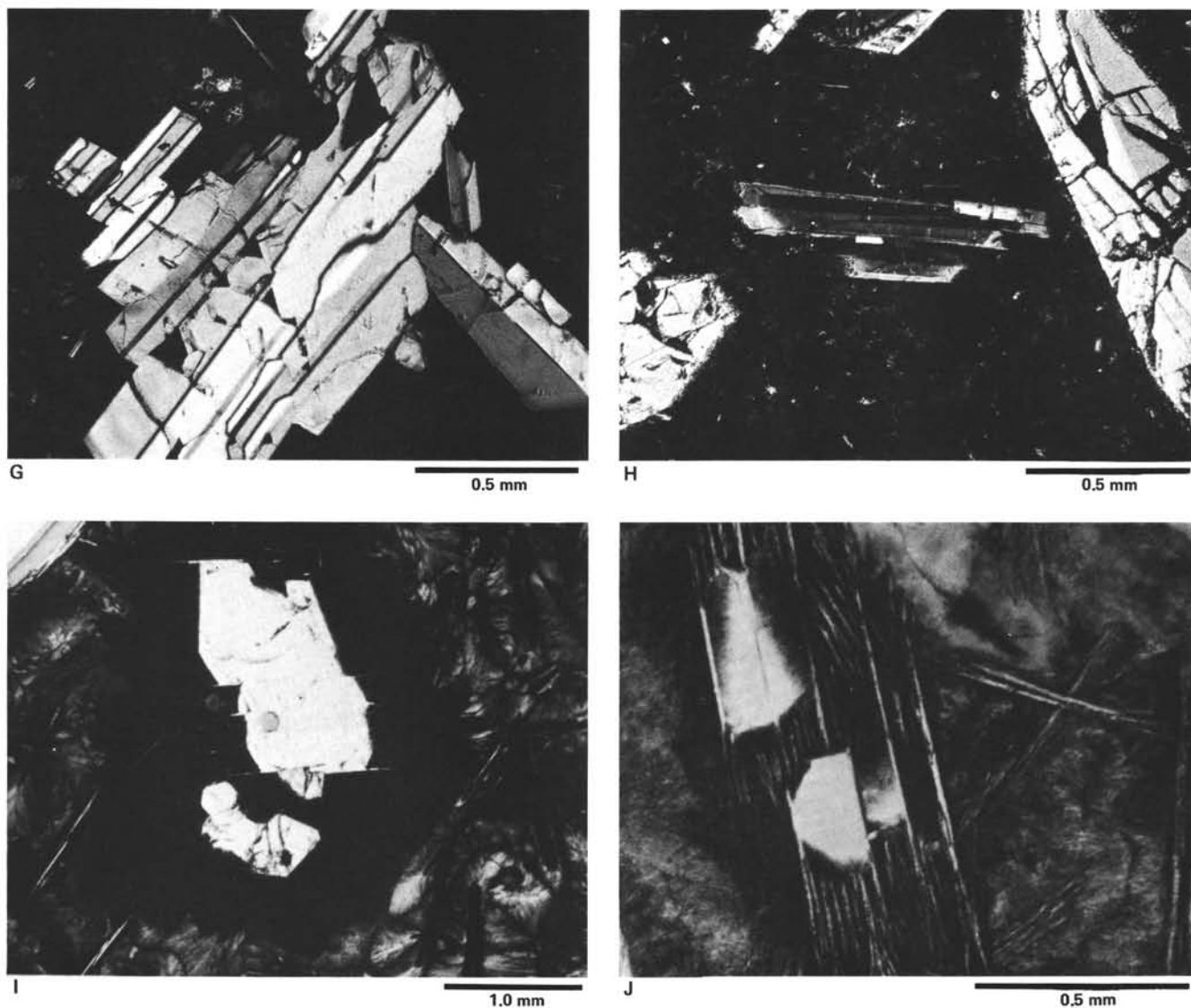


Figure 7. (Continued).

ly so) or whether they formed at two different times and later joined to form glomerocrysts. The circles plotted in Figure 13 are therefore only those for which clinopyroxene demonstrably formed after plagioclase, and thus enclose it. Plagioclases simply attached to, or plated against, clinopyroxenes are plotted as X's. There are consequently few circles plotted in Figure 13, but these show clearly the association of high-MgO, high-Cr₂O₃ clinopyroxene with very calcic plagioclases and the close correlation between compositions of associated clinopyroxenes and plagioclases.

A comparison of Figures 11 and 13 shows that plagioclases in equilibrium with Group G glass should have a composition of about An₇₉. This composition is close to that of the single phenocryst rim for Group G samples in the reconnaissance data (An₇₇, Table 8), but it is far more sodic than the compositions of tiny plagioclase euhedra in glass in the two Group G samples studied in detail (indicated by the lowest bar on Fig. 13). Possibly an insufficient number of these were analyzed. Alterna-

tively, crystallization of plagioclase is readily suppressed at high undercooling (Kirkpatrick, 1979; Lofgren, 1980); hence, even small crystals in glass need not represent crystals in equilibrium with that glass.

More surprising is that the compositions of two plagioclases in large glomerocrysts with (altered) olivine (upper bar, Fig. 13) are more sodic than those intergrown with high-Cr₂O₃ clinopyroxene. We do not know the original compositions of the particular altered olivines, but the most magnesian olivine in Groups K (mixed-assembly) and O (clinopyroxene-assembly) samples is Fo₈₇ (Table 5); that is, it is less magnesian than the olivine calculated to be in equilibrium with the highest Cr₂O₃ (ca. 1.1%), clinopyroxenes (Fo_{88.9}; Fig. 11). The crystallization sequence was plagioclase, clinopyroxene, and then olivine. Olivine and clinopyroxene do not occur together in any glomerocryst, and, as mentioned earlier, they seem to be incompatible, with clinopyroxenes especially strongly resorbed in basalts with abundant olivine.

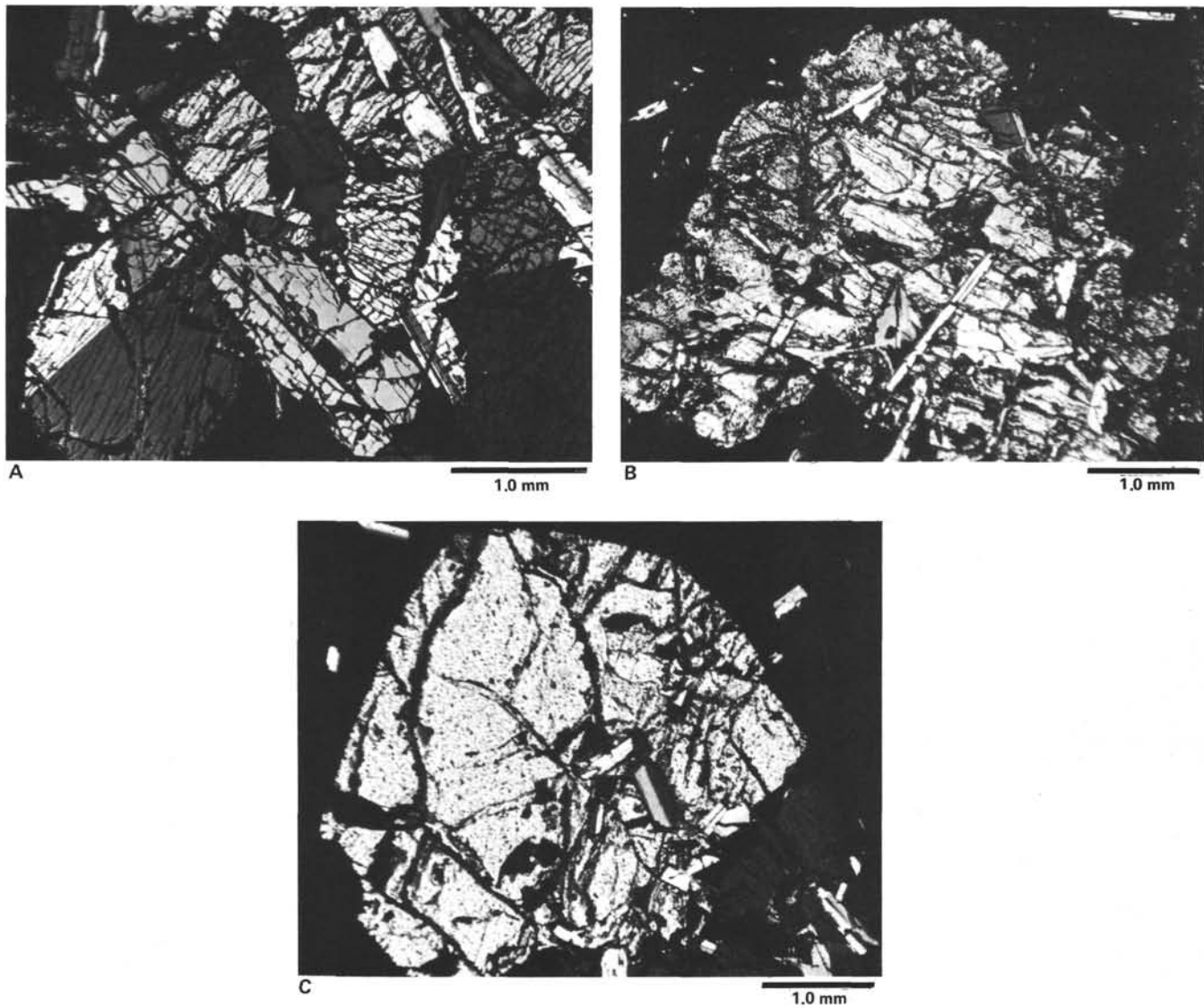


Figure 8. Clinopyroxene phenocrysts, megacrysts, xenocrysts, and gabbro xenoliths in clinopyroxene assemblage basalts, all with nichols crossed. A and B are gabbro (clinopyroxene-plagioclase) xenoliths in Sample 504B-24-2, 58–62 cm (Piece 1361 of detailed study). C. Sample 504B-24-1, 12–15 cm. Rounded clinopyroxene megacryst enclosing plagioclases. D. Sample 504B-23-1, 115–118 cm (Piece 1326 of detailed study). Distinctly rounded clinopyroxene megacryst partially plated and rimmed with attached plagioclases. E. Sample 504B-24-1, 12–15 cm (Piece 1361). Clinopyroxene-plagioclase glomerocryst with the plagioclases both enclosed by and attached to the clinopyroxene. F. Sample 504B-23-1, 115–118 cm (Piece 1326). Large, nearly euhedral clinopyroxene phenocryst enclosing a small, tabular plagioclase. G. Sample 504B-24-1, 12–15 cm (Piece 1361). Euhedral twinned clinopyroxene phenocryst largely enclosing a small tabular plagioclase.

Summary

Hypotheses for the origin of clinopyroxene-assemblage basalts thus must account for the following relationships, some of which are apparently contradictory: (1) lack of Cr-spinel, even in olivine-plagioclase glomerocrysts; (2) early separation of high-MgO, high-Cr₂O₃ calcic pyroxene from high-Mg melts; (3) continuous crystallization of pyroxenes, sharply decreasing in Cr₂O₃ as melt Mg/Mg + Fe²⁺ decreases only slightly; (4) coexistence of high-Cr₂O₃ clinopyroxenes with very calcic plagioclases, which become more albitic as Cr₂O₃, Al₂O₃, and MgO all drop in associated clinopyroxenes; (5) evidence for formation of olivine also with calcic plagioclases, but not as calcic as those formed in associ-

ation with clinopyroxenes; (6) no indication from glomerocrysts that olivine and clinopyroxene precipitated together; (7) evidence for considerable resorption of clinopyroxene phenocrysts, glomerocrysts, and gabbroic xenoliths of all ranges of composition, particularly pronounced in samples containing olivine-plagioclase glomerocrysts; and (8) occurrence of gabbro xenoliths and xenocrysts containing clinopyroxenes more iron-rich, and plagioclases more albitic, than those in equilibrium with host glass compositions.

MINERALS IN GROUPS B AND J (spinel-assemblage) SAMPLES

Although glass Groups B and J have similar phenocryst assemblages, they have different geochemical char-

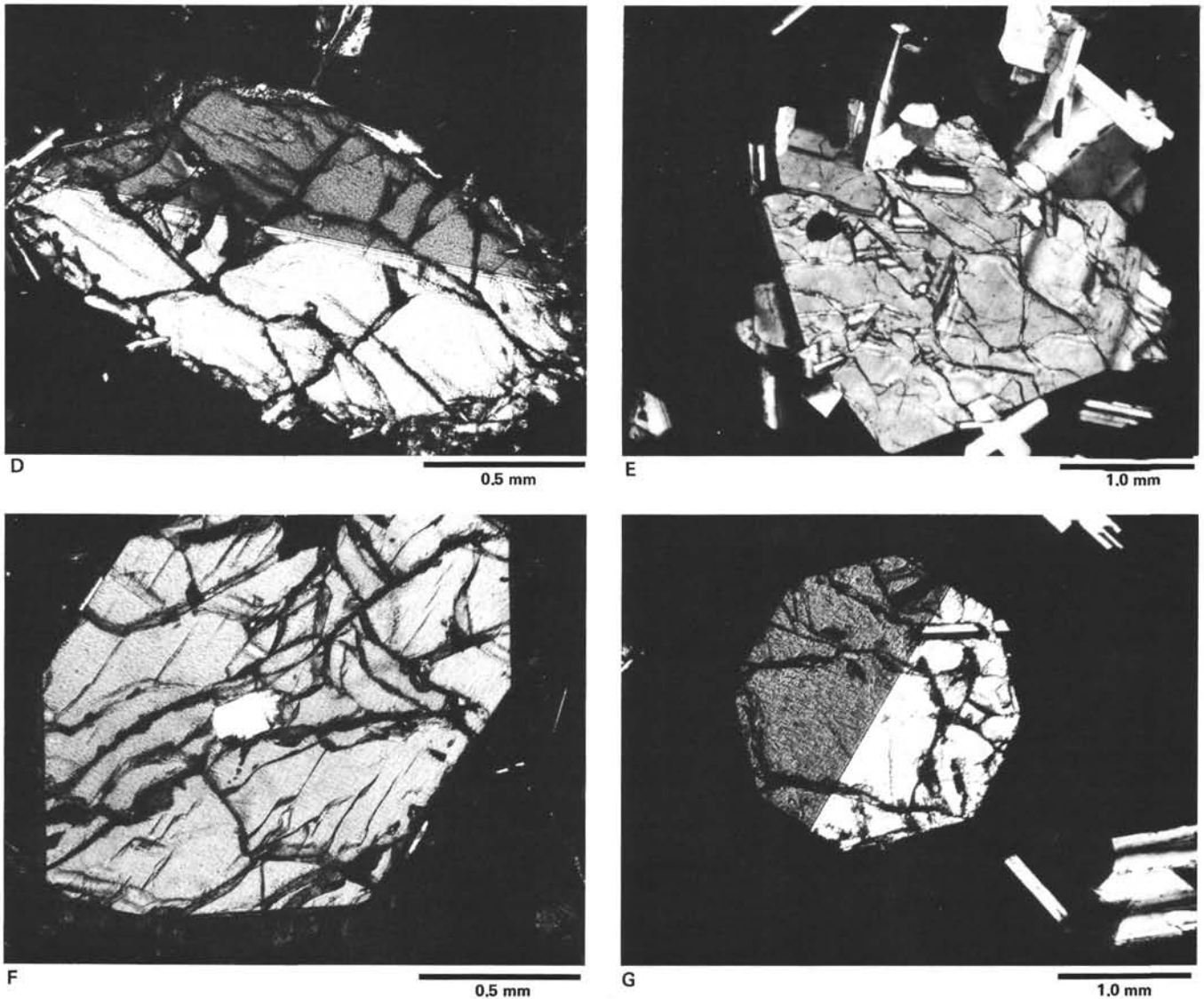


Figure 8. (Continued).

acteristics (Table 3), exemplified by their rather great separation on the ternary normative diagrams (Figs. 3 and 4). One might therefore expect the minerals in samples of these two groups to differ in composition, a difference that might cause one to consider again the possibility that the more evolved Group B lavas derived from a parental magma similar in composition to that of Group J. The possibility seems unlikely on the basis of the glass compositions alone, but the mineral data may still provide support for it.

Olivines

The olivine compositions are slightly different; the sample from Group J averages 1.5 mol% Fo greater than the sample from Group B. If the Roeder and Emslie (1970) relationship is used and K_D is assumed to be 0.30, Group B liquid should have been in equilibrium with olivine of composition Fo_{85.8}, slightly less magnesian than measured in phenocrysts (Fo_{86.3-87.0}). The most magne-

sian olivine should have been in equilibrium with liquid having $Mg/Mg + Fe^{2+} = 0.667$. The most magnesian olivine in the Group J sample calculates to be in equilibrium with a liquid with $Mg/Mg + Fe^{2+} = 0.725$, and the average (which is probably more appropriate to use in a comparison, inasmuch as it allows for some analytical imprecision) in equilibrium with a liquid having $Mg/Mg + Fe^{2+} = 0.710$ (compared with host glass, 0.689).

Cr-Spinels

Chrome spinels show much wider variation, and contrast strongly between the two samples. $Mg/Mg + Fe^{2+}$ in the spinels is plotted versus $Cr/Cr + Al$ in Figure 14. The Group J sample includes one spinel with low $Cr/Cr + Al$ (≈ 0.3), another with $Cr/Cr + Al$ slightly higher, and one remarkable grain in which this ratio ranges across it from 0.31 to 0.47. As $Cr/Cr + Al$ increases in this grain, its $Mg/Mg + Fe^{2+}$ drops. The higher $Cr/Cr + Al$ values in part of this single grain are comparable

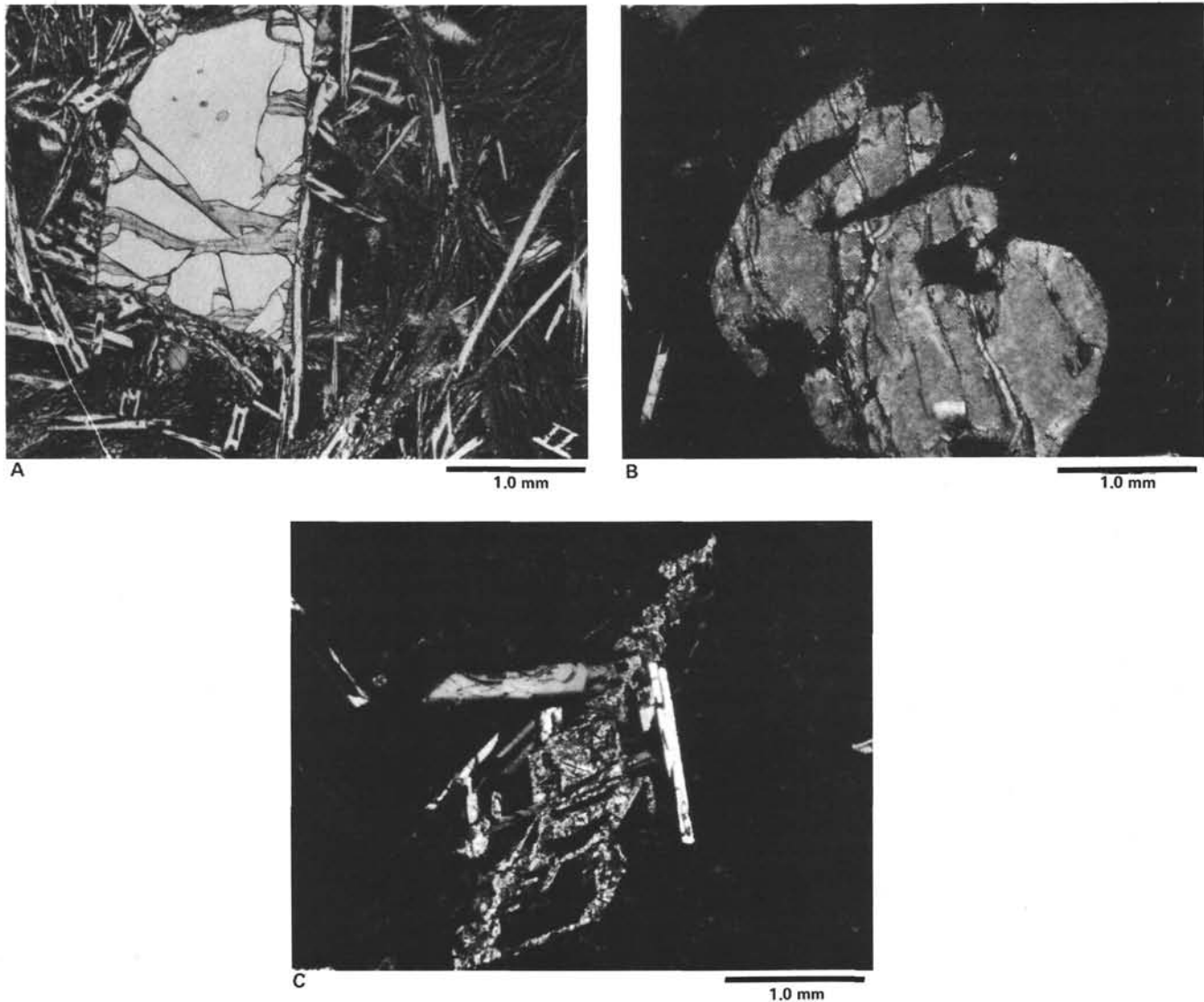


Figure 9. Olivines and spinels in Costa Rica Rift basalts. All photomicrographs except B are of spinel-assembly basalts. A. Sample 505B-5-1, 14–17 cm. Plane polarized light. A granular olivine phenocryst partly altered to clay minerals, in a microlitic groundmass. B. Sample 505-26-1, 33–35 cm, mixed-assembly basalt, crossed nichols. A large, fresh olivine phenocryst showing the typical rounded and embayed morphology characteristic of skeletal growth at moderate undercooling. C. Sample 504B-4-5, 87–89 cm, crossed nichols. An entirely altered olivine replaced by clays, but maintaining a strikingly skeletal morphology. D. Same sample as C, plane polarized light. A tiny euhedral olivine set in glass with wisps of spherulitic material next to the crystal, which contain several fluid inclusions. E. Sample 505B-3-1, 76–79 cm, plane polarized light. A typical small euhedral Cr-spinel in a fairly crystalline basalt, near a segregation vesicle with spherulitic texture in the material lining the vesicle. Pale clay minerals coat the vesicle interior. F. Sample 504B-4-5, 87–89 cm, combined plane polarized and reflected light. Spherulitic material in glass nucleating upon euhedral Cr-spinel. G. Same sample as F, away from glass, plane polarized light. Large euhedral Cr-spinel with round inclusions of spherulitic material. H. Sample 505B-3-2, 135–137 cm, and I. Sample 505B-5-1, 14–17 cm, both in reflected light. Large euhedral, but highly skeletal Cr-spinels.

to those of all three spinels analyzed from the Group B sample, except that those are displaced to the right on Figure 14, to lower $Mg/Mg + Fe^{2+}$.

The aluminous Group J spinels approach the compositions of the Mid-Atlantic-Ridge Group I chromian spinels (Fig. 14) of Sigurdsson and Schilling (1976), which they believe crystallized at high pressure, and which Wilkinson (1982) includes among the high-pressure minerals found in abyssal tholeiites. The Group B spinels (and Group P spinels reported in Furuta and Tokuyama [this volume], indicated by the dashed boundary in Fig. 14)

correspond to the magnesiochromite Group II low-pressure spinels of Sigurdsson and Schilling (1976).

The three solid arrows labelled EPR-1, EPR-2, and EPR-3 on Figure 14 are average trends for the range of spinels found in three separate samples from the Siqueiros Fracture Zone at $8^{\circ}30'N$ near its intersection with the crest of the East Pacific Rise (Natland and Melchior, unpublished data). From left to right on the diagram, the arrows show that the spinels followed three separate crystallization paths. They precipitated from liquids systematically lower in $Mg/Mg + Fe^{2+}$ (0.71 for EPR-1 to

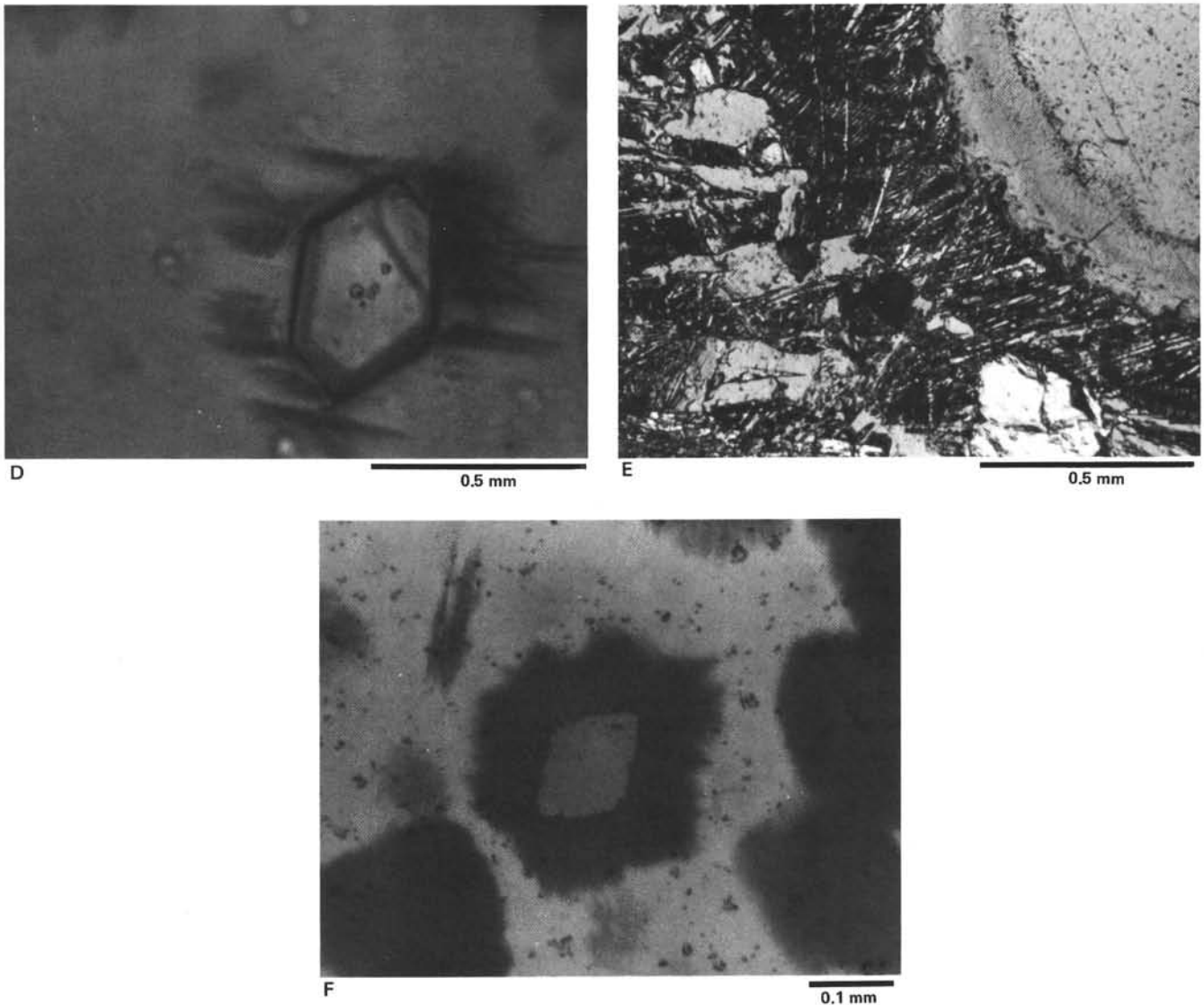


Figure 9. (Continued).

0.65 for EPR-3), essentially bridging the gap between chromian spinels (near Group I) and magnesiochromites (Group II) seen in the Mid-Atlantic-Ridge samples. Such parallel trends have been predicted to occur on the basis of thermodynamic calculations (e.g., Dick and Bullen, in press). The field for the Group J analyses, which is dominated by the wide range of compositions in a single spinel, parallels these trends and is quite similar to that of EPR-1, which was obtained from spinels in a strongly olivine-phyric picrite of the oceanite type (Natland, 1980a). The average of glass compositions obtained from several pillow rims of this oceanite (glass Group D of Natland and Melson, 1980) is shown in terms of normative components as an asterisk in Figure 3. It plots very close to the position of Costa Rica Rift glass Group J of Table 2. We thus can infer a broadly similar origin for the two, including the possibility that Group J stemmed from an originally picritic parental composition, even though it differs in some aspects of chemistry and in location. The sample we investigated from Group

B is evidently too fractionated to preserve relict high-pressure aluminous spinels, but the EPR trends seem to indicate that the Group B spinels would plot to the right of the Group J spinels on Figure 14.

This interpretation also suggests that the fairly broad range of magnesiochromites found in Group P (Site 505) samples by Furuta and Tokuyama (this volume) is atypical and may have been produced by magma mixing. The dashed arrows within the Group P spinel field on Figure 14 indicate that separate trends occur in the Site 505 spinels enclosed in olivines and plagioclases. The inset diagram in Figure 14 shows how these trends may have resulted from mixing of two distinct spinel-assemblage magmas, each of which on its own would crystallize spinels with different $Mg/Mg + Fe^{2+}$ but the same $Cr/Cr + Al$. Continued spinel crystallization as mixing occurred, we propose, flattened the trends to those in the inset indicated by 3A (enclosed in olivine), 3B (enclosed in plagioclase) and 3C (groundmass spinels). 3B is particularly flat and even shows a reduction

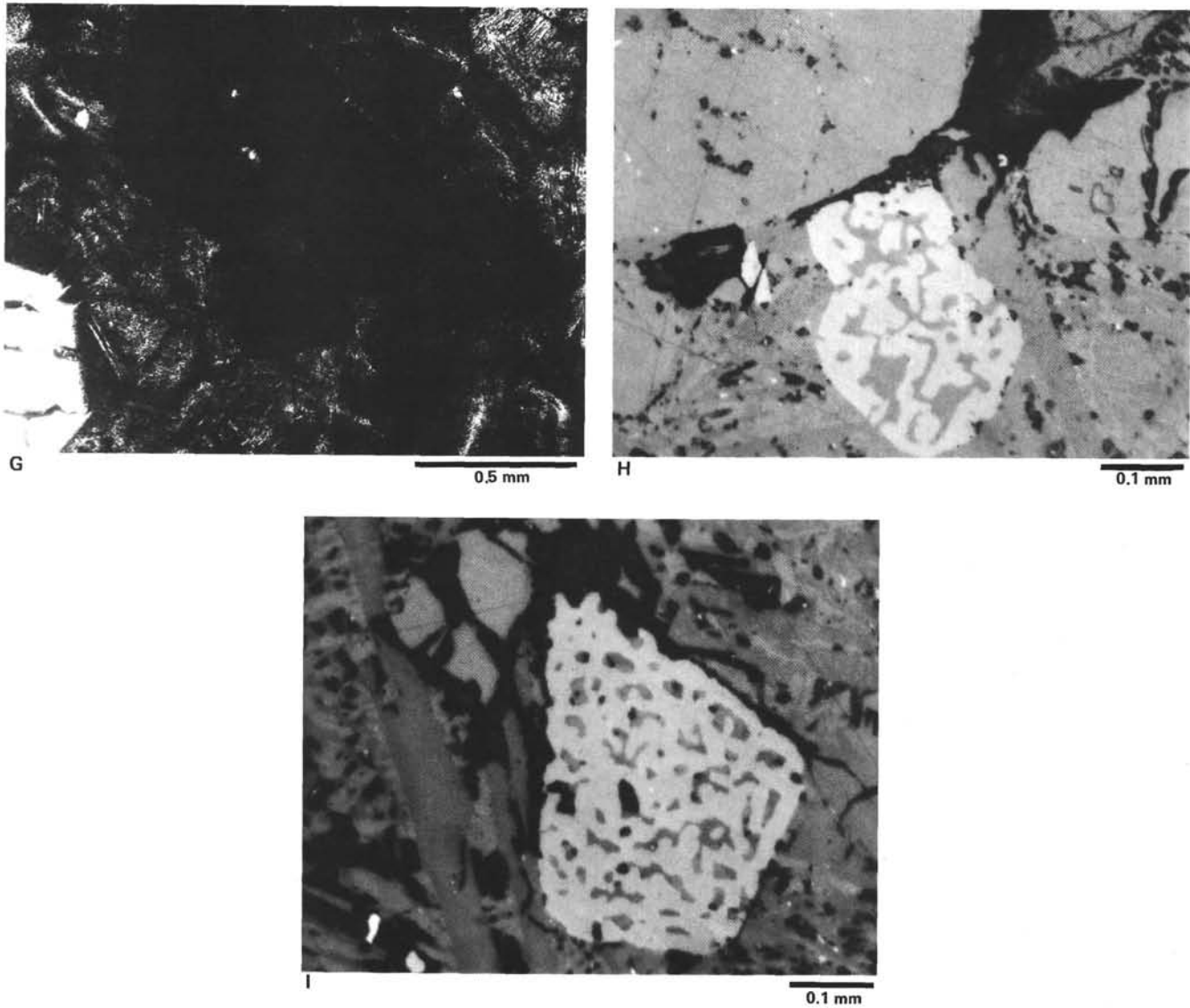


Figure 9. (Continued).

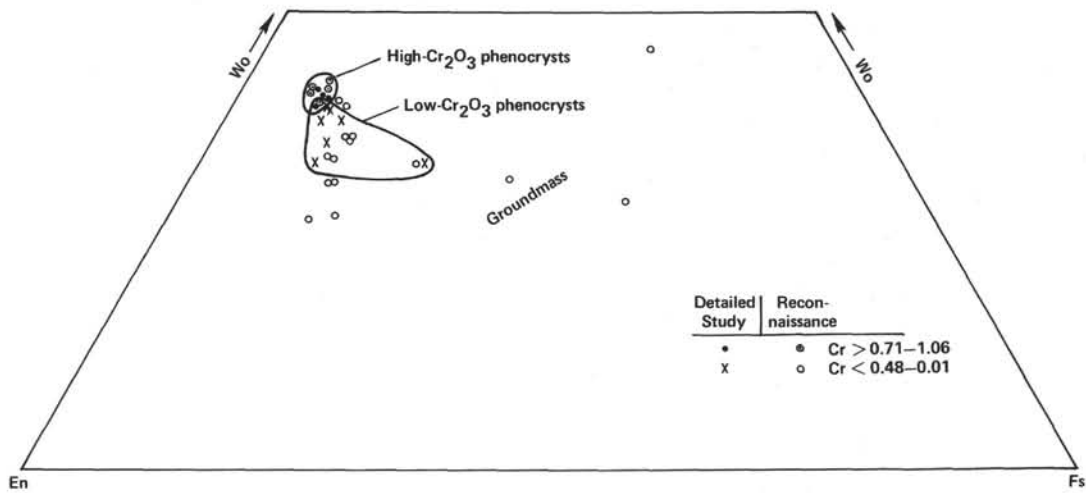


Figure 10. Pyroxene quadrilateral giving proportions of Wo, En, and Fs calculated from structural formulae of reconnaissance (Table 7) and detailed study (Table 12) clinopyroxenes.

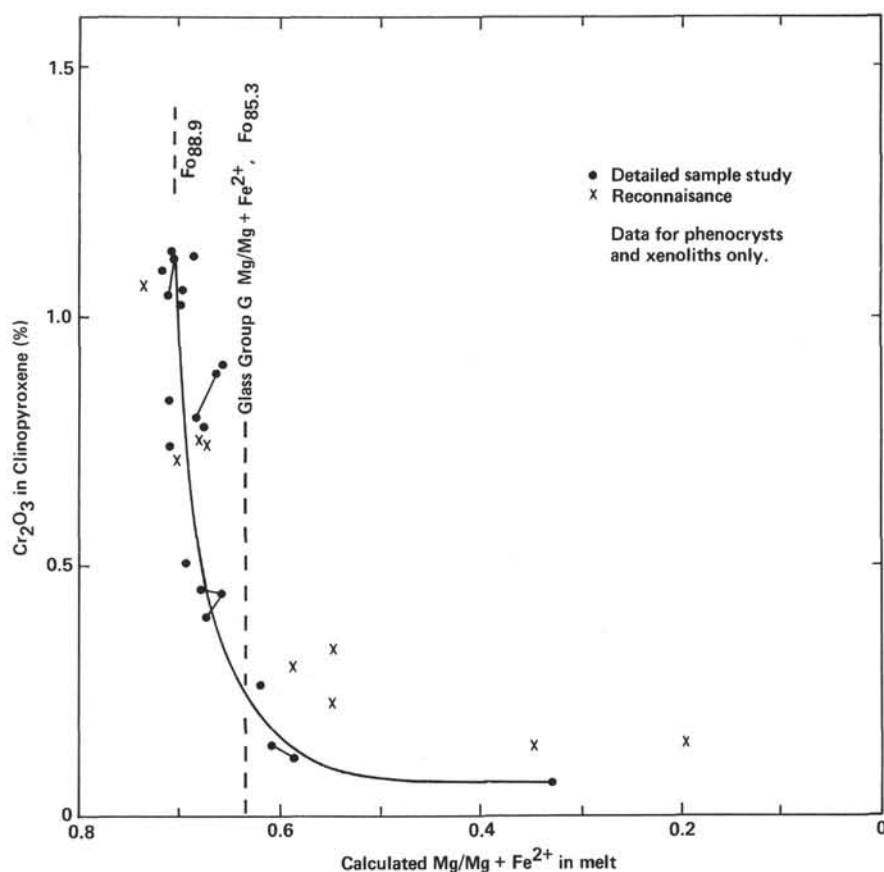


Figure 11. Cr_2O_3 in reconnaissance (Table 7) and detailed study (Table 12) clinopyroxenes versus $\text{Mg}/\text{Mg} + \text{Fe}^{2+}$ of melts calculated to be in equilibrium with them using equation of Duke (1976). The left vertical dashed line is taken as the average melt ($\text{Mg}/\text{Mg} + \text{Fe}^{2+} = 0.705$) in equilibrium with the cluster of clinopyroxenes with $\text{Cr}_2\text{O}_3 > 1.0\%$. The composition of olivine calculated to be in equilibrium with this glass is $\text{Fo}_{88.9}$. The right vertical dashed line is the $\text{Mg}/\text{Mg} + \text{Fe}^{2+}$ of Glass Group G (from Table 2), which is calculated to be in equilibrium with olivine having $\text{Fo}_{85.3}$ composition.

in $\text{Cr}/\text{Cr} + \text{Al}$ with decreasing $\text{Mg}/\text{Mg} + \text{Fe}^{2+}$, because plagioclase competes during crystallization with magnesiochromites for Al (Furuta and Tokuyama, this volume).

The contrast in spinel compositions between the Group J and Group B samples further corroborates the inference from glass compositions that the two magma types were not related by crystal fractionation. Chemically similar but mineralogically distinct spinel-assemblage magma types arose beneath the Costa Rica Rift as they did in the Siqueiros Fracture Zone near the East Pacific Rise. They followed separate crystallization histories until they arrived at shallow magma reservoirs. In some cases (e.g., Group P), the primary characteristics of the magma batches were incompletely blurred by mixing. Such processes have often been inferred for other spreading ridges, particularly the Mid-Atlantic Ridge, from lava geochemistry and mineral data (e.g., Dungan and Rhodes, 1979; Rhodes et al., 1979). But here, we have obtained both mineral and geochemical evidence that these processes acted on distinctive magma types, only very subtly different chemically, and occurring as lavas now in the same DSDP hole.

Plagioclases

The Group J sample analyzed contained no large plagioclase megacrysts intergrown with olivine or glass inclusions. Plagioclase phenocrysts have compositions $\text{An}_{85.6-88.9}$, and a groundmass plagioclase microlite has composition $\text{An}_{80.7}$. The analyzed Group B sample contains a very large plagioclase megacryst with a solid core and rim but a highly skeletal mantle between the core and rim (Fig. 8E). There are also two smaller but similarly skeletal plagioclase phenocrysts and a number of tabular plagioclase phenocrysts and small glomerocrysts without glass inclusions. Two of the skeletal phenocrysts show reverse zoning, from about An_{87} to $\text{An}_{90.5}$ (Table 12), and the glass inclusions are trapped basaltic melts (Table 13). The formation of these huge megacrysts with glass inclusions is a complex process that warrants careful consideration.

Glass Inclusions in Plagioclases

The compositions of the glass inclusions suggest intricate crystallization histories for the megacrysts. They are quite heterogeneous, they have high $\text{Mg}/\text{Mg} + \text{Fe}^{2+}$

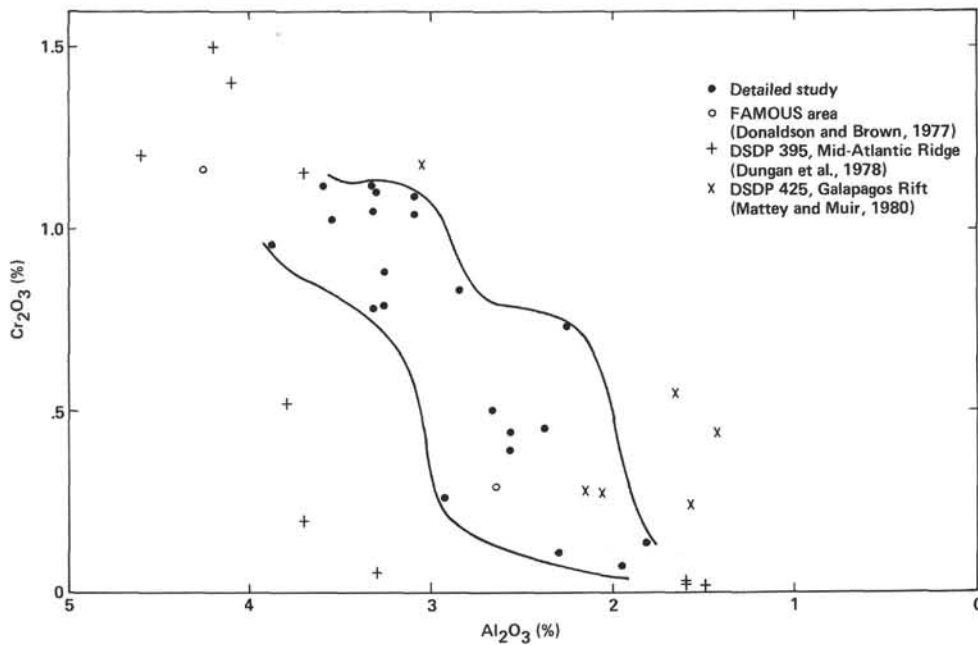


Figure 12. Al_2O_3 versus Cr_2O_3 for detailed study clinopyroxenes (Table 12). There is a broad correlation (indicated by the wavy bounding lines) more evident in the Hole 504B samples than samples from previous studies, also plotted on the diagram.

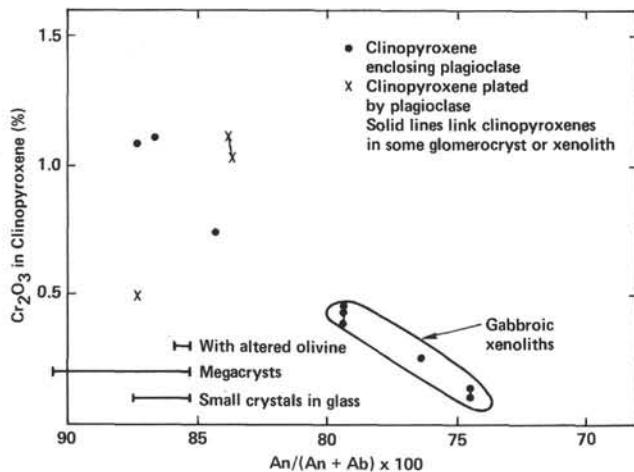


Figure 13. Cr_2O_3 contents of clinopyroxenes plotted against $\text{An}/(\text{An} + \text{Ab}) \times 100$ of plagioclases either enclosed in (dots) or plating (x's) the clinopyroxenes. Solid lines link compositions of clinopyroxenes in the same glomerocrysts or xenoliths. Bars give ranges of plagioclase compositions (from top down) coexisting with altered olivine, occurring as isolated megacrysts, or occurring as small crystals in glass (all data from detailed study, Tables 11 and 12).

and low $\text{CaO}/\text{Al}_2\text{O}_3$, and several of them have unusually high K_2O and P_2O_5 compared with the composition of the glass margin measured in the same sample (Column 1 of Table 13B, which compares favorably to the average of Group B in Column 2).

The heterogeneity is unlikely to stem from variations in composition across the inclusions induced by spherulitic crystallization within them, because the probe beam was defocused to a spot 10 or 15 microns in diameter, depending on the size of the inclusion. The spherulites in the inclusions are plagioclases, which would tend to

produce both high Al_2O_3 and CaO values if the beam diameter were too small. Although some of the inclusions have high Al_2O_3 , there is no correlation of this with CaO .

Additional heterogeneity might have resulted from continued crystallization of plagioclase from the inclusions following entrapment. However, the microphenocrysts in the glass (An_{87}) are as sodic in composition as the portions of the megacrysts near the inclusions. Melt temperatures seem to have dropped only slightly between the entrapment of inclusions and the quenching of pillow rims, so additional plagioclase would not have crystallized from the inclusions.

The probable reason for the high K_2O and P_2O_5 contents and other variations in composition is that the inclusions were trapped during periods of skeletal crystal growth, that is, during some interval of supercooling of the melt. The diffusion of species in the melt was inhibited by increased melt viscosity (Kirkpatrick, 1975) and caused those species that contained cations rejected during the formation of the plagioclase crystals to become highly concentrated in the parts of the melts next to the crystals. These melts later became trapped between the arms of growing dendrites. Relative enrichments were greatest for those species with lowest diffusion coefficients (the large cations in general, and probably potassium in particular, because of its affinity for tetrahedrally coordinated Al in the melt [Bottinga and Weill, 1972]). For potassium cations, enrichments approached a factor of 20 in some inclusions. Also, since the crystallizing plagioclase had low SiO_2 contents ($\sim 45\%$), relatively high SiO_2 abundances built up in melts adjacent to the crystals. For this reason, the normative projections of even those melt inclusions with lowest K_2O plot far toward the silica apex on Figure 3, making that projection

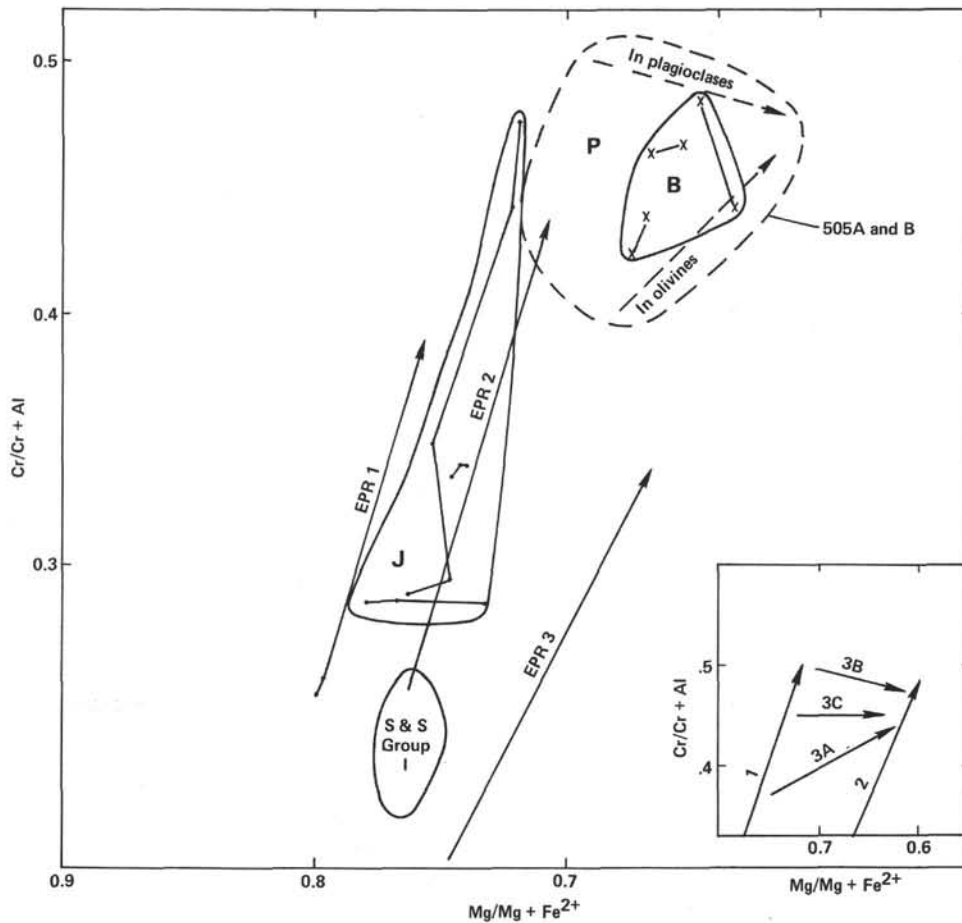


Figure 14. Cr/Cr + Al versus Mg/Mg + Fe²⁺ for Cr-spinels analyzed in Groups J (dots) and B (x's) detailed study samples (Table 9). Data points linked by lines are from the same mineral grain. Dashed field boundary and arrows are based on Group P (Site 505) spinel compositions reported by Furuta and Tokuyama (this volume). The boundary for S and S Group I is from Sigurdsson and Schilling's (1976) high-Al spinels in Mid-Atlantic Ridge FAMOUS region basalts. See text for discussion of EPR trends and inset diagram.

useless for attempting to infer the conditions of origin of the inclusions, or for relating them to host glass compositions.

However, ratios of excluded species already in high concentration in the melt probably did not change greatly. Therefore the values of Mg/Mg + Fe²⁺ for inclusions in Table 13 should be reasonably representative of those in the original melts. All of the values are higher than that of host glass Group B (0.645), and two of them have values near 0.72, nearly identical to those calculated to be in equilibrium with the most magnesian olivines analyzed (in the Group J samples).

Ratios of species strongly concentrated in the plagioclase will be modified according to the partition coefficients of the particular cations. The crystallization of plagioclase with low CaO/Al₂O₃ (~0.5) should increase this ratio in the adjacent melt, if it is higher than that in the melt to begin with. Thus the low values of CaO/Al₂O₃ for the melt inclusions in Table 13 compared with the host glass were probably even lower to begin with.

The concentrations of cations in moderate abundance in the melt, and either moderately or strongly excluded

from the plagioclase, are probably enriched in the glass inclusions. Thus, both Na₂O and TiO₂ contents were probably originally lower in the original glass than in the present inclusions. In the two inclusions with the least K₂O (Pieces 1 and 6 in Table 13), the TiO₂ abundances should be closest to their original concentrations. Not surprisingly, these are the two largest inclusions analyzed and have the highest Mg/Mg + Fe²⁺.

What is peculiar about the melt inclusions, in spite of all these potential complications, is the heterogeneity expressed by the ratios CaO/Al₂O₃ and Mg/Mg + Fe²⁺, even in the same plagioclases. It is difficult to imagine how such variety could arise from crystal growth in a homogeneous melt, even one suddenly supercooled. Kuo and Kirkpatrick (1982) have argued that similar inclusions in the mantles of plagioclases in Mid-Atlantic-Ridge basalts from DSDP Sites 395 and 396 resulted from injection of magmas carrying plagioclases into cooler melts crystallizing more sodic plagioclases. Both the diffusion effects evident in our inclusions and the ranges of their CaO/Al₂O₃ and Mg/Mg + Fe²⁺ ratios support a similar interpretation here. During such supercooling,

diffusion rates would be suppressed, and the enrichments in K_2O and P_2O_5 would result. Before mixing was complete, the plagioclases could come into contact with both end-member melt compositions and a variety of hybrids that would be reflected in different major cation ratios. However, in Kuo and Kirkpatrick's (1982) samples, such plagioclases are normally zoned, whereas here they are reversely zoned. Moreover, such mixing beneath the Costa Rica Rift was between magmas with very little-fractionated compositions, to judge from the highly calcic compositions of the plagioclases and the compositions of the melt inclusions themselves. In the Mid-Atlantic-Ridge samples, compositional differences between the mixing magmas were greater.

The reverse zoning can be explained by the mixing of magma carrying crystals formed at high pressure with magma carrying crystals formed at lower pressure. Given that the magmas had very similar compositions, the plagioclases formed at high pressure would be more sodic than those formed at low pressure (Lindsley, 1968; Yoder, 1969). Therefore, the solid cores of the megacrysts could have formed in the deeper magma, and the inclusion-filled mantles could have grown when the host magma was injected into a shallower magma reservoir, even though the magma compositions were very similar. However, we cannot appeal to significant differences in magma composition, hence temperature, to produce the skeletal mantles. Instead, skeletal growth may have occurred simply because of the mixing, and the need, we suggest, to supply (or extract) the heat of mixing. Alternatively, rifting and fracturing of the crustal lid above the magma chamber, induced by injection of magma into the chamber, may have allowed sudden access of circulating seawater deep into the crust (Cann and Strens, 1982). The sudden cooling resulting from this may have resulted in skeletal growth of phenocrysts.

The solid core of the plagioclase megacryst of Figure 8E is quite rounded. Thus in addition to the crystal growth effects during mixing just described, the crystal was partly resorbed prior to the growth of its skeletal mantle. Subsequent growth of the crystal has tended to restore a more typical faceted crystal outline. However, this process was not completed, and the final outline of the crystal is quite irregular.

Our interpretation of the growth of these crystals differs from that of Dungan and Rhodes (1978), who favored a resorption origin for melt inclusions with irregular shapes in plagioclase megacrysts. For our crystals, at least, the compositions of the melt inclusions preclude such a mechanism.

COMPARISON OF PLAGIOCLASES IN SPINEL- AND CLINOPYROXENE-ASSEMBLAGE LAVAS

An unusual phenomenon, and one difficult to explain, is systematic differences between plagioclase compositions in lavas of the two phenocryst assemblages when compared at the same An or atomic Si content. From Table 11, clinopyroxene-assemblage plagioclase phenocrysts are lower in Ca and higher in Al at the same Si (Figs. 15A and B) than spinel-assemblage plagioclases. There is some overlap, probably reflecting analytical

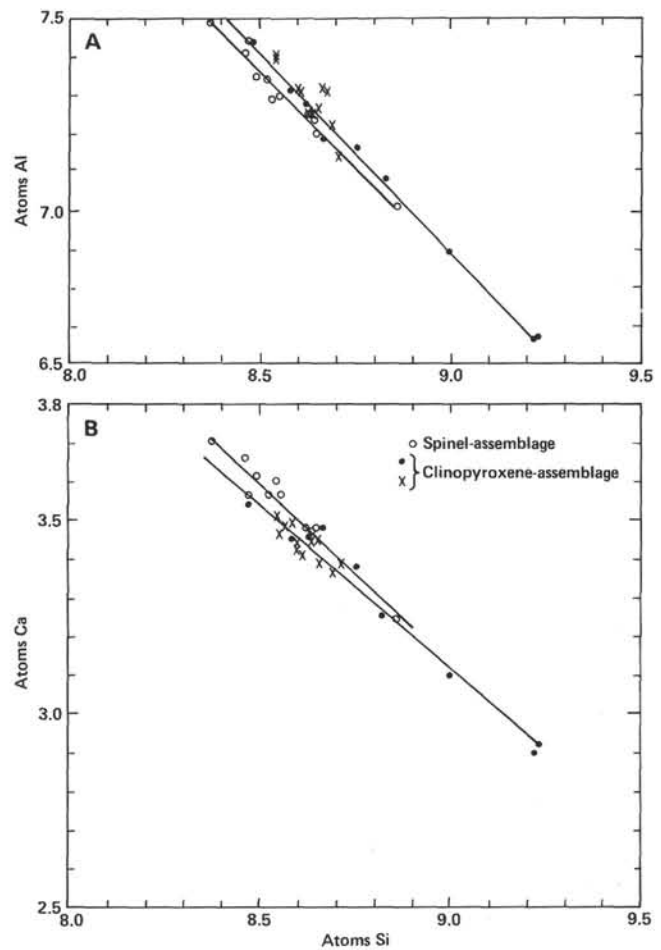


Figure 15. Contrasts in plagioclase compositions found in spinel-assemblage and clinopyroxene-assemblage basalts, from detailed study (Table 11). A. Atoms Al versus atoms Si. B. Atoms Ca versus atoms Si. Lines give linear regressions through data points for the two assemblages (see text). Circles, spinel-assemblage samples; x's, clinopyroxene assemblage Piece 1326; dots, clinopyroxene assemblage Piece 1361 (with gabbroic xenoliths).

imprecision, but the same relationships exist in the reconnaissance data, although not as distinctly. The phenomenon was thus detected by three different electron microprobes each operated by different investigators. Linear regressions on Figure 15 have correlation coefficients (r^2) ranging from 0.946 to 0.990. Consideration of the reconnaissance and detailed-study data together suggests that the contrasts are most pronounced for plagioclases in the range An_{88-94} , those we have termed first-generation plagioclases (the large megacrysts, glomerocrysts, and phenocrysts with glass inclusions). There are insufficient data to compare second-generation plagioclases very well, but there is a suggestion that the chemical differences may be restricted completely to the population of larger plagioclases. The lower Ca and higher Al are particularly evident in the plagioclases of clinopyroxene-assemblage Group G sample (Piece 1326, Fig. 16A), which is the one with abundant clinopyroxene phenocrysts and few xenoliths. The other Group G sample (Piece 1361) includes a number of plagioclases from gabbroic xenoliths that do not show the compositional

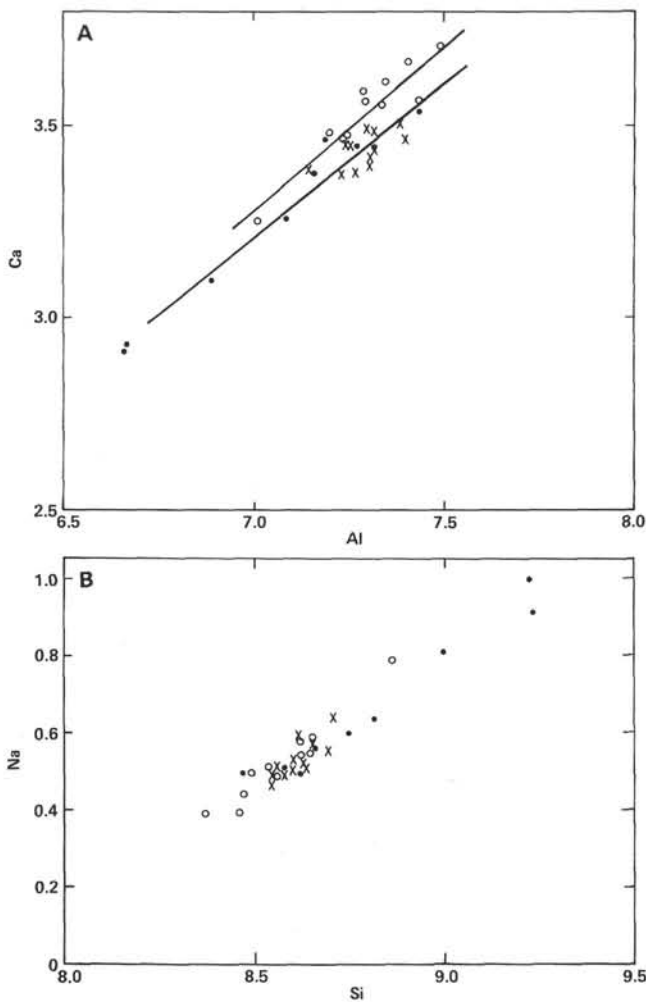


Figure 16. A. Atoms Ca versus atoms Al, and B. Atoms Na versus Si, for plagioclases from spinel- and clinopyroxene-assemblage lavas. Data from detailed study (Table 11). Symbols, linear regressions are as in Figure 15.

contrast. Since the xenolith minerals crystallized from melts more evolved than their Group G host, the disparity in plagioclase compositions may not exist among the more sodic plagioclases. We cannot be certain of this, however, since we cannot specify the lineage of the melts that produced the xenoliths.

There is no obvious difference in the Na contents of the plagioclases belonging to the two lava suites (Fig. 16B), although this may reflect the limits of instrumental resolution. Together, the differences in Ca and Al with respect to Si imply that there is some departure from ideal stoichiometry, since the two vary in opposite senses, not together as they would if there were ideal albite-anorthite solid solution. In the general plagioclase formula, MT_4O_8 , there must be more Si and less Al in the T sites of spinel-assemblage plagioclases than in clinopyroxene-assemblage plagioclases. To maintain charge balance, there must be deficiencies of Ca and Na in the M sites.

Both the effects of pressure and of competition for the components of plagioclase by other phases may be

involved here. For example, Ca-species in clinopyroxene-assemblage melts entered lattice sites in both clinopyroxene and plagioclase, but only plagioclase took up Ca in spinel-assemblage melts. However, in the spinel-assemblage melts, chromian spinel competed with plagioclase for Al. Together, the two effects could have modified the activities of the various melt species enough to produce the contrasts shown in Figures 15 and 16. This might have been enhanced at higher pressure. Smith (1974) cites experimental data showing that simple application of pressure greater than 5 kbars on anorthite resulted in separation of corundum from the feldspar, resulting in high SiO_2 anorthite. At pressures close to the upper limit of plagioclase stability in the mantle (about 9 kbars; e.g., Presnall et al., 1979) or in typical abyssal tholeiites (e.g., Fujii et al., 1979), the formation of plagioclases with defect structures should be expected. This problem is clearly worthy of more detailed mineralogical investigation.

These differences in plagioclase compositions suggest that the lavas with the two phenocryst assemblages underwent different crystallization sequences. The lavas contain no plagioclase phenocrysts, megacrysts, or glomerocrysts to indicate that they diverged from a common parental magma at a particular pressure and temperature. Decrease in pressure and/or magma mixing resulted in crystallization of subsequent (second-generation) plagioclases with overlapping Ca/Si and Al/Si, but the earliest stages of crystallization were entirely separate.

CRYSTALLIZATION OF PHENOCRYST ASSEMBLAGES

A number of aspects of phenocryst crystallization in the Costa Rica Rift basalts stand out amidst all these mineral data. Of fundamental importance is that within the population of phenocrysts there are minerals that crystallized from melts as little evolved as any that have ever been found in the ocean crust. Based on Fe-Mg partitioning between olivine and melt, and between clinopyroxene and melt, plus melt inclusion compositions, these melts had a surprisingly consistent $Mg/Mg + Fe^{2+} = 0.71 \pm 0.01$.

The clinopyroxene-assemblage lavas are important because they demonstrate the existence of a type of abyssal tholeiite in which first plagioclase and then clinopyroxene formed during the earliest traceable stages of crystallization (both minerals usually form after significant intervals of crystallization of olivine, or of olivine plus plagioclase). There is no evidence that olivine precipitated either before or during the crystallization of the magnesian Cr-rich clinopyroxene, although some quite obviously formed later. Clinopyroxene-assemblage basalts may be fairly common in the ocean crust since they are not only the most abundant porphyritic basalt type in the Costa Rica Rift drill sites, but they have also been described from a number of places on the Mid-Atlantic Ridge (e.g., Blanchard et al., 1976; Donaldson and Brown, 1977; Natland, 1979b). At DSDP Site 395, in fact, there are five porphyritic basalt types, of which three are similar to the clinopyroxene-assemblage lavas

of the Costa Rica Rift and two are similar to the spinel-assembly lavas (Natland, 1979a, b). The megacryst and glomerocryst mineral associations are almost identical to those described here, even to the extent that clinopyroxene and olivine do not occur together in the same glomerocrysts (Natland, 1979b), and some of the clinopyroxenes are high-Cr₂O₃ endiopsides (Fig. 12; see also Dungan and Rhodes, 1978).

The mineral data here also constitute evidence for the compositional integrity of magma batches, at least until they arrived at shallow levels in the crust from sources in the mantle. Not only are the lavas with the two phenocryst assemblages mineralogically distinct, but so are lava types with the same phenocryst assemblage (i.e., glass Groups J and B, with their different Cr-spinels). This level of diversity has been found increasingly among abyssal tholeiite suites by combining bulk chemical and mineral data (e.g. le Roex et al., 1981; Natland and Melchior, unpublished). But it is in the context of this diversity that the small range of glass compositions at Sites 501, 504, and 505 must be understood. Why, for example, do glass Groups B and G, which are so nearly identical, carry different phenocryst populations? Did they arrive at the same point from two different directions, or are other explanations possible?

Finally, among the minerals we have analyzed are those that appear to require an origin at elevated pressure (the Cr-rich clinopyroxenes and aluminous chromian spinels). By implication, therefore, associated plagioclases and olivines also formed at high pressure, and we have indicated some aspects of the composition and reverse zoning of plagioclases that support crystallization over a range of pressures, or at different pressures. The case for a high-pressure origin for Cr-rich calcic pyroxene, aluminous Cr-spinel, associated plagioclase, and olivine megacrysts has been summarized by Wilkinson (1982) and need not be repeated here. However, we believe that at the Costa Rica Rift these minerals crystallized from the melt and are not exotic fragments of mantle wall rock, despite evidence for resorption that, in other instances, has led some workers to the conclusion that the minerals were xenocrysts or xenoliths.

Phase relationships of ocean crust basalts have been determined at various pressures in several studies (Kushiro and Thompson, 1972; Fujii et al., 1979; Bender et al., 1978; Green et al., 1979; Stolper, 1980; Jaques and Green, 1980). Studies have also been made of a number of synthetic systems pertinent to their crystallization (e.g. Presnall et al., 1978, 1979). These systems are all relevant to the origin of the phenocryst assemblages. In some cases, 1-atm. relations of natural basalts have been integrated with the high-pressure results to extrapolate phase relations at higher pressures (Fisk et al., 1980). Although such extrapolations should be used with caution, they suggest that basalts of the ocean crust exhibit a wide variety of phase relations, and that inferences based on any of these studies in the absence of similar data on the particular rocks of interest must be drawn with great care. In our case, the principal difficulty is in selecting a phase-diagram analog relevant to the crystallization of phenocryst assemblages when it is

likely that the basalts studied (as well as those used in the experiments) (1) underwent at least some shallow fractionation; (2) probably underwent crustal-level mixing; and (3) in some cases were affected by the accumulation of phenocrysts by mechanical processes. Therefore, the current host rocks need not, and probably do not, resemble the melts from which the phenocrysts formed, and the melts are not precisely represented by the samples used in the experiments. There has also been a tendency to use olivine tholeiites in such experiments, on the understandable assumption that they should more closely approximate parental compositions than other basalt types. However, the results of the experiments on olivine tholeiites are probably pertinent mainly to what we have called spinel-assembly lavas; our data imply that clinopyroxene-assembly lavas require a somewhat different parent.

Typical experimental results on natural olivine tholeiites show a convergence of field boundaries on pressure-temperature (P-T) diagrams (Fig. 17A) such that at 8 to 9 kbars, all the principal silicate phases crystallize within a very narrow temperature interval. One interpretation of these experiments in terms of melting is that at these pressures, the basalts could have melted in equilibrium with plagioclase lherzolite (e.g., Kushiro and Thompson, 1972; Fujii et al., 1979). Presnall et al. (1979) noted the coincidence of this 8-to-9-kbar convergence of phase

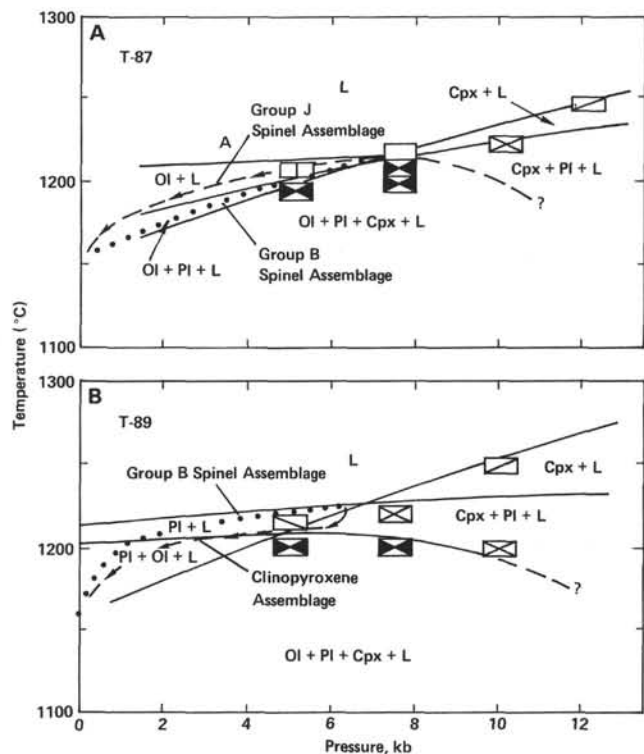


Figure 17. Possible phase diagrams for abyssal tholeiites parental to Costa Rica Rift porphyritic basalts, with hypothetical high-to-low pressure fractionation sequences indicated as shown. A. Olivine tholeiite. B. Plagioclase-phyric basalt. Ol, olivine; Pl, plagioclase; L, lherzolite; Cpx, clinopyroxene. After Kushiro and Thompson (1972).

boundaries with the experimentally determined pressure range for the zone of transition between plagioclase and spinel lherzolite in the mantle. They propose that this pressure range effectively acts as an invariant point on the mantle solidus during melting and that in a steady-state spreading regime most melting would take place near this transition in the mantle. The basalts produced in this way therefore naturally should have been in equilibrium with both plagioclase and spinel lherzolite at 8 to 9 kbars.

Other investigators, however, are of the opinion that basaltic magmas are produced at a variety of depths beneath spreading ridges and stem principally from picritic parents (O'Hara, 1968; Frey et al., 1974; Elthon, 1979; Stolper, 1980; Jaques and Green, 1980). We have used Figures 3 and 4 to show possible relationships between the Costa Rica Rift glass groups in Table 2, sequences of crystallization at different depths (Stolper, 1980), and the subsequent polybaric fractionation of olivine (arrows) to positions at or near the 1-atm. cotectic boundary. The rarity of picrites in the ocean crust has been attributed by some workers to fractionation of olivine near the base of shallow magma chambers. When charged with olivine, the magmas are too dense to mix with overlying olivine-poor liquids (Sparks et al., 1980; Huppert and Sparks, 1980); hence, olivine must generally fractionate from all picrites entering the magma chamber. This view is not held by Wilkinson (1982), however, who notes not only the rarity of picrites but also the rarity of dunites, troctolites, and other olivine-rich cumulates in dredge collections from fracture zones and other structures that expose the plutonic foundation of the ocean crust (see also Dick and Bullen, in press).

It is conceivable, therefore, that Figures 3 and 4 suggest relationships to picritic parental magmas produced at a variety of depths. After the attainment of shallow cotectic crystallization, the fractionation of all three major silicate phases moved residual liquids down the cotectic to give the present glass groups.

This sequence, however, is contradicted for Costa Rica Rift basalts by our mineral data. Only one glass group, Group J, possibly had a picritic parent, as suggested earlier. Group I may have had as well. But even spinel-assembly Group B contains plagioclase megacrysts with inclusions of high-Mg melts. And the clinopyroxene-assembly lavas also precipitated both plagioclase and Cr-rich clinopyroxene from high-Mg melts. Every porphyritic lava, and many of the sparsely phyric ones, have at least some highly calcic plagioclase (Table 4), which certainly also precipitated from similarly high-Mg melts. Consequently, almost all the lavas that reach shallow magma chambers in the crust of the Costa Rica Rift were saturated in plagioclase, and many were also saturated in clinopyroxene; they were not picrites.

If we try to interpret the crystallization of phenocryst assemblages in terms of conventional P-T diagrams like that of Figure 17A, we face the additional difficulty of accounting for the failure of olivine to occur in glomerocrysts with plagioclase and clinopyroxene in the clinopyroxene-assembly basalts. Their crystallization sequence, based on phenocrysts and glomerocrysts, was

plagioclase, clinopyroxene, and then olivine. Figure 17A, which depicts the phase relations of an olivine tholeiite, does not show such a crystallization sequence at any pressure. Up to about 8 kbars, olivine is the first phase to crystallize. Above that, clinopyroxene precedes both olivine and plagioclase.

A second type of phase diagram is shown in Figure 17B and is based on the phase relations of a plagioclase-olivine phyric tholeiitic basalt (Kushiro and Thompson, 1972) that was first described from the Mid-Atlantic Ridge by Miyashiro et al. (1969). In that sample, accumulated plagioclase phenocrysts expanded the stability field of plagioclase, making it precede olivine in the crystallization sequence at low pressures. However, between 5 and 8 kbars, clinopyroxene follows plagioclase in the crystallization sequence, which is the sequence in our clinopyroxene assemblage basalts. One can thus imagine that a decrease in pressure during magma ascent might shift the crystallization path (dashed line) into the field of stability of plagioclase plus olivine (but not clinopyroxene), and at this point clinopyroxene phenocrysts would tend to go into solution as olivine crystallized. This sequence has the advantage of explaining several of the enigmatic aspects of the clinopyroxene-assembly basalts, namely (1) lack of evidence for early crystallization of olivine, (2) resorption of clinopyroxene and some plagioclase phenocrysts, and (3) failure of olivine and clinopyroxene to occur together in the same glomerocrysts. The difficulty is in trusting the applicability of a phase diagram for a basalt that does not represent a liquid composition. Perhaps removal of the phenocrysts in the original experiment would have resulted in a somewhat similar diagram, with the plagioclase field reduced, but not to the extent that olivine would crystallize first. This would have narrowed the interval within which clinopyroxene could follow plagioclase in the crystallization sequence, forcing it closer to the 8-to-9-kbar convergence of phase boundaries.

This is of some importance in that it suggests that melting may indeed have occurred in a very narrow pressure interval at or about the depth of the transition between plagioclase and spinel lherzolite in the mantle. The cluster of clinopyroxene-assembly lavas in Figures 3 and 4 could then be derived from a parental composition produced at about a 10-kbar pressure, or slightly less, and have reached their current position near the low-pressure cotectic by some crystallization pathway such as that indicated by the heavy arrows. The spinel-assembly lavas, however, apparently had deeper sources, and they are displaced toward the olivine apex on Figures 3 and 4.

Thus, elements of both the hypotheses for origin of abyssal tholeiites are plausible. Picrites indeed do exist, and they are produced at a variety of depths. But at least on the Costa Rica Rift, differentiates of picrites are not the most abundant rock types. Far more abundant are the clinopyroxene-assembly lavas that appear to have originated at 8 to 9 kbars, or at about a 30-km depth in the mantle, perhaps at the inferred near-invariant point on the lherzolite solidus. Presnall et al. (1979) proposed that melting at this invariant point (or cusp, as they call

it) should produce melts of almost identical composition, regardless of the degree of melting, which would tend to cause variations in oxides of elements with low-partition coefficients only (e.g., K_2O , P_2O_5 , TiO_2 , etc.). This prediction seems almost perfectly realized among the clinopyroxene-assemblage glass groups, which had the greatest number of equivalences and near-equivalences we were able to identify. A major reason for the equivalences, then, could be that most of the magma types were nearly identical to begin with.

Crystallization sequences for the spinel-assemblage lava groups can be interpreted by using both Figures 17A and 17B. The dashed line on Figure 17A would be for a picrite or olivine tholeiite in which plagioclase did not begin to crystallize until the magmas reached some fairly shallow level in the crust (i.e., Group J lavas). The dotted lines on Figures 17A and 17B could represent the crystallization pathways of magma types similar to glass Group B, in which plagioclase crystallized at depth, was partially resorbed upon ascent, and then began to crystallize again as temperatures dropped at some shallow crystal level. Glass Groups B and G may be so similar because contrasting crystallization sequences (Figs. 17A and B) produced the same residual liquid, or because the two melts were similar to begin with, and the small differences in the course of fractionation during magma ascent were insufficient to produce noticeable differences in their composition.

Experimental data bearing on the crystallization of Cr-spinel in abyssal tholeiites are thus far restricted to picritic basalts (e.g., Fisk and Bence, 1980) and have been obtained primarily to explain differences in spinel compositions. That clinopyroxene and Cr-spinel do not precipitate simultaneously in tholeiitic magmas has been established on the basis of detailed study of gabbroic intrusions (e.g., Irvine, 1980) and experimental investigations (Irvine, 1977). These observations, however, apply to rather fractionated basaltic compositions in which Cr has already been depleted in the melt by chromite fractionation. The first clinopyroxenes to form in such basaltic systems are augitic, not diopsidic, in composition. Moreover, this applies only to tholeiitic magmas with low oxygen fugacity. Higher oxygen fugacity can greatly expand the stability of Cr-spinel, as is observed in some backarc basin basalts (Melchior, 1981), but in all likelihood, the Costa Rica Rift basalts did not have oxygen fugacity as high.

Both Figures 17A and 17B show the stability field of clinopyroxene to expand with pressure; hence, it is plausible that the reaction relation between Cr-spinel and clinopyroxene found by Irvine (1977) at 1 atmosphere extends in some form to high pressures as well. It is likely that Cr-spinels would be considerably more aluminous at higher pressures than at 1 atm.; hence, phase relations between spinel and other phases on the join anorthite-forsterite-diopside in the synthetic system $CaO-Al_2O_3-SiO_2-MgO$ (Presnall et al., 1978) might bear on the phenocryst assemblages observed in Costa Rica Rift and other abyssal tholeiite suites. On this join, there is rapid expansion of the fields of diopside and spinel at the expense of anorthite and forsterite as pressure increases

(Fig. 18). Above 7 kbars, in fact there is a common boundary between the spinel and diopside fields. However, it is clear that any melt on this join that first crystallizes plagioclase would be most likely to crystallize diopside next rather than spinel. Moreover, fractional (not equilibrium) crystallization of the plagioclase would move liquids across the diopside field so that they could not intersect the spinel field. Polybaric fractionation during magma ascent would result in resorption of clinopyroxene formed at higher pressure and eventual coprecipitation of plagioclase and olivine.

In spinel-assemblage basalts, spinel is enclosed in olivine, enclosed in plagioclase, enclosed in both minerals, or occurs as a separate phenocrysts. Spinel does not occur in basalts with clinopyroxene phenocrysts, as it does, for example, in some alkalic basalts. The common boundary between the fields of spinel and diopside on Figure 18 at elevated pressures thus does not seem to be a factor in generation of these abyssal tholeiites.

The high Cr_2O_3 of the calcic clinopyroxenes in these basalts almost certainly implies that the clinopyroxene was sufficient to take in any available Cr without the formation of Cr-spinel. There is no indication, for example, that Cr is necessarily more abundant in spinel-assemblage basalts than in clinopyroxene-assemblage basalts (Table 3), although it may be higher in some samples. Our observational data, at any rate, imply that the two minerals were incompatible in parental Costa Rica Rift tholeiites and occur in the same rocks only if mixing has taken place. Similar observations were made on a suite of 78 samples from DSDP Leg 37 (37°N, Mid-Atlantic Ridge) by Donaldson and Brown (1977). They found Cr-rich clinopyroxene megacrysts in 16 of those samples, and in only two of these were olivine and clinopyroxene in the same glomerocrysts (compositions were unspecified). Cr-spinel was only found enclosed in oliv-

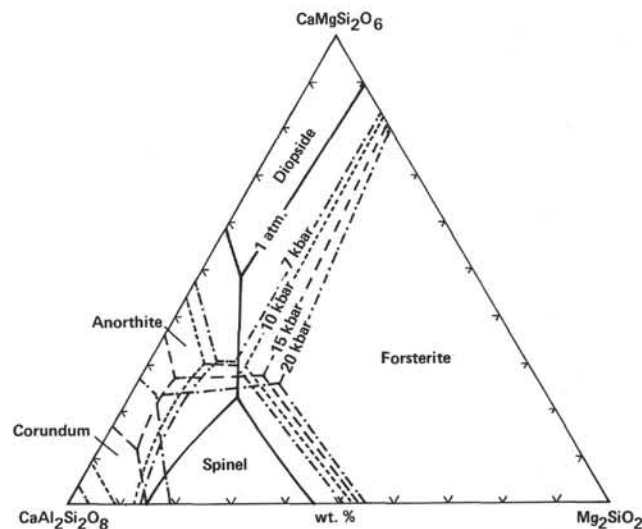


Figure 18. Composite diagram showing changes in liquidus boundaries on the join $CaMgSi_2O_6-Mg_2SiO_4-CaAl_2Si_2O_8$ at 1 atm., 7 kbar, 10 kbar, 15 kbar, and 20 kbar, after Presnall et al. (1978, fig. 5). Mineral stability fields are indicated for 1 atm. except corundum at 15 kbar.

ines (whether in the same samples with clinopyroxene megacrysts was also not specified). The mineral relationships therefore are similar to those of the Costa Rica Rift basalts, although the details of this have not been worked out.

If the two minerals are fundamentally incompatible in abyssal tholeiites at elevated pressures, hypotheses of high-pressure clinopyroxene fractionation may be discounted for basalts carrying chromian spinel. O'Donnell and Presnall (1980) deduced that low-pressure crystal fractionation could not produce the range of compositions found in a suite of Mid-Atlantic-Ridge basalts having spinel-assemblage phenocrysts, but they obtained better quantitative results by presuming that high-pressure clinopyroxene fractionation had occurred. Some of the spinels in these basalts are similar to the highly aluminous variety described here and elsewhere that is inferred to have crystallized at elevated pressure (e.g., Sigurdsson and Schilling, 1976). O'Donnell and Presnall (1980) explained the lack of clinopyroxene megacrysts in the basalts as resulting from resorption upon ascent of the magmas. However, our study implies that clinopyroxene could not have fractionated from spinel-bearing tholeiites at high pressure. Therefore, some other explanation for the chemical variations must be found.

EFFECTS OF AN AXIAL MAGMA CHAMBER

The phenocryst assemblages may be virtually independent of host rock compositions. Suppose that the uniformity of glass compositions reflects primarily the capacity of a steady-state axial magma chamber to buffer liquid compositions to a consistent homogeneous average, hybridizing small injected magma increments with a much larger quantity of magma in the chamber itself. Suppose also that between injections of new magma, all phenocrysts and glomerocrysts that are not erupted settle or attach to the walls and floor of the chamber so that the magma within it becomes substantially aphyric. Then, no matter whether this remaining magma was produced by mixing of batches exclusively of one phenocryst assemblage or both, the phenocrysts of the next injected magma batch, whatever they may be, would become the phenocrysts of the entire magma chamber, unless some were stirred in from the bottom and sides of the chamber itself. If the injected magma increment were small, it would modulate the bulk composition of the magma chamber only slightly. If it were close to the composition of the magma already in the chamber, it need not have been a particularly small increment, nor necessarily one excessively charged with phenocrysts.

Thus the identical glass Groups B and G, erupted at different times from the top of such a chamber, could readily have different phenocryst assemblages. Eruptions would have had to follow closely after episodes of injection, before separation of melts and phenocrysts. But it is likely that episodes of eruption would be linked to magma-chamber inflation. Such a hypothesis would explain the occurrence of nearly aphyric and strongly porphyritic lavas of the same glass group, as well as the petrographic distinction between spinel- and clinopyroxene-assemblage lavas. Complete separation of phe-

nocrysts from melts need not have occurred after every episode of magma injection, and this would explain the uncommon occurrence of lavas having both spinel and clinopyroxene phenocrysts (Hole 505), and the occurrence of two phenocryst assemblages in different samples of the same chemical type (mixed Group K of Hole 504B).

The near uniformity of Hole 504B glass groups places special constraints on mechanisms for fractionation. Fractionation is commonly inferred to take place in shallow (crustal) magma chambers beneath axes of spreading, especially along eastern Pacific intermediate- and fast-spreading rises and rifts (e.g., Clague and Bunch, 1976; Batiza et al., 1977). On the basis of such features as uniform crustal structure, modest axial topographic expression, and microtopography revealed by near-bottom surveys, long-lived, essentially steady-state magma chambers have been proposed to exist at the crests of faster spreading ridges (Rosendahl, 1976; Lonsdale, 1977; Sleep and Rosendahl, 1979; Natland, 1980). Earlier, we mentioned the lack of either positive or negative axial relief on the present Costa Rica Rift, and the flat basement topography around Sites 501 and 504. Crustal generation was thus a very uniform process, without much tectonic disruption, during the late Miocene. Such a situation could have been conducive to the development of a long-term, steady-state spreading magma chamber at this location.

Usselman and Hodge (1978) used numerical modeling to calculate variation in lava compositions and cryptic variation among cumulus minerals in a periodically replenished, periodically tapped magma chamber such as might characterize spreading ridges. By varying the proportions of magma entering the base of the chamber, and the time between such episodes of injection, a fair variation in lava compositions, produced primarily by fractionation, was predicted. By keeping the proportion of material injected relatively small and of uniform composition, and by increasing the frequency of injection, the range of erupted compositions became very limited, and on the average evolved only slightly from the compositions injected into the chamber from below. In terms of $Mg/Mg + Fe^{2+}$, parental compositions were assumed to have a ratio of 0.71 (similar to that calculated to have been in equilibrium with the earliest crystallizing phenocrysts in Costa Rica Rift basalts). Small injections of about 5 to 10% every 5000 yr. with eruption of equivalent volumes from the top of the chamber resulted in eruptive compositions having $Mg/Mg + Fe^{2+}$ no lower than 0.65. Most important, at least conceptually, a steady-state eruptive composition could be achieved.

It is rare to see the components of a theoretical model so closely realized in nature, but almost exactly these compositions, both of injected and erupted lavas, occur at Sites 501 and 504. The uniformity of compositions is unmatched by any other DSDP hole, nor even a group of very similar basalts sampled by subsurface at 21°N on the East Pacific Rise, where the same type of magma-chamber processes have been inferred (Juteau et al., 1980).

Two factors evidently were involved in producing the uniform compositions at Sites 501 and 504. First, many of the magma types were very similar, and perhaps were produced, as suggested earlier, by melting at a near-invariant thermal cusp in the mantle (Presnall et al., 1979). Following this, the magma chamber itself appears to have removed much of the small remaining diversity in magma types that reached the crust, by serving as a locus for mixing and homogenizing. Usselman and Hodge (1978) argue that achieving multiphase fractionation stabilizes melt compositions in a magma chamber. Autio and Rhodes (this volume) determined the 1-atm. phase relationships of seven nearly aphyric samples from Hole 504B and found them all to crystallize olivine, plagioclase, and clinopyroxene in a very narrow temperature interval, lending support to this suggestion. The only significant change in bulk compositions within the chamber recorded by the lavas occurred with injection of unfractionated spinel-assemblage magmas, which led to eruption of lavas with glass Groups J and I in that order. It is probably not fortuitous that these are adjacent stratigraphically; at least two cycles of magma injection were necessary before that particular chemical perturbation was no longer evident.

The alkali-enriched Groups E and M stand out as genuine anomalies, however. These magma types must somehow have bypassed the principal magma conduit and reservoir system which supplied all the other glass groups. Therefore, the principal long-lived magma chamber, which supplied most of the glass groups, was not entirely interconnected with other conduit-chamber systems. There was some lateral discontinuity among such systems along the axis of the Costa Rica Rift.

Enrichments in K_2O , P_2O_5 , and hygromagmatophile trace elements are predicted for steady-state magma chambers that are periodically tapped and replenished (O'Hara, 1977; O'Hara and Mathews, 1981; Robson and Cann, 1982; and Cann, 1982). Such enrichments, though, are not evident among the Costa Rica Rift basalts. On the contrary, the general level of depletion in the basalts is among the most remarkable features of the samples. However, enrichment factors must be calculated by comparison with the compositions of injected magmas, for which we have no data. Moreover, probably there were not many more pulses of injected magma than eruptions, of which we sampled only 11 in Hole 504B (excluding Groups E and M, which were not part of the principal magma chamber and conduit system). This may be too few to detect significant build-ups of these elements, or changes in their ratios, particularly if the fractions of magma in the chamber that both crystallized and erupted in each cycle were small compared with the size of the chamber. In this situation, only modest enrichments in elements with very low partition coefficients need have occurred (cf. O'Hara and Mathews, 1981, fig. 19).

Green et al. (1979) postulate the existence of widespread depleted magmas in the uppermost mantle beneath spreading ridges from which very calcic plagioclase, calcic clinopyroxene, and olivine more forsteritic than Fo_{88} crystallize. They believe that these magmas

become entrained in less depleted but more typically picritic magmas originating at greater depth, giving the mineralogical indications for mixing observed in Mid-Atlantic-Ridge basalts (Dungan and Rhodes, 1979). Autio and Rhodes (this volume) consider the depleted Costa Rica Rift basalts to be chemically equivalent to the magmas from which the megacrysts found in Mid-Atlantic-Ridge porphyritic basalts segregated, based on comparison to glass inclusions in those megacrysts. Costa Rica Rift basalts may thus be a sort of missing link in abyssal tholeiite petrogenesis, one widespread at many spreading ridges, but one whose existence until now has been obscured by mixing processes. The Costa Rica Rift is a place where depleted mantle sources dominate; elsewhere they can only be deduced by unravelling the mixing history of the basalts. We do not hold that any of the megacrysts in these basalts were entrained in rising picritic magmas, however.

Ferrobasalts did not erupt at the Costa Rica Rift, even though they are especially abundant on the nearby Galapagos Rift (e.g., Clague and Bunch, 1976; Byerly, 1980; Christie and Sinton, 1981; Clague et al., 1981). Natland (1980b) and Byerly (1980) both proposed that magma chamber shape is a critical factor in production of ferrobasalts. Natland (1980b) argued that even where ferrobasalts are abundant, the compositions of magmas in large axial magma chambers do not become much more evolved than those, for example, of Hole 504B. There is no geochemical evidence for mixing between olivine tholeiites and ferrobasalts at the East Pacific Rise near the Siqueiros Fracture Zone, implying physical isolation of ferrobasalts from olivine tholeiite magmas injected into the base of the axial magma chamber. Ferrobasalts thus appear to form by means of crystal fractionation in small isolated magma bodies such as dikes, lava lakes, or shallow intrusives above larger magma chambers. Such small bodies should be more commonly tapped at spreading ridges with wide, relatively unstable, and shifting loci of dike injection. The orientation and location of these would be sensitive to the distribution of stresses in the thin, comparatively flat crustal lid above the principal magma chamber. For ferrobasalts to be uncommon, stresses must be such as to prevent isolation and probably even formation of such small magma bodies. Thus the magma chamber should have a more triangular cross section with a narrow, apical top, which would constrain dike injection to a very narrow zone.

Natland and Melson (1981) proposed that magma chambers with comparatively flat tops, where ferrobasalts are abundant, are produced by excessive production of magmas compared with spreading rate, resulting in formation of positive axial relief (a horst or shield volcano). More balanced magma production at a given spreading rate does not produce such an overinflated magma chamber, and in such situations ferrobasalts should be less common. With a narrow dike injection zone, the only magmas likely to be tapped are within the main magma chamber itself, that is, the relatively unfractionated compositions carrying the phenocrysts of primitive precursors that began crystallizing at elevated pres-

sure. In contrast, ferrobasalts are almost always aphyric (cf. Natland, 1980a), supporting the hypothesis that they indeed evolve in magma bodies isolated from principal magma chambers. If the uniform lava compositions in Hole 504B are any indication, the dike injection zone was narrow, such small bodies were never intercepted by dikes emanating from the main magma chamber, and a well developed sheeted dike complex should exist beneath the extrusive section.

Recently, Hey (1981) proposed that the Costa Rica Rift was tectonically unusual in that asymmetric spreading has occurred, with the southern flank consistently accreting 20% faster than the northern flank. Most asymmetric spreading results from ridge crest jumps. Many of these have been shown to result from rift propagation. No jumps are evident in the Costa Rica Rift magnetic anomalies, indicating either that spreading was truly asymmetric or that the crust consists largely of

very small failed rifts which transferred less than 2 or 3 km of crust to the southern flank every million years or so. Petrologic data cannot specifically prove or disprove either alternative. However, the tectonic instability implicit in the shifting-rift hypothesis is unlikely to be conducive to the production of so uniform a suite of lavas as is present at Sites 501 and 504. Eruption of at least some more evolved basalts, perhaps including ferrobasalts, would probably have occurred, as briefly outlined in the preceding paragraphs.

Finally, we can use the compositions of fractionated rock types to specify something about the proportions of possible parental compositions supplied to axial magma chambers in different settings. In Figure 19, summary fractionation pathways are shown for the Galapagos and Costa Rica Rifts combined (GR-CRR; solid line with arrows) and the East Pacific Rise near the Siqueiros Fracture Zone, where spreading rates are nearly

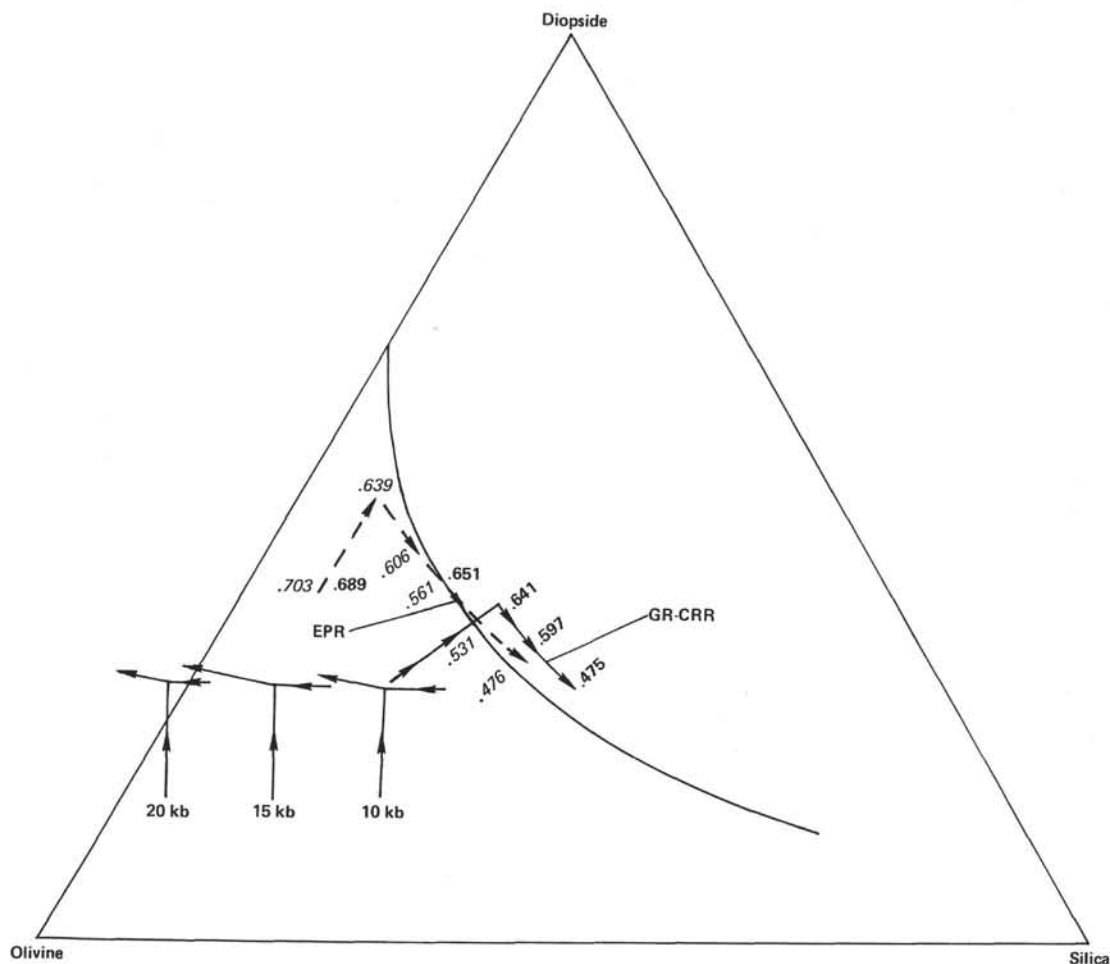


Figure 19. Same diagram as Figure 3, except the values of $Mg/Mg + Fe^{2+}$ of representative East Pacific Rise glass compositions (italicized, from Natland and Melson, 1980) and Costa Rica-Galapagos Rift glass compositions (not italicized, from Natland and Melson, 1980, this study and unpublished) are plotted in the positions of the corresponding data points. The dashed East Pacific Rise (EPR) fractionation trend is as in Figure 3. The solid line with arrows originating at the 10 kbar pseudo-invariant point and turning parallel to the 1-atm. cotectic (GR-CRR) is an inferred pathway for Costa Rica Rift clinopyroxene-assembly lavas and Galapagos Rift ferrobasalts. Note that Costa Rica Rift clinopyroxene-assembly lavas with $Mg/Mg + Fe^{2+} > 0.6$ plot in the same positions as East Pacific Rise ferrobasalts with $Mg/Mg + Fe^{2+} = 0.48-0.53$ on this projection.

three times as great as they are in the Panama Basin (EPR; dashed line with arrows). The pathways are based on data from Table 2 (see also Fig. 3) and of Natland and Melson (1980). Next to these at various points are indicated values of $Mg/Mg + Fe^{2+}$ (italicized in figure and in following discussion for EPR; not italicized for GR-CRR) appropriate to their position on the diagram. This shows clearly that the Costa Rica Rift glass compositions corresponding to clinopyroxene-assemblage lavas of Figure 3 ($Mg/Mg + Fe^{2+} = 0.641 - 0.597$) plot close to the low-pressure cotectic in the same position as occupied by East Pacific Rise ferrobasalts ($Mg/Mg + Fe^{2+} = 0.531 - 0.476$). Galapagos Rift ferrobasalts (e.g., $Mg/Mg + Fe^{2+} = 0.475$) plot significantly closer to the silica apex along the cotectic than East Pacific Rise ferrobasalts with comparable $Mg/Mg + Fe^{2+}$.

Natland and Melson (1980) inferred that an olivine tholeiite with glass having $Mg/Mg + Fe^{2+} = 0.703$ was representative of parental compositions of the fractionated East Pacific Rise tholeiite suite. This glass is similar to Costa Rica Rift glass Group J ($Mg/Mg + Fe^{2+} = 0.689$; Fig. 19). Thus, the most abundant magma type supplied to an East Pacific Rise axial magma chamber differed substantially from that supplied most frequently to Costa Rica Rift and Galapagos Rift magma chambers. In essence, spinel-assemblage magma types, many of them conceivably having picritic parents, were the most abundant precursors of East Pacific Rise ferrobasalts. Clinopyroxene-assemblage lavas predominated at the Galapagos and Costa Rica Rifts. Both types occur at the Costa Rica Rift (although the spinel-assemblage lava types are in the minority), and compositions akin to clinopyroxene-assemblage lavas occur in the Siqueiros Fracture Zone near the East Pacific Rise (Natland and Melchior, unpublished). But the proportions of these supplied to magma chambers in the two places were clearly different, to judge from the compositions of derivative lavas.

Figure 19 also suggests that the pressure regimes were different for production of parental magmas in the two regions. Extrapolating back to the high-pressure phase boundaries on Figure 19 (Stolper, 1980), most of the Costa Rica Rift parental compositions apparently originated at shallower depths (8–10 kbar pressure) than those of the East Pacific Rise (≈ 15 kbars). Bryan et al. (1981) observed similar relationships in samples from the Kane Fracture Zone and nearby portions of the Mid-Atlantic Ridge, except that the derivatives of parental magmas produced at different depths were both abundant in a small geographical area. Magma generation processes beneath slow-, intermediate-, and fast-spreading ridges are thus quite similar.

In general, this would seem to deny the efficacy of a thermal cusp, or invariant point, on the mantle solidus, in constraining abyssal tholeiites to a uniform composition (Presnall et al., 1979), although this mechanism may be important in some places, such as the Costa Rica Rift. It is particularly important that such an effect evidently did not operate beneath the East Pacific Rise, where uniform crustal structure so strongly suggests that steady-state spreading was achieved (Rosendahl,

1976). The diversity of probable parental compositions inferred by Stolper (1980) is confirmed by this analysis, although the role of picrites is considerably less than he suggested. That spreading ridges should have significant differences in the compositions of the most abundant parental materials supplied to magma chambers is a surprise, and the possibility that these originated at different depths may have important bearing on the dynamics of ridges spreading at different rates.

CONCLUSIONS

We have reconstructed in some detail the history of magmas supplied to one portion of the Costa Rica Rift in the late Miocene, some 5.9 Ma. By outlining the history of crystallization of phenocrysts and comparing crystallization sequences to assorted phase diagrams and projections, we conclude that there were two very depleted primary magmas supplied to the Costa Rica Rift, with $Mg/Mg + Fe^{2+} = 0.71$ and originating at two different depths. The majority of these depleted melts came from 25 to 30 km (8–10 kbars) and first crystallized highly calcic plagioclase and Cr-rich endiopsidite in that order. Removal of these magmas to shallow depths caused partial resorption of clinopyroxenes plus early plagioclase and crystallization of olivine. A lesser number of magma batches originated at depths of 45 to 50 km and first crystallized aluminous chrome spinel, olivine, and in some cases plagioclase in that order. Removal of these batches to shallower depths caused compositional changes in the spinels, partial resorption of some plagioclases, and reverse zoning of plagioclases. Mixing between unfractionated magma batches occurred at depth, causing skeletal plagioclase growth and trapping inclusions with high, but variable $Mg/Mg + Fe^{2+}$.

These two magma types were fed at different times into an axial magma chamber that was usually free of high-pressure phenocrysts from earlier episodes of magma injection. These had either settled to the floor of the chamber or adhered to its walls. A second generation of smaller phenocrysts and overgrowths on injected phenocrysts formed from the more evolved melt compositions in the chamber. Injections of new magma were probably small compared with the volume of the chamber, they were regularly spaced in time, and their compositions were very similar, allowing eruptive lavas only a very limited range in composition. High-pressure phenocrysts in the lavas were usually only those of the particular injected magma causing inflation of the chamber and eruption, and are abundant only in some (less than half) of the lavas of each chemical type. They are not necessarily related to the compositions of their current hosts, which are averages of many previous injected magmas. The greatest departures from the average bulk composition of material in the chamber followed infrequent injection of the higher pressure spinel-assemblage magmas. Although rare xenocrysts occur that crystallized from more evolved magmas than typical host lavas, materials in the magma chamber never achieved ferrobasalt bulk compositions, and none were erupted. This suggests that eruptions were constrained to above a very narrow dike injection zone on top of the chamber; hence

only magmas from the principal chamber itself, carrying high-pressure phenocrysts, could be tapped.

The eruption of two lava types with less depleted compositions implies that there were variations in the compositions of mantle sources in large-ion-lithophile and related elements, and that conduit magma chamber systems supplying these magmas from different sources were not entirely interconnected. The predominant Costa Rica Rift basalt type, however, is extremely depleted, having glasses with K_2O , P_2O_5 , Na_2O , and TiO_2 abundances less than in typical depleted abyssal tholeiites. Comparison with East Pacific Rise glass compositions suggests that a higher-pressure (15 + kbar) possibly picritic parent was more commonly supplied to the Rise axial magma chamber than to the Costa Rica Rift, although both high- and low- (8–10 kbar) pressure parental compositions produced derivative lavas in both places.

The low pressure parental compositions at the Costa Rica Rift were not picritic, but instead first precipitated phenocrysts of calcic plagioclase and Cr-rich, aluminous clinopyroxene, in which takeup of Cr prevented crystallization of chromian spinel. The clinopyroxenes are definitely phenocrysts and not fragments of upper mantle source rocks. Their compositions imply that early clinopyroxene crystallization may be more common in basalts of the ocean crust than previously realized. It is erroneous to suppose that they can only have formed after significant intervals of plagioclase and olivine crystallization. We propose that clinopyroxene-assemblage basalts of the type described here are an important lava type in the ocean crust and that their phase relationships and place in abyssal tholeiite petrogenesis are significant topics for further research.

ACKNOWLEDGMENTS

We thank all the marine technicians who skillfully prepared the many thin sections examined during Legs 68, 69, and 70, and our shipboard colleagues, Yves Noack and Nick Pertsev, for their participation in the initial descriptions of the rocks. Joe Cann offered insight and helpful discussion at several points. Finally, we thank Russ Merrill and Sherman Bloomer for reviewing the manuscript.

REFERENCES

- Anderson, R. N., and Noltimer, H. C., 1973. A model for the horst and graben structure of mid-ocean ridge crests based upon spreading velocity and basalt delivery to the oceanic crust. *Geophys. J. R. Astron. Soc.*, 34:137–147.
- Batiza, R., Rosendahl, B. R., and Fisher, R. L., 1977. Evolution of oceanic crust, 3, petrology and chemistry of basalts from the East Pacific Rise and Siqueiros transform fault. *J. Geophys. Res.*, 82:265–276.
- Bender, J. F., Hodges, F. N., and Bence, A. E., 1978. Petrogenesis of basalts from the Project FAMOUS area: experimental study from 0 to 15 kilobars. *Earth Planet. Sci. Lett.*, 41:277–302.
- Blanchard, D. P., Rhodes, J. M., Dungan, M. A., Rodgers, K. V., Donaldson, C. H., Brannon, J. C., Jacobs, E. W., and Gibson, E. W., 1976. The chemistry and petrology of basalts from Leg 37 of the Deep-Sea Drilling Project. *J. Geophys. Res.*, 81:4231–4246.
- Bottinga, Y., and Weill, D. F., 1972. The viscosity of magmatic silicate liquids: a model for calculation. *Am. J. Sci.*, 272:438–475.
- Bryan, W. B., Thompson, G., and Ludden, J. N., 1981. Compositional variation in normal MORB from 22°–25°N: Mid-Atlantic Ridge and Kane Fracture Zone. *J. Geophys. Res.*, 86:11,815–11,836.
- Byerly, G., 1980. The nature of differentiation trends in some volcanic rocks from the Galapagos spreading center. *J. Geophys. Res.*, 85:3797–3810.
- Cann, J. R., 1982. Rayleigh fractionation with continuous removal of liquid. *Earth Planet. Sci. Lett.*, 60:114–116.
- Cann, J. R., and Strens, M. R., 1982. Black smokers fuelled by freezing magma. *Nature*, 298:147–149.
- Christie, D. M., and Sinton, J. M., 1981. Evolution of abyssal lavas along propagating segments of the Galapagos Spreading Center. *Earth Planet. Sci. Lett.*, 56:321–335.
- Clague, D. A., and Bunch, T. E., 1976. Formation of ferrobasalt at east Pacific midocean spreading centers. *J. Geophys. Res.*, 81:4247–4256.
- Clague, D. A., Frey, F. A., Thompson, G., and Rindge, S., 1981. Minor and trace element geochemistry of volcanic rocks dredged from the Galapagos Spreading Center: role of crystal fractionation and mantle heterogeneity. *J. Geophys. Res.*, 86:9469–9482.
- Dick, H. J. B., and Bullen, T., in press. Chromian spinel as a petrogenetic indicator in oceanic environments. *Contrib. Mineral. Petrol.*
- Donaldson, C. H., and Brown, R. W., 1977. Refractory megacrysts and magnesium-rich melt inclusions within spinel in oceanic tholeiites: indicators of magma mixing and parental magma composition. *Earth Planet. Sci. Lett.*, 37:81–89.
- Duke, J. M., 1976. Distribution of the period four transition elements among olivine, calcic clinopyroxene and mafic silicate liquid: experimental results. *J. Petrol.*, 17:499–521.
- Dungan, M. A., Long, P. E., and Rhodes, J. M., 1979. The petrology, mineral chemistry, and one-atmosphere phase relations of basalts from Site 395. In Melson, W. G., Rabinowitz, P. D., et al., *Init. Repts. DSDP 45*: Washington (U.S. Govt. Printing Office), 461–477.
- Dungan, M. A., and Rhodes, J. M., 1978. Residual glasses and melt inclusions in basalts from DSDP Legs 45 and 46: evidence for magma mixing. *Contrib. Mineral. Petrol.*, 67:417–431.
- Elthon, D., 1979. High magnesia liquids as the parental magma for ocean floor basalts. *Nature*, 278:514–518.
- Fisk, M. R., and Bence, A. E., 1980. Experimental crystallization of chrome spinel in FAMOUS basalt 527-1-1. *Earth Planet. Sci. Lett.*, 48:111–123.
- Fisk, M. R., Schilling, J.-G., and Sigurdsson, H., 1980. An experimental investigation of Iceland and Reykjanes Ridge tholeiites: I. Phase relations. *Contrib. Mineral. Petrol.*, 74:361–374.
- Frey, F., Bryan, W. B., and Thompson, G., 1974. Atlantic Ocean floor: geochemistry and petrology of basalts from Legs 2 and 3 of the Deep Sea Drilling Project. *J. Geophys. Res.*, 79:5507–5527.
- Fujii, T., Kushiro, I., and Hamuro, K., 1979. Melting relations and viscosity of an abyssal olivine tholeiite. In Melson, W. G., Rabinowitz, P. D., et al., *Init. Repts. DSDP, 45*: Washington (U.S. Govt. Printing Office), 513–516.
- Graham, A. L., Symes, R. F., Bevan, J. C., and Din, V. K., 1979. Chromium-bearing spinels in some rocks of Leg 45: phase chemistry, zoning, and relation to host basalts chemistry. In Melson, W. G., Rabinowitz, P. D., et al., *Init. Repts. DSDP, 45*: Washington (U.S. Govt. Printing Office), 581–586.
- Green, D. H., Hibberson, W. O., and Jaques, A. L., 1979. Petrogenesis of mid-ocean ridge basalts. In McElhinny, M. W. (Ed.), *The Earth: its Origin, Structure and Evolution*: London (Academic Press), pp. 265–299.
- Hey, R. N., 1981. Anomalous tectonics of the Costa Rica Rift. *Eos*, 62:1027.
- Huppert, H. E., and Sparks, R. S. J., 1980. The fluid dynamics of a basaltic magma chamber replenished by influx of hot, dense, ultrabasic magma. *Contrib. Mineral. Petrol.*, 75:279–289.
- Irvine, T. N., 1977. Chromite crystallization on the join Mg_2SiO_4 - $CaMgSi_2O_6$ - $CaAl_2Si_2O_8$ - $MgCr_2O_4$ - SiO_2 . *Year Book Carnegie Inst. Washington*, 76:465–472.
- , 1980. Magmatic infiltration metasomatism, double-diffusive fractional crystallization, and adcumulus growth in the Muskov intrusion and other layered intrusions. In Hargraves, R. B. (Ed.), *Physics of Magmatic Processes*: Princeton (Princeton Univ. Press), pp. 325–418.
- Jaques, A. L., and Green, D. H., 1980. Anhydrous melting of peridotite at 0–15 kb pressure and the genesis of tholeiitic basalts. *Contrib. Mineral. Petrol.*, 73:287–310.
- Jarosewicz, E., Nelen, J., and Norberg, J., 1979. Electronic microprobe reference samples for mineral analyses. In Fudali, R. F. (Ed.), *Smithson. Contrib. Earth Sci.*, 22:68–72.

- Juteau, T., Eissen, J. P., Francheteau, J., Needham, D., Choukroune, P., Rangin, C., Seguret, M., Ballard, R. D., Fox, P. J., Normark, W. R., Carranza, A., Cordoba, D., and Guerrero, J., 1980. Homogeneous basalts from the East Pacific Rise at 21°N: steady state magma reservoirs at moderately fast spreading centers. *Oceanol. Acta*, 3:487-503.
- Kay, R., Hubbard, N. J., and Gast, P. W., 1970. Chemical characteristics and origin of ocean ridge volcanic rocks. *J. Geophys. Res.*, 75:1585-1613.
- Kirkpatrick, R. J., 1975. Crystal growth from the melt: a review. *Am. Mineral.*, 60:798-814.
- , 1979. Processes of crystallization in pillow basalts, Hole 396B, DSDP Leg 46. In Dmitriev, L., Heirtzler, J., et al., *Init. Repts. DSDP*, 46: Washington (U.S. Govt. Printing Office), 271-282.
- Kirkpatrick, R. J., Kuo, L.-C., and Melchior, J., 1981. Crystal growth in incongruently melting compositions: programmed cooling experiments with diopside. *Am. Mineral.*, 66:223-241.
- Kuo, L.-C., and Kirkpatrick, R. J., 1982. Pre-eruption history of phytic basalts from DSDP Legs 45 and 46: evidence from morphology and zoning patterns in plagioclase. *Contrib. Mineral. Petrol.*, 79:13-27.
- Kushiro, I., and Thompson, R. N., 1972. Origin of some abyssal tholeiites from the Mid-Atlantic Ridge. *Year Book Carnegie Inst. Washington*, 71:403-406.
- le Roex, A. P., Erlank, A. J., and Needham, H. D., 1981. Geochemical and mineralogical evidence for the occurrence of at least three distinct magma types in the "Famous" region. *Contrib. Mineral. Petrol.*, 77:24-37.
- Lindsley, D. H., 1968. Melting relations of plagioclase at high pressures. *Mem. N. Y. State Mus. Sci. Serv.*, 18:39-46.
- Lofgren, G., 1980. Experimental studies on the dynamic crystallization of silicate melts. In Hargraves, R. B. (Ed.), *Physics of Magmatic Processes*: Princeton (Princeton Univ. Press), pp. 487-551.
- Lonsdale, P., 1977. Structural geomorphology of a fast-spreading rise crest: the East Pacific Rise near 3°25'S. *Marine Geophys. Res.*, 3:251-293.
- Lonsdale, P., and Klitgord, K. D., 1978. Structure and tectonic history of the eastern Panama Basin. *Geol. Soc. Am. Bull.*, 89:981-999.
- Lonsdale, P., and Spiess, F. N., 1980. Deep-tow observations at the East Pacific Rise, 8°45'N, and some interpretations. In Rosendahl, B. R., Hekinian, R., et al., *Init. Repts. DSDP*, 54: Washington (U.S. Govt. Printing Office), 43-62.
- Mattey, D. P., and Muir, I. D., 1980. Geochemistry and mineralogy of basalts from Galapagos Spreading Center, Deep Sea Drilling Project Leg 54. In Rosendahl, B. R., Hekinian, R., et al., *Init. Repts. DSDP*, 54: Washington (U.S. Govt. Printing Office), 755-772.
- Melchior, J., 1981. Chromite, olivine, and glass compositions from Mariana back-arc basin basalts: estimates of oxidation state of the magmas. *Eos*, 62:408.
- Melson, W. G., 1979. Chemical stratigraphy of Leg 45 basalts: electron probe analyses of glasses. In Melson, W. G., Rabinowitz, P. D., et al., *Init. Repts. DSDP*, 45: Washington (U.S. Govt. Printing Office), 507-511.
- Melson, W. G., Vallier, T. L., Wright, T. L., Byerly, G. T., and Nelen, J. A., 1976. Chemical diversity of abyssal volcanic glass erupted along Pacific, Atlantic, and Indian Ocean sea-floor spreading centers: Washington (Am. Geophys. Union), *Geophys. Monogr.*, 19: 351-368.
- Miyashiro, A., Shido, F., and Ewing, M., 1969. Diversity and origin of abyssal tholeiite from the Mid-Atlantic Ridge near 24° and 30° north latitude. *Contrib. Mineral. Petrol.*, 23:117-127.
- Muir, I. D., and Tilley, C. E., 1964. Basalts from the northern part of the rift zone of the Mid-Atlantic Ridge. *J. Petrol.*, 5:272-279.
- Natland, J. H., 1979a. Comparison of the chemical and magnetic stratigraphy of DSDP Sites 332 and 395. In Melson, W. G., Rabinowitz, P. D., et al., *Init. Repts. DSDP*, 45: Washington (U.S. Govt. Printing Office), 657-677.
- , 1979b. Crystal morphologies in basalts from DSDP Site 395, 23°N, 46°W, Mid-Atlantic Ridge. In Melson, W. G., Rabinowitz, P. D., et al., *Init. Repts. DSDP*, 45: Washington (U.S. Govt. Printing Office), 423-445.
- , 1980a. Crystal morphologies in basalts dredged and drilled from the East Pacific Rise near 9°N and the Siqueiros Fracture Zone. In Rosendahl, B. R., Hekinian, R., et al., *Init. Repts. DSDP*, 54: Washington (U.S. Govt. Printing Office), 605-633.
- , 1980b. Effect of axial magma chambers beneath spreading centers on the compositions of basaltic rocks. In Rosendahl, B. R., Hekinian, R., et al., *Init. Repts. DSDP*, 54: Washington (U.S. Govt. Printing Office), 833-850.
- Natland, J. H., and Melson, W. G., 1980. Compositions of basaltic glasses from the East Pacific Rise and Siqueiros Fracture Zone, near 9°N. In Rosendahl, B. R., Hekinian, R., et al., *Init. Repts. DSDP*, 54: Washington (U.S. Govt. Printing Office), 705-723.
- , 1981. Crustal stratigraphy and magmatic processes at slow-, intermediate-, and fast-spreading ridges revealed by the compositions of natural basaltic glasses. In Presnall, D. C., Hales, A. L., and Frey, F. A. (Convenors), *The Generation of the Oceanic Lithosphere*. (Abstract).
- O'Donnell, T. H., and Presnall, D. C., 1980. Chemical variations of the glass and mineral phases in basalts dredged from 25°-30°N along the Mid-Atlantic Ridge. *Am. J. Sci.*, 280-A:845-868.
- O'Hara, M. J., 1968. The bearing of phase equilibria studies in synthetic and natural systems on the origin and evolution of basic and ultrabasic rocks. *Earth Sci. Rev.*, 4:69-133.
- , 1977. Geochemical evolution during fractional crystallization of a periodically refilled magma chamber. *Nature*, 266:503-507.
- O'Hara, M. J., and Mathews, R. E., 1981. Geochemical evolution in an advancing, periodically replenished, periodically tapped, continuously fractionated magma chamber. *J. Geol. Soc. London*, 138:237-277.
- Poldervaart, A., and Hess, H. H., 1951. Pyroxenes in the crystallization of basaltic magma. *J. Geol.*, 59:472-489.
- Presnall, D. C., Dixon, J. R., O'Donnell, T. H., and Dixon, S. A., 1979. Generation of mid-ocean ridge tholeiites. *J. Petrol.*, 20:3-35.
- Presnall, D. C., Dixon, S. A., Dixon, J. R., O'Donnell, T. H., Brenner, N. L., Schrock, R. L., and Dycus, D. W., 1978. Liquidus phase relations on the join diopside-forsterite-anorthite from 1 atm. to 20 kbar: their bearing on the generation and crystallization of basaltic magma. *Contrib. Mineral. Petrol.*, 66:203-220.
- Rhodes, J. M., Dungan, M. A., Blanchard, D. P., and Long, P. E., 1979. Magma mixing at mid-ocean ridges: evidence from basalts drilled near 22°N on the Mid-Atlantic Ridge. *Tectonophysics*, 55: 35-61.
- Robson, D., and Cann, J. R., 1982. A geochemical model of mid-ocean ridge magma chambers. *Earth Planet. Sci. Lett.*, 60:86-92.
- Roeder, P. L., and Emslie, R. F., 1970. Olivine-liquid equilibrium. *Contrib. Mineral. Petrol.*, 29:275-289.
- Rosendahl, B. R., 1976. Evolution of oceanic crust, 2: constraints, implications, and inferences. *J. Geophys. Res.*, 81:5305-5314.
- Sigurðsson, H., and Schilling, J.-G., 1976. Spinels in Mid-Atlantic Ridge basalts: chemistry and occurrence. *Earth Planet. Sci. Lett.*, 29:7-20.
- Sleep, N., and Rosendahl, B. R., 1979. Topography and tectonics of mid-oceanic ridge axes. *J. Geophys. Res.*, 84:6831-6839.
- Smith, J. V., 1974. *Feldspar Minerals, 2. Chemical and Textural Properties*: New York (Springer-Verlag).
- Sparks, R. S. J., Meyer, P., and Sigurðsson, H., 1980. Density variation amongst mid-ocean ridge basalts: implications for magma mixing and the scarcity of primitive lavas. *Earth Planet. Sci. Lett.*, 46:419-430.
- Stolper, E., 1980. A phase diagram for mid-ocean ridge basalts: preliminary results and implications for petrogenesis. *Contrib. Mineral. Petrol.*, 74:13-27.
- Usselman, T. M., and Hodge, D. S., 1978. Thermal control of low-pressure fractionation processes. *J. Volcanol. Geotherm. Res.*, 4:265-281.
- Walker, D., Shibata, T., and DeLong, S. E., 1979. Abyssal tholeiites from the Oceanographer fracture zone II. Phase equilibria and mixing. *Contrib. Mineral. Petrol.*, 70:111-125.
- Wilkinson, J. F. G., 1982. The genesis of mid-ocean ridge basalts. *Earth Sci. Rev.*, 18:1-57.
- Yoder, H. S., 1969. Experimental studies bearing on the origin of anorthosite. In Isachsen, Y. W. (Ed.), *Origin of Anorthosite and Related Rocks*. Mem. N.Y. State Mus. Sci. Serv., 18:13-22.

APPENDIX
Analytical Procedures for the Detailed Sample Study

Mineral and glass analyses for the detailed sample study were obtained on a Camebax automated electron microprobe aligned with a PDP-11 computer at Scripps Institution of Oceanography. Counting time was 20 s, at 15 kV and 30 mA. A defocused beam of 20-micron diameter was used for all mineral analyses except olivine and Cr-spinel, for which a 2-micron beam was used. Glass inclusions were analyzed by using either a 5- or 10-micron beam, depending on the size of the inclusion. Drift was corrected electronically, and dead time and absorption effects were corrected by using programs CORREX and QUANTI, which were supplied by Camebax Instruments, Inc.

Oxides were calibrated by using a combination of Smithsonian (U.S. National Museum [USNM] and BRGM standards as follows: K₂O—Kakanui, N.Z., hornblende (USNM 143965); FeO—San Car-

los, Ariz., olivine (USNM 111312/444); Na₂O—BRGM albite; CaO—BRGM wollastonite; Cr₂O₃—Tiebaghi Mine, New Caledonia, chromite (USNM 117175); TiO₂ and MnO—Ilmen Mountains, U.S.S.R., ilmenite (USNM 96189); MgO—San Carlos, Ariz., olivine; Al₂O₃—BRGM corundum; P₂O₅—Durango, Mex., fluorapatite (USNM 104021); NiO—BRGM nickel oxide; and SiO₂—San Carlos, Ariz., olivine. This allowed all mineral types and glass to be analyzed at one time. Minor corrections were then made for particular oxides by comparing results for individual mineral or glass standards run as unknowns to published analyses for those standards. These corrections were made for plagioclases by comparison to Lake County, N.Y., labradorite (USNM 115900), clinopyroxenes to Natural Bridge, N.Y., diopside (USNM 117733), olivine to San Carlos, Ariz., olivine, Cr-spinels to Tiebaghi Mine, New Caledonia, chromite, and glasses to Juan de Fuca Ridge basaltic glass (USNM 111240/52 VG-2). Published values for USNM standards can be found in Jarosewich et al. (1979).